# Synthesis and Photophysical Properties of Donor/Acceptor Substituted Pyrene-Based Fluorophores


**March 2018**

**Department of Advanced Technology Fusion,**
**Graduate School of Science and Engineering,**
**Saga University, Japan**

**Wang ChuanZeng**

# Synthesis and Photophysical Properties of Donor/Acceptor Substituted Pyrene-Based Fluorophores


**A dissertation presented to the Graduate School of Science and Engineering of Saga University in partial fulfillment of the requirements for the degree of Doctor of Philosophy**

**March 2018**

By

**Wang ChuanZeng**

Supervisor:

**Professor Dr. Takehiko Yamato**

# CERTIFICATE OF APPROVAL
# Ph.D Dissertation

This is to certify that the Ph.D Dissertation of

## Wang ChuanZeng

has been approved by the Examining Committee for the dissertation requirement for the Doctor of Philosophy degree in Chemistry at the March, 2018 graduation.

Dissertation committee: Supervisor: Prof. Takehiko Yamato

_____

Member, Prof. Tsugio Kitamura

_____

Member, Prof. Takeshi Hanamoto

_____

Member, Prof. Michinori Takeshita

_____

# ACKNOWLEDGEMENTS

Firstly, I would like to express my deepest gratitude to my supervisor, Professor *Takehiko Yamato*, for his invaluable guidance, limitless helping and understanding. His profound knowledge, constructive advices inspired me during the whole doctor course.

I would like to express great appreciate to professor *Tsugio Kitamura*, professor *Mishinori Takeshita*, and professor *Takeshi Hanamoto* and the rest of my thesis committee for their kind cooperation and suggestions. I also wish to convey my sincere thanks to professor *Zhu Tao*, professor *Xin-Long Ni*, professor *Hang Cong* and other professors at Guizhou University, China, due to their inspiriting discussions and constant encouragement. Furthermore, I must acknowledge to Prof. *Carl Redshaw* and Dr. *Mark R. J. Elsegood* (United Kingdom) for single-crystal X-ray analysis and valuable suggestions during my research.

I also would like to express my deep gratitude to all of the members in Yamato Lab., especially to Dr. *Hirotsugu Tomiyasu*, Dr. *Zannatul Kowser*, Dr. *Jiang-Lin Zhao*, Dr. *Xue-Kai Jiang*, Dr. *Chong Wu*, Dr. *Tahmina Akter*, Mr. *Yuki Noda*, *Hisashi Ichiyanagi*, *Kouya Sakaguti*, *Akisumi Ageno*, and Miss *Rie Kihara* and who made my research work more enjoyable. Special thanks are given to the staffs and faculty in the International Division of Saga University for their acting concerns.

Finally, I would like to express my deeply appreciation to my parents, my girlfriend *Wen-Xuan Zhao*, my sister *Fu-Ling Wang* for their endless encouragement, understanding and sacrifice. Without their careful assistance, it would not have been possible to complete my doctoral study. I would like to dedicate this thesis to my family.

Wang Chuanzeng

March, 2018, Saga University, Japan

# ABSTRACT

Pyrenes as typical polycyclic aromatic hydrocarbons (PAHs) possess unique optoelectronic properties and features that can be readily modified, which have allowed them to be extensively explored as fluorophores, particularly in view of their additional favorable stability and high fluorescence efficiency. Based on this excellent extended carbon-rich sp2-hybridized scaffolds, pyrene-based derivatives have been used in organic electronic devices and organic semiconductors. In this thesis, we investigated the emission properties of pyrene-based fluorophores by constructing the different type molecules, such as such as D–$\pi$–D, D–$\pi$–A, and A–$\pi$–A pyrene-based derivatives.

Firstly, a facile strategy to tune the emission color of pyrene-based chromophores has been established by simple functional group modification at the para position to the diphenylamino on the donor building block. The results obtained could be explained by the Hammett method and by density functional theory (DFT) calculations. This positive correlation can be used to develop a predictive method for these types of systems.

Secondly, a controllable regioselective approach to achieve dipolar functionalization at the active sites and K-region of pyrene is demonstrated. Further, by adjusting the substituents at the 5,9-positions of pyrene, the pyrene-based dipolar molecules exhibit wide tunable emission from blue to orange-red, which opens up new avenues to explore strategy to functionalize pyrene and to greatly expand the scope for developing highly efficient pyrene-based photoelectric materials.

Thirdly, a rational design of pyrene-based dipolar molecules with two-photon absorption (TPA) properties is presented, and a series of 1,3-diphenyl-6,8-diarylethynylpyrene compounds with wide-range color tuning and large TPA cross-sections (up to 2.8 $\times$ 103 GM) are reported. These results indicate that they are promising candidates for several applications in practical photics and biological imaging applications.

Finally, A set of extended $\pi$-conjugated pyrene derivatives, namely 1,3-di(arylethynyl)-7-tert-butylpyrenes were synthesized by a Pd-catalyzed Sonogashira coupling reaction in

good yields. All the compounds exhibit blue or green emission with high quantum yields (QYs) in dichloromethane. In addition, with strong electron-donating (-$N(CH_3)_2$) or electron-withdrawing (-CHO) groups, these molecules displayed efficient intramolecular charge-transfer (ICT) emissions with solvatochromic shifts from blue to yellow (green) on increasing the solvent polarity.

In summary, several kinds of pyrene-based fluorophores were investigated. Different strategies to design and synthesize pyrene-based organic materials with tunable emission properties were established. In this work, we have presented a novel and significative result, which can expand the new fundamental concepts, synthetic strategies, and application in organic electronics.

# TABLE OF CONTENTS

**ACKNOWLEDGMENTS**····· i

**ABSTRACT**····· ii

**TABLE OF CONTENTS**····· iii

**Chapter 1**

**Recent Development of Pyrene Based Fluorophores**····· 1

1.1 General Introduction of Pyrene····· 2

1.1.1 What Is Pyrene? ····· 2

1.1.2 Modification of Pyrene Core ····· 3

1.2 General Introduction of Organic Light Emitting Diodes (OLEDs)····· 12

1.2.1 What Is OLEDs? ····· 12

1.2.2 The History of OLEDs ····· 13

1.2.3 The Main Parts of OLEDs Devices····· 13

1.2.4 The Development of Organic Host Materials for OLEDs····· 15

1.2.5 The Future of OLEDs····· 18

1.3 Working Mechanisms of Luminescence····· 19

1.3.1 Excimer Emissions····· 20

1.3.2 Charge-Transfer (CT) Emission····· 23

1.4 Objects and Motivation····· 25

1.5 References····· 26

**Chapter 2**

**Acceptor substituted π-Conjugated Pyrene Derivatives: Structural, Photophysical and Electrochemical Properties**····· 33

2.1 Introduction····· 34

2.2 Results and Discussion……36
2.2.1 Syntheses and characterization……36
2.2.2 Crystallography……37
2.2.3 Photophysical Properties……42
2.2.4 Electrochemical Properties……45
2.2.3 Density Functional Theoretical Calculation……46
2.3 Conclusions……48
2.4 Experimental Section……49
2.4.1 General……49
2.4.2 Synthetic Procedures……49
2.5 References……52
**Chapter 3**
**Synthesis and tunable emission properties of 1, 3-bis(N, Ndiaryl)amino substituted pyrene-based fluorophores**……55
3.1 Introduction……56
3.2 Results and Discussion……58
3.2.1 Synthesis procedures of monomers 3……58
3.2.2 Crystallography……58
3.2.3 Density Functional Theoretical Calculation……61
3.2.4 Optical Properties……62
3.3 Conclusions……69
3.4 Experimental Section……70
3.4.1 General……70
3.4.2 Synthetic Procedures……70
3.4.3 X-ray crystallography……73
3.5 References……75

**Chapter 4**

**Synthesis and photophysical properties of regioselective substituted pyrene-based fluorophores**……78

4.1 Introduction……79

4.2 Results and Discussion……81

4.2.1 Synthesis and Characterization……81

4.2.2 Crystallography……83

4.2.3 Density Functional Theoretical Calculation……84

4.2.4 Optical Properties……86

4.3 Conclusions……92

4.4 Experimental Section……93

4.4.1 General……93

4.4.2 Synthetic Procedures……94

4.4.3 X-ray crystallography……97

4.5 References……99

**Chapter 5**

**Regioselective substituted at 1, 3- and 6, 8-positions to achieve pyrene-based dipolar molecules: synthesis and large two-photon absorption cross sections**……102

5.1 Introduction……103

5.2 Results and Discussion……105

5.2.1 Syntheses procedures of 2……105

5.2.2 Crystallography……105

5.2.3 Density Functional Theoretical Calculation……108

5.2.4 LinearOptical Properties……109

5.2.5 Two-Photon Absorption (TPA) Properties……113

5.3 Conclusions……117

5.4 Experimental Section……118
5.4.1 General……118
5.4.2 Synthetic Procedures……118
5.4.3 X-ray crystallography……120
5.5 References……122
**Summary**……125
**Publications**……128

# Chapter 1

# Recent Development of Pyrene Based Fluorophores

*In this chapter, a shortly review focus on the development of electronic and optoelectronic organic materials based on pyrene chemistry, including the general introduction of pyrene, general introduction of organic light emitting diodes (OLEDs), general introduction of luminescence mechanisms, and objects and motivation in our present work.*

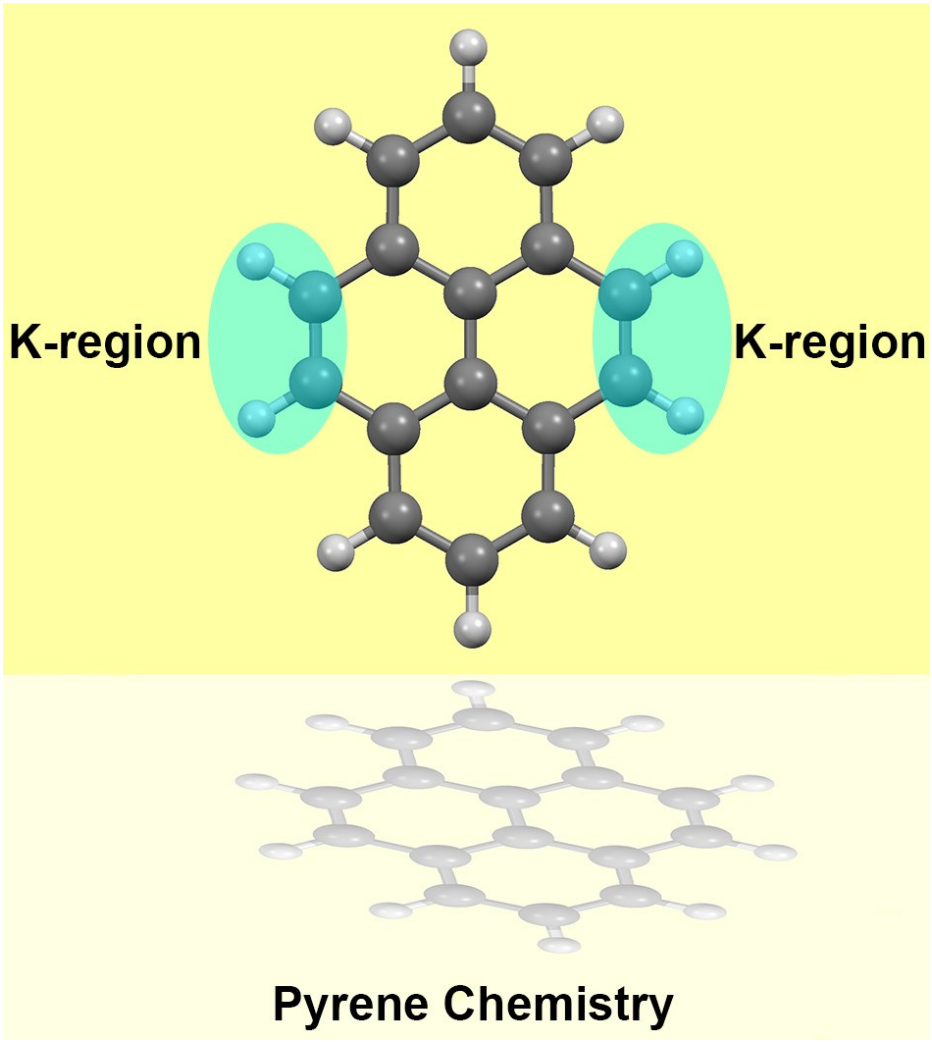

## 1.1 General Introduction of Pyrene

### 1.1.1 What Is Pyrene?

Pyrene is a polycyclic aromatic hydrocarbon (PAH) consisting of four fused aromatic rings. Its sum formula is $C_{16}H_{10}$. LAURENT was the first to isolate the hydrocarbon from coal tar.[1] this polycyclic aromatic hydrocarbon has been the subject of tremendous investigation. The name "pyrene" derives from the ancient Greek word for "fire", as LAURENT believed pyrene to be formed when organic substances react with fire. About one hundred and twenty years later, advances in industrial chemistry turned pyrene into a readily available, inexpensive building block for dye industry.[2] Coke-oven coal tar is an abundant source of polycyclic aromatic hydrocarbons (approx. 20*106 t/a) which is relatively rich in pyrene (2 - 2.1 %). Nowadays, pyrene is prepared on a multi-ton scale and utilized in its own right, especially due to its outstanding photophysical properties (e.g. as optical brightener Fluolite XMF™,[3] reactive dye C.I. Direct Blue 109[4] or fluorescent dye Pyranine[5]).

Pyrene also can be synthesized in laboratory, for instance, Weitzenböck first developed an effective synthetic route for pyrene from o,o'-ditolyl in 1913.[6] after that, several preparative routes toward pyrene were released.[7] Generally, pyrene was prepared from [2,2]metacyclophane (MCP) with bromine in the presence of iron powder, afforded the tetrahydropyrene via the addition-elimination mechanism, in the other hand, reaction of MCP with iodine monochloride (ICI) or with iodine and silver perchlorate gave same compound,[8] subsequently, dehydrogenation of tetrahydropyrene with 2,3-dichloro-5,6-dicyano-1,4-benzoquinone (DDQ) in benzene afford pyrene in good yield (Figure 1).[9]

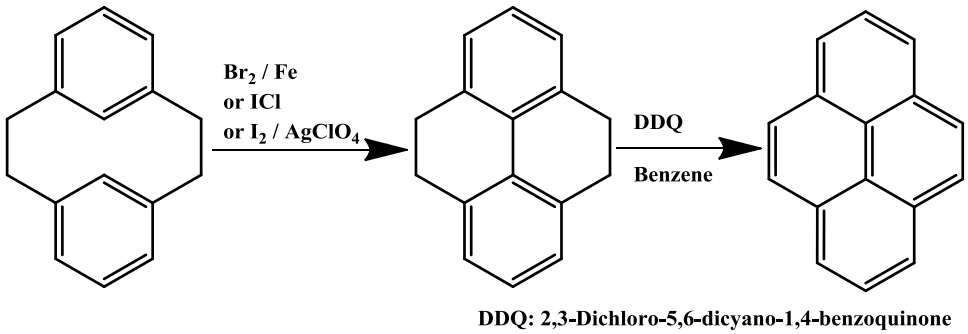


**Figure 1**. General strategy to pyrene from metacyclophane.

### 1.1.2 Modification of Pyrene Core

Pyrene and its derivatives as an excellent chromophore possesses high fluorescence (FL) quantum yield in high saturated color emission with efficient excimer formation. Although the excimer FL of them have been employed to detect guest molecules,[10] and as single-molecule excimer-emitting compounds for OLED application,[11] more attempts to the preparation of pyrene as an organic electroluminescence material for utilizing in full-flat panel displays[12] and solid-state lighting and OPV,[13] due to that can offer many advantages: (1) solution processable, (2) good thermal stability, (3) enhanced charge carrier mobility, and (4) intense luminescence efficiency. However, the great drawback of employing pyrene as an organic luminescence material is the formation of excimer emission which quenches the efficiency at high concentration or in the solid-state. Thus, in order to obtain highly efficient optical devices, the key step is functionalizing pyrene core (Figure 2) by effective chemical methods.

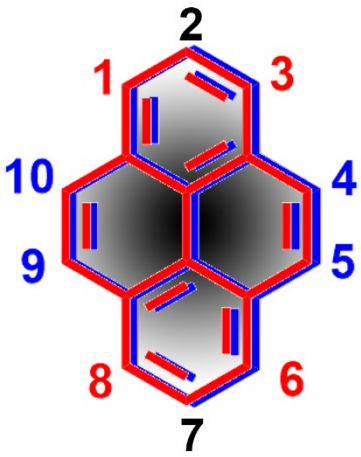


**Figure 2.** General structure of pyrene with 10 modifiable sites.

It is well known that electrophilic reagents prefer to attack the positions of 1-, 3-, 6- and 8- of pyrene, but not the other positions (2-, 4-, 5-, 7-, 9-, and 10-). Based on experimental[1] and theoretical calculation,[14] the 1, 3, 6, 8- positions of pyrene exhibited significantly active than others, such as 4, 5, 9, 10- positions or 2,7- positions. For example, the energy of 1, 3, 6, 8- position is lower 8.8 kcal/mol than 2, 7- position, and the substitution order followed by the 1- > 8- > 6- > 3- position.[15] With the development of synthetic technology, continuous progress has contributed to explore effectively approach to functionalization pyrene, not only at the

active sites 1-, 3-, 6- and 8- position, but also at the K-region of 4-, 5-, 9- and 10- position, as well as the node plane of the 2- and 7- positions.

### 1.1.2.1 1-Substituted Pyrenes

The most common chemical reactions used to synthesis 1-substituted pyrenes for use in molecular electronics are metal-catalyzed cross-coupling reactions. In this way it is possible to obtain larger $\pi$–systems by coupling more than one or more pyrenes to another $\pi$–system. Among these cross-coupling reactions, one of the most employed is the palladium-catalyzed carbon–carbon bond-forming Suzuki coupling reaction, which involves the palladium-mediated coupling of organic electrophiles, such as aryl halides, with organoboron compounds in the presence of a base. The Suzuki coupling reaction is a particularly useful method for the construction of conjugated dienes and higher polyene systems of high stereo isomeric purity, as well as of biaryl and related systems. Thus, 1-bromopyrene, obtained without difficulty with 1 equiv. of bromine at room temperature, can further be involved in Suzuki cross-couplings.[16] One example is the Suzuki reaction of 1-bromopyrene and 1,4-benzeneboronacidether in the presence of sodium tert-butoxide and $PdCl_2(PPh_3)_2$ in toluene to afford 1,4-di-1-pyrenylbenzene (Figure 3).[17]

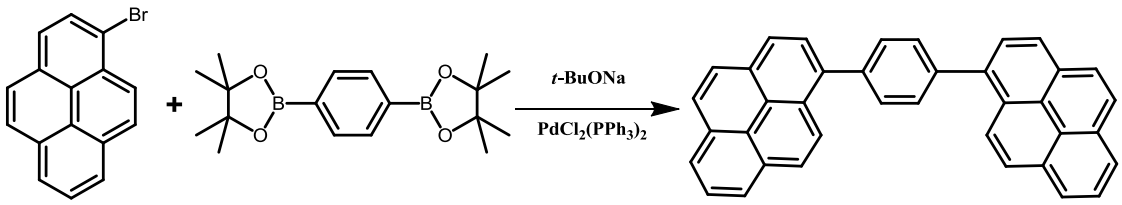


**Figure 3.** Suzuki coupling to 1,4-di-1-pyreneylbenzene.

Another possibility is to use the 1-pyreneboronic acid in the Suzuki coupling, as demonstrated in Figure 3. The 1-pyreneboronic acid could be obtained by lithiation of 1-bromopyrene at 0 °C followed by treatment with trimethylborate at –78 °C and subsequent acidic workup.[18] In this case, pyrene 4 reacted with different aryl bromides in the presence of $Pd(PPh_3)_4$ and sodium carbonate in toluene to give the three dipyrenylbenzenes in 63–66% yields (Figure 4).[19] The use of these dipyrenylbenzenes as blue emitters for the fabrication of OLED devices will be analyzed in the next section. Depending on the attachment of different

building blocks, it is possible to choose the appropriate cross-coupling reaction to afford different pyrene-based semiconductor materials.

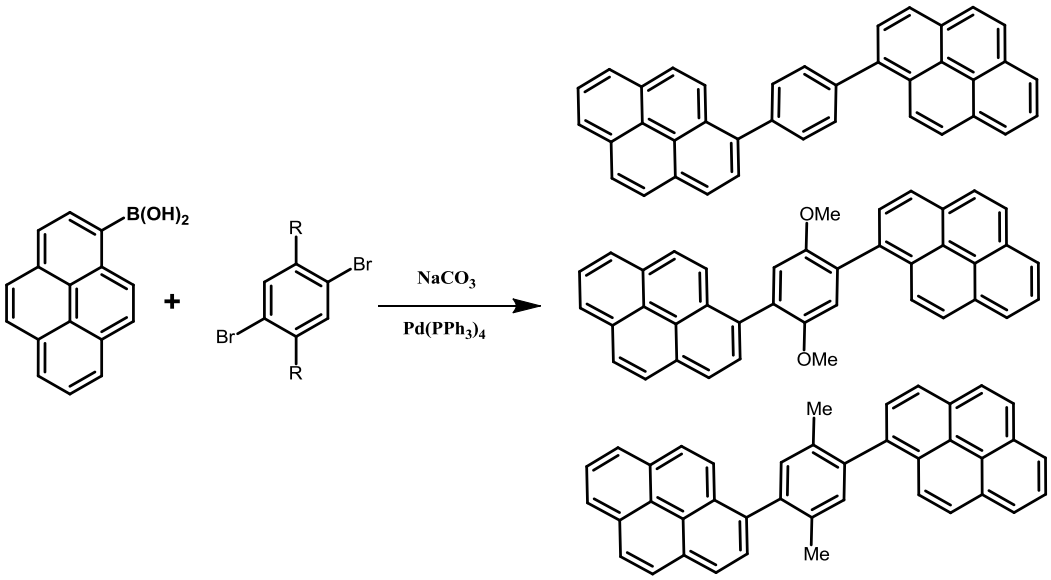


**Figure 4.** Suzuki coupling to dipyreneylbenzenes.

Metal-catalyzed reactions as a mainstream synthetic tool have attracted much attention in organic synthesis in recent years, due to the low cost, high-efficiency and ease of manipulation. More importantly, judicious choice of metal complex allows for regio-selective functionalization to the desired product.[20] Given that the active 1-position site preferentially undergoes electrophilic substitution, the pyrene-1-carbaldehyde is directly obtained from pyrene using either the Vollmann approach[16a] or by a Lewis acid-catalyzed method in good yield.[21] As shown in Figure 5, the reaction of pyrene with dichloromethyl methyl ether in $CH_2Cl_2$ solution using $TiCl_4$ as a catalyst, afforded in 90% yield.

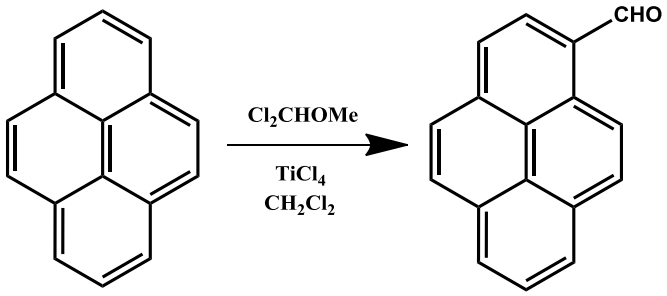


**Figure 5.** Synthesis of pyrene-1-carbaldehyde.

The Sonogashira reaction provides a valuable method for the synthesis of conjugated acetylenic systems, allowing the design of molecules including pyrene with interest in molecular electronic devices such as OLEDs as well in nanotechnology. 1-Ethynylpyrene can be easily obtained from trimethyl-(pyren-1-ylethynyl)silane in good yields (Figure 6).[22] Thus, reaction of 1-bromopyrene with ethynyltrimethylsilane in the presence of $PdCl_2(PPh_3)_2$ and CuI/$Et_3N$ in toluene provided intermediate in 80% yield (Figure 6). The TMS protecting group was eliminated using KOH in a mixture of THF/MeOH, giving 1-ethynylpyrene in 86% yield (Figure 6).[22]

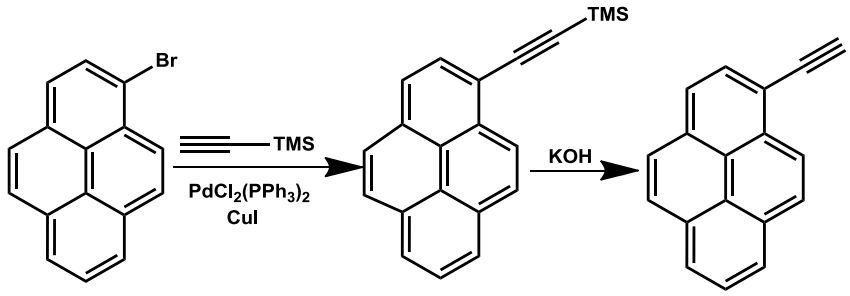


**Figure 6.** Synthesis of 1-ethynylpyrene.

The Ullmann coupling has also be used to prepare 1-substituted pyrenes with interest in molecular electronics. For example, the 10-pyren-1-yl-10*H*-phenothiazine was prepared in 55% yield via Ullmann-type reaction of phenothiazine and 1-iodopyrene (Figure7). The 1-iodopyrene was previously prepared from the 1-bromopyrene in the presence of CuI and KI.[23] Direct iodination of pyrene is not commonly used, due to the poor yield of the reaction and insolubility of the iodide derivative. Only one reference mentions the iodine cyanide promoted iodination of pyrene to afford 1-iodopyrene.[24]

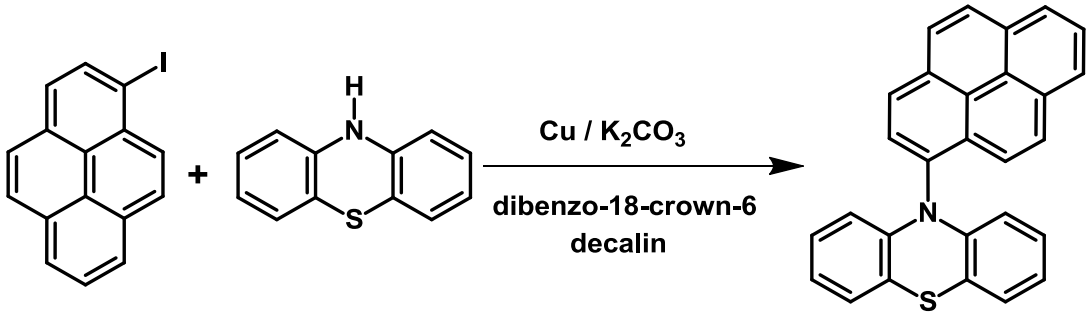


**Figure 7.** Ullmann coupling to 10-pyren-1-yl-10*H*-phenothiazine.

### 1.1.2.2 1,3,6,8-Tetrasubstituted Pyrenes

Owing to the equivalent active positions of 1-, 3-, 6- and 8- carbon atom of pyrene, which is a tendency to randomly undergo electrophilic substituent reactions ($S_EAr$) afford multi-component substituted product depending on the stoichiometric ratio of starting product. The 1,3,6,8-tetrabromopyrene as an intermediate compound in precursor, which has proven to be general and compatible with many substitution patterns and functional groups. 1,3,6,8-tetrabromopyrene can be involved in classical Suzuki, Sonogashira, Heck reaction. [25] Since the first example of *p*-type organic field effect transistors (OFETs) star-shaped pyrene-based molecular was reported by Zhu and co-workers,[26] 1,3,6,8-substituted compounds have been attracted research interesting in material science, the tetrabromopyrene has opened a door to the construction of more appropriate pyrene building blocks for organic optoelectronics application.

Tang et al. presented an AIE-active tetraphenylethene pyrenebased,[27] 1,3,6,8-tetrakis[4-(1,2,2-triphenylvinyl) phenyl]pyrene (TTPEPy), which was prepared by Suzuki coupling reaction between 1,3,6,8-tetrabromopyrene and 4- (1,2,2-triphenylvinyl) phenylboronic acid in 50%. The tetraphenylethene units were located at 1,3,6,8-position of pyrene-core as peripheral ornaments, resulting in an aggregation-induced emission enhancement (AIEE) effect (Figure 8).

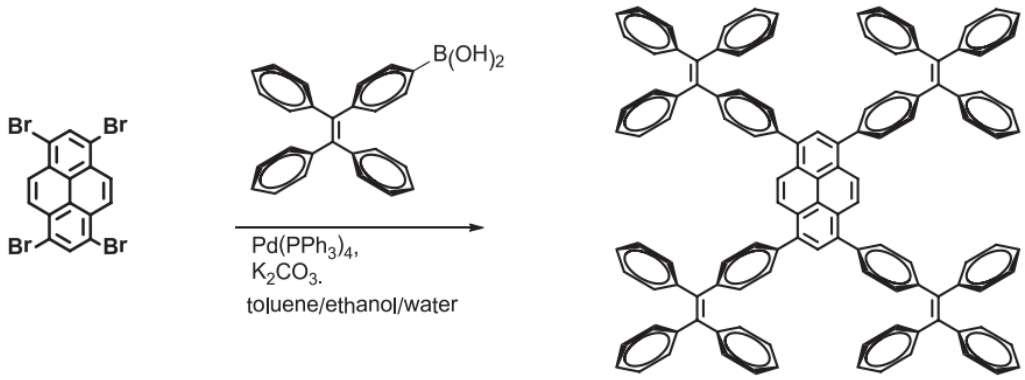


**Figure 8.** Synthesis route to TTPEPy.

An acetylene group is one option among other (such as ethylene) choice to extend the $\pi$-conjugation of molecular skeletons, and the advantage over ethylene linker is a better stability, in addition, it's very convenient to prepare this kind of compounds by Pdcatalyzed coupling

reaction. The Sonogashira reaction between 1,3,6,8-tetrabromopyrene 43 and different acetylene reagent using palladium catalyst could furnish different tetrasubstituted pyrenes; and the effect of extended acetylenic conjugation on their absorption and fluorescence properties have been thoroughly studied. Kim et al.[28] reported a series of alkynylpyrene molecules, which the *N*, *N*-dimethylaniline and 1-(trifluoromethyl) benzene are randomly introduced into 1,3,6,8-position of pyrene by stepwise Sonogashira coupling. In this case, the substitution groups are arranged randomly in nature and the substitution positions are controlled by feeding. Those results strongly indicate that substitution groups can be used to tune the photophysical properties of the pyrene chromospheres, as well as to improve the solubility or prevent aggregation. Indeed, they may be potential new photo-functional materials for application (Figure 9).

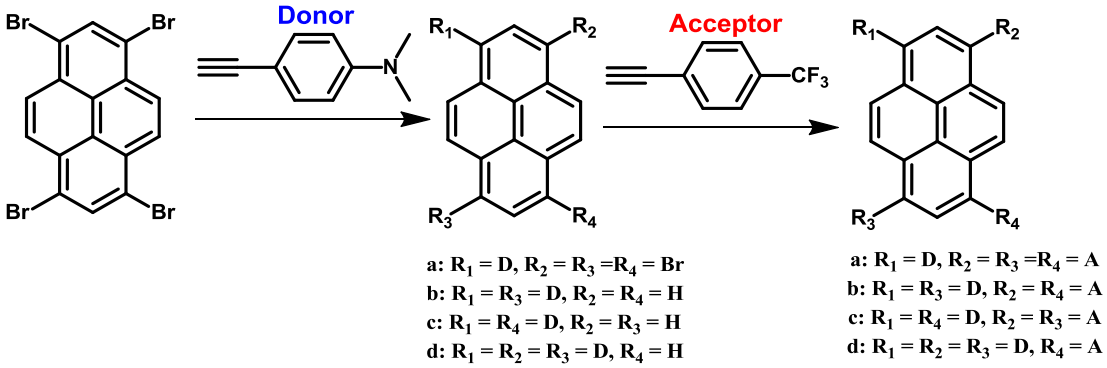


**Figure 9.** Synthesis of Donor (D)/Acceptor (A) substituted pyrene derivatives.

### 1.1.2.3 2,7-Disubstituted Pyrenes

Up to date, various of 2- and 2,7-functionalized pyrene derivatives with unusually long fluorescence lifetimes have been released.[29] Zhu et al. Presented a novel series of 2,7-functionalized pyrene derivatives for effective field-effect transistors as *p*-type semiconductors; especially, the field-effect mobility as high as 0.018 $cm^2$ $V^{-1}s^{-1}$ and current on/off ratio of $10^6$.[29b] Substitution of pyrene at the 2- and 7-positions represents a general problem, as these positions are not directly accessible by electrophilic substitution of pyrene itself, thus demanding an indirect route. Otherwise, Liu investigated the effect the substituted-position of pyrenes for optical properties.[30] For example, Suzuki reaction of pyrene-2-boronate esters with 4-bromo-toluene in the presence of $Pd(PPh_3)_4$ and sodium carbonate in toluene furnished 2-4-

tolyl-pyrene. Furthermore, for comparison, compounds 2,7-di-4-tolyl-pyrene 2,7,4-tri-4-tolylpyrene were synthesized under similar condition (Figure 10).

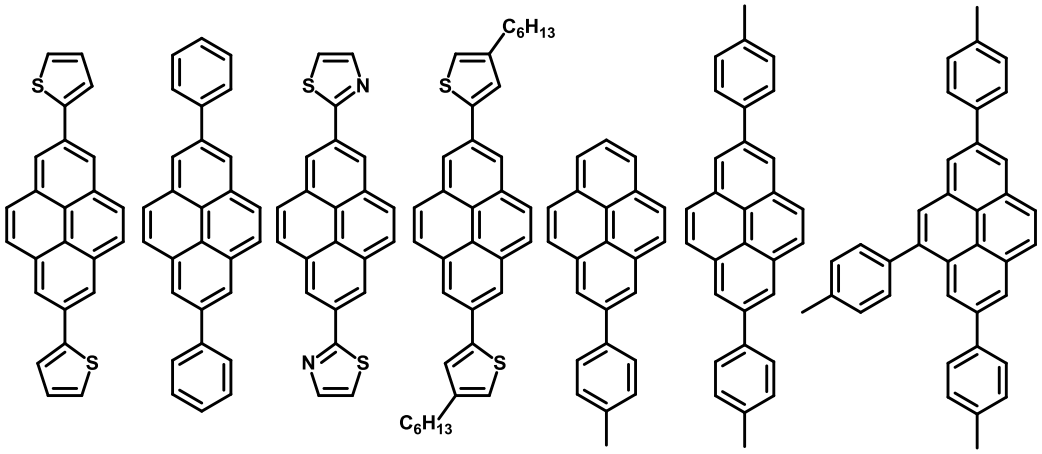


**Figure 10.** Molecular structures of 2- / 2,7- substituted pyrene derivatives.

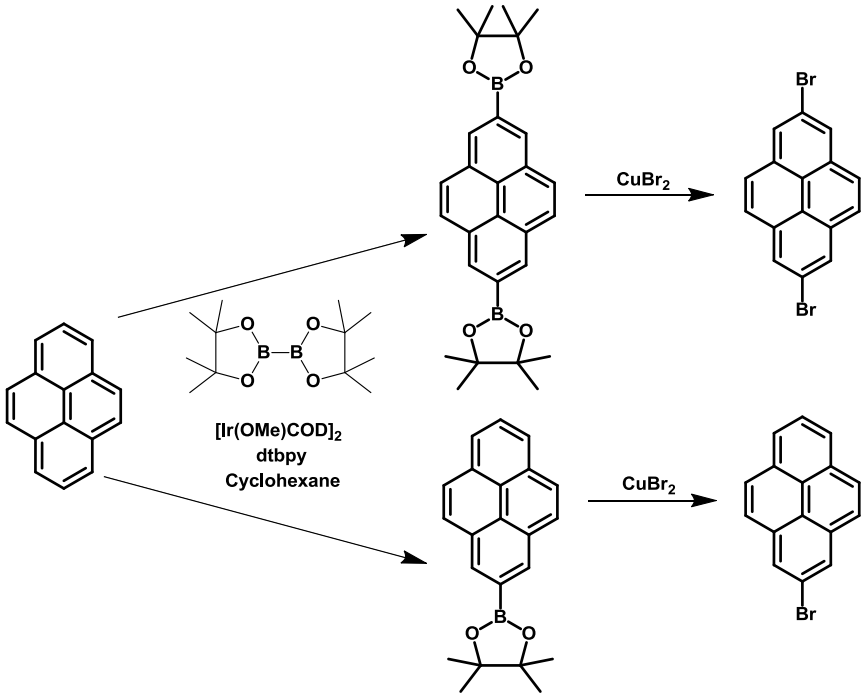


**Figure 11.** A novel method to synthesis 2-bromopyrene and 2,7-dibromopyrene.

Recently, a one-step synthesis was reported to obtain pyrene-2,7-bis(boronate)ester in high yields using an iridium-based catalyst.[31] The pyrene-2,7-bis(boronate)ester and the pyrene-2-(boronate)ester obtained following this method can be directly used in several Suzuki couplings. On the basis of this boronation reaction, our group developed a new synthetic

method to synthesize the 2,7-dibromopyrene in only two steps and in high yields (Figure 11). Bromination of pyrene-2,7-bis(boronate)-ester with $CuBr_2$ afforded 2,7-dibromopyrene in the good yield of 70%. Following the same strategy, pyrene-2-boronate ester provided 2-bromopyrene in 75% yield (Figure 11).

This strategy circumvents difficulties in obtaining 2,7-dibromopyrene and 2-bromopyrene and opens many possibilities in terms of using these attractive building-blocks in different coupling reactions.

### 1.1.2.4 4,5,9,10-Tetrasubstituted Pyrenes

Using tert-butyl group as protective group, the K-region of 4-, 5-, 9-and 10-position can be selectively modified. Bromination of 2,7-di-*tert*-butylpyrene afforded 4,5,9,10-tetrabromopyrene, (Figure 12) which can be involved in Suzuki, Sonogashira and Migita-Kosugi-Stille coupling reactions. Yamato lab. demonstrated that three types of cruciform shaped pyrene derivatives as blue emitter. As shown in Figure 13, Sonogashira reaction of 2,7-*tert*-butyl-4,5,9,10-tetrabromopyrene with different phenylacetylenes produced the corresponding 2,7-di-*tert*-butyl-4,5,9,10-tetrakis (p-R-phenylethynyl) pyrenes in excellent yields.[32] Similarly, mixture of 2,7-*tert*-butyl-4,5,9,10-tetrabromopyrene with quinolinylboronic acids to obtain 2,7-di-*tert*-butyl-4,5,9,10-tetraquinolinylpyrene, which has the potentially serve as binucleating ligands;[33] Dramaticlly, Müllen reported a fourfold Stille coupling of 2,7-*tert*-butyl-4,5,9,10-tetrabromopyrene with tri-n-butyl (thiophen-2-yl) stannane gave 2,7-di-*tert*-butyl-4,5,9,10-tetra (thien-2-yl) pyrenes in 48% yield; subsequently, irradiation of the cruciform-shaped molecules in the presence of iodine as an oxidant instead of iron (III) chloride afford a large $\pi$-system nonplanar polycyclic aromatic hydrocarbons in 60% yield by photoinduced cyclization reaction (Figure 13).[34]

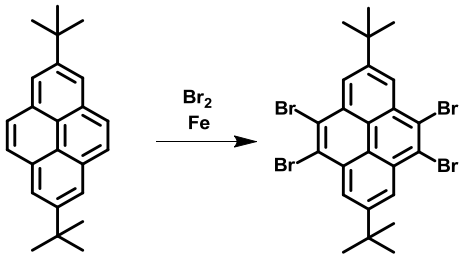


**Figure 12.** Bromination to afford 2,7-*tert*-butyl-4,5,9,10-tetrabromopyrene.

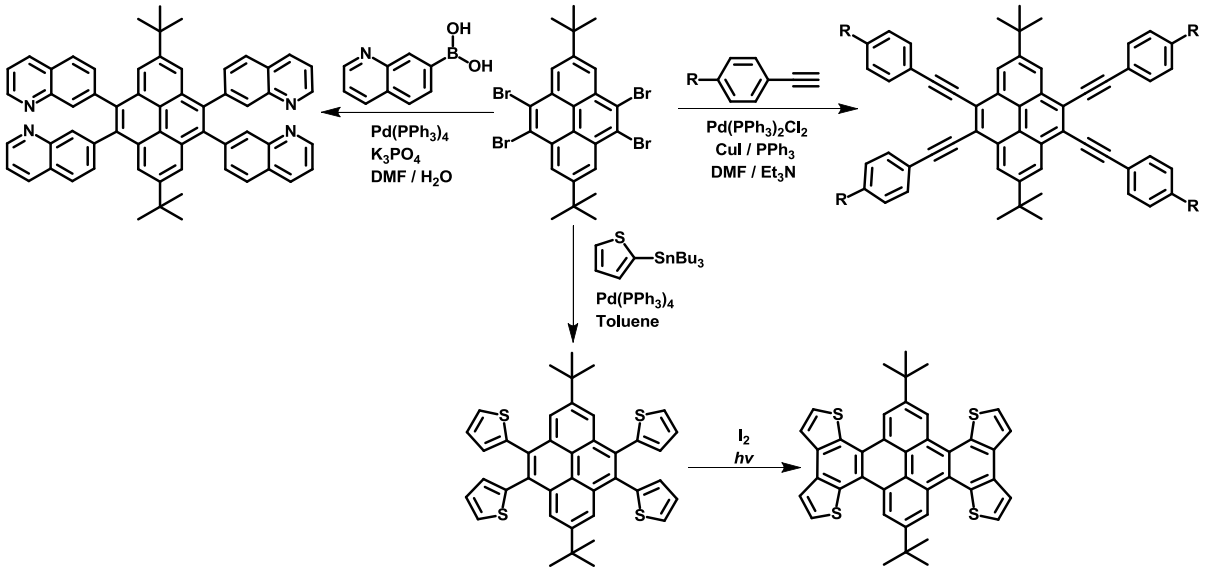


**Figure 13.** Synthesis of cruciform shaped pyrene derivatives.

Meanwhile, several attempts have been made to prepare pyrene-4,5-diones and pyrene-4,5,9,10-tetraones directly from pyrene. Pyrene-4,5-dione has been prepared in low yield by the oxidation of pyrene with the highly toxic osmium tetroxide.[35] The pyrene-4,5-dione and pyrene-4,5,9,10-tetraone have been also prepared by multistep synthetic routes.[36] To avoid such multistep routes to the tetraones, the oxidation of pyrene was reported using a heterogeneous mixture of ruthenium(III)chloride ($RuCl_3$) and sodium periodate ($NaIO_4$) in $CH_2Cl_2$, $H_2O$, and $CH_3CN$, which selectively provided pyrene-4,5-dione and pyrene-4,5,9,10-tetraone, depending on the reaction temperature and the amount of oxidant used (Figure 14).[37] This strategy opened many possibilities in terms of extension of the pyrene conjugated system by simple condensation reactions.[38]

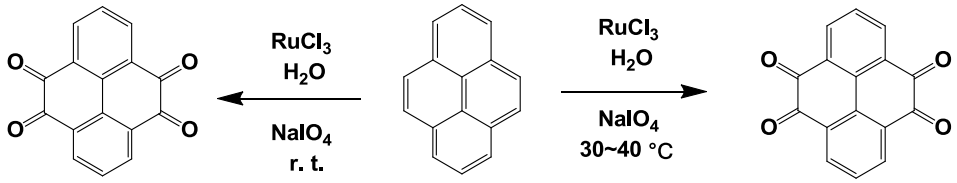


**Figure 14.** One-step synthesis to pyrene-4,5-dione and pyrene-4,5,9,10-tetraone.

## 1.2 General Introduction of Organic Light Emitting Diodes (OLEDs)

### 1.2.1 What Is OLEDs?

Light has played a crucial role in the evolution of the whole human history. With the development of technology, the great revolution is that human can create the light from utilizing the natural light since 1879.[39] The Nobel Prize in physics 2014 was awarded to Japanese Professor Isamu Akasaki and Hiroshi Amano, and American scientist Shuji Nakamura Shirakawa for "The invention of efficient blue light-emitting diodes (LED) which has enabled bright and energy saving white light sources".[40]

Organic light-emitting diodes (OLEDs)[41] are semiconductors made of layers of thin organic materials only a few nanometers thick, which potentially can be deposited on a variety of substrates such as glass, flexible metal or plastic foil.

OLEDs emit light as an ultra-flat area light source in a diffuse, glare free-way. They are a key part of a revolution in the rapidly-growing display market - fulfilling the dream of paper-thin, flexible, highly efficient displays with brilliant colors and amazing design flexibility. OLEDs have a broad color spectrum and can provide an exceptional warm, natural white light. OLEDs are considered to represent the future of a vast array of completely new lighting applications. By combining color with form factor, OLEDs can create new ways of decorating and personalizing personal surroundings with light (Figure 15).


**Figure 15.** The world's first curves 3D OLED TV.

### 1.2.2 The History of OLEDs

The first profound breakthrough since Tang and Van Slyke[42] who reported double layer organic light-emitting diodes (OLEDs) with lowvoltage and attractive luminance efficiency in 1987, which combined modern thin film deposition techniques with suitable materials with structure form p-$\pi$ heterostructure devices. This novel application of the principle caused a resurgence of interest in the subject sparking increased research in the technology. After 3 years, the Friend group at the University of Cambridge discovered the EL from polymers for the development of large-area OLEDs,[43] which exhibited light emission in the green-yellow part of the spectrum with considerable high efficiency. Forrest et al. reported a fluorescent red organic light emitting device containing emissive triplet phosphors with nearly 100% efficiency.[44] Since then, many efforts to improve color gamut, luminance efficiency and device reliability of OLEDs material for research interesting and commercial value.[45] And the growing interest is largely motivated by the promise of the use of this technology toward full-color flat panel displays.

Since the intensity research on OLED field in 1990s, over than 12000 papers were published within 30 years, and the research interests involving in fundamental and application research are increasing trend as time has gone on.

### 1.2.3 The Main Parts of OLEDs Devices

As shown in Figure 16, the basic OLEDs structure likes sandwich which consists of a layer of a luminescent organic chromophore between anode and hole transport layer. As current flows from the cathode to the anode through the organic layers, holes and electrons move from the corresponding conducting layers into the emissive layer where they recombine. As the electrons drop into the holes, they release extra energy as light, thus generating an organic light source. Specifically, the anode is usually made of transparent conducting oxide (TCO) anode, such as indium tin oxide (ITO); while the cathode is reflective and made of metal with low work function electrode, like aluminum (Al) and magnesium (Mg). The luminescent organic chromophore always involved conjugated monomer, polymer or complex and the thickness of the organic layer is around 100 and 150 nm. When the electricity passed, the holes are injected from the anode and the electrons are injected from cathode, respectively. Charge carriers

migrate through the organic layer, then recombine to form singlet and triplet excitons with 1:3 ratio.[46]

This process occurred at the emissive layer (EML) due to the location of the recombination zone in the diode is a function of the charge mobility of the organic material as well as of the electric field distribution. After diffusion, the exciton recombines and a photon is emitted.[47] The singlet excitons return to ground state directly by decaying rapidly, yielding prompt electroluminescence (fluorescence). Or two triplet excitons return to a multiplicity state and combine to form a singlet exciton through triplet–triplet annihilation, which leads to radiative delayed electroluminescence (phosphorescence).

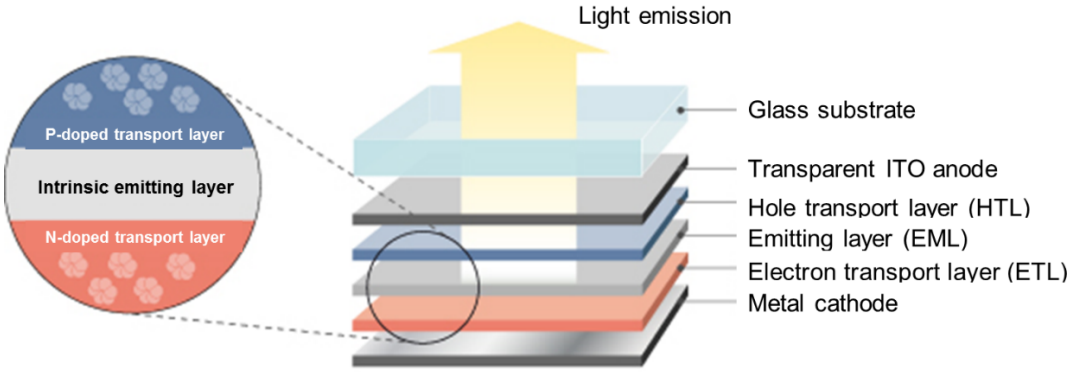


**Figure 16.** The main parts of an OLED.

In a basic monolayer OLED structure, the emitting layer (EML) was composed of materials with the capabilities of holetransporting, electron-transporting and emissive. Tang and his group have reported a new OLED devices with double-layer structure that can dramatically improved power conversion efficiencies by the addition of a hole transport layer (HTL) with the thin amorphous film stacking in the device structure.[48] The HTL provides an efficient site for the recombination of the injected hole-electron pair and resultant electroluminescence. Subsequently, multi-layer structure configurations to improve the device performance were implemented by inserting several layers like buffer layer between anode and hole transport layer (HTL),[49] electron transport layer (ETL), hole blocking layer (HBL)[50] or interlayer between cathode and ETL[51] in the device structure. Thus, the luminescent or recombination layer can be chosen to have a desired EL color as well as high luminance efficiency.

## 1.2.4 The Development of Organic Host Materials for OLEDs

Phosphorescent organic light-emitting diodes (PhOLEDs) unfurl a bright future for the next generation of flat-panel displays and lighting sources due to their merit of high quantum efficiency compared with fluorescent OLEDs. Numerous studies focus on small-molecular organic host materials as triplet guest emitters in PhOLEDs. At first, some typical hole and electron transport materials used in OLEDs are briefly introduced. Then the hole transport-type, electron transport-type, bipolar transport host materials and the pure-hydrocarbon compounds are comprehensively presented. The molecular design concept, molecular structures and physical properties such as triplet energy, HOMO/LUMO energy levels, thermal and morphological stabilities, and the applications of host materials in PhOLEDs are reviewed.

### 1.2.4.1 Typical Hole Transport Materials

Generally, the molecular structures of hole transport materials usually contain electron-donating moieties, such as triarylamine, diphenylamine, carbazole etc. A useful hole transport material for electrophosphorescence should possess good hole mobility, a high glass transition temperature ($T_g$) to form thermally and morphologically stable thin films, an appropriate HOMO level to ensure a low energy barrier for hole injection from the anode and then into the emissive layer, a suitable LUMO level to block electron injection from the EML to the HTL, and a high triplet energy to confine triplet excitons in the EML. Figure 17 displays the chemical structures of the most frequently used hole transporting materials in PhOLEDs.

4,4'-bis[N-(*p*-tolyl)-*N*-phenylamino]biphenyl (TPD) is commonly used as a hole transporter in PhOLEDs materials, especially for those based on organolanthanide complexes as emitters.[52] The HOMO and LUMO levels of TPD are 5.4 and 2.4 eV, respectively; its triplet energy is 2.34 eV,[53] and its hole drift mobility is known to be as high as $1.1 \times 10^{-3}$ cm2 $V^{-1}$ $s^{-1}$. However, it lacks thermal and morphological stability and tends to readily crystallize, as its $T_g$ is as low as 65 °C.[54] *N*,*N*'-Di(1-naphthyl)-*N*,*N*'-diphenylbenzidine (NPB) is a structural modification of TPD through replacing the tolyl by the bulky naphthyl group, showing an improved $T_g$ (95 °C)[54] and almost comparative hole mobility ($8.8 \times 10^{-4}$ $cm^2$ $V^{-1}$ $s^{-1}$)[53a] with TPD. The HOMO and LUMO levels of NPB are the same as TPD, while its triplet energy slightly lowers to 2.29 eV.[53] Up to date, NPB is the most widely used hole transport material

either in fluorescent or phosphorescent OLEDs. However, the much lower triplet energy of these two compounds prevent them to using as hole transport materials in blue and white PhOLEDs, which leads to the utilization of high triplet-energy 4,4',4''-tris(*N*-carbazolyl)triphenylamine (TCTA)[55] and 1-Bis[4-[*N*,*N*-di(4-tolyl)amino]phenyl]-cyclohexane (TAPC)[42] as both triplet exciton blocker and transitional hole transport layer. The HOMO level of TPAC (5.5 eV) is close to those of TPD and NPB, however its LUMO rises to 2.0 eV,[56] which is beneficial to electron blocking. Together with its high triplet energy (2.87 eV),[53b, 57] TAPC is a good HTL material for highly efficient blue PhOLEDs, although its morphological instability makes it undesirable for long lifetime OLEDs.[58]

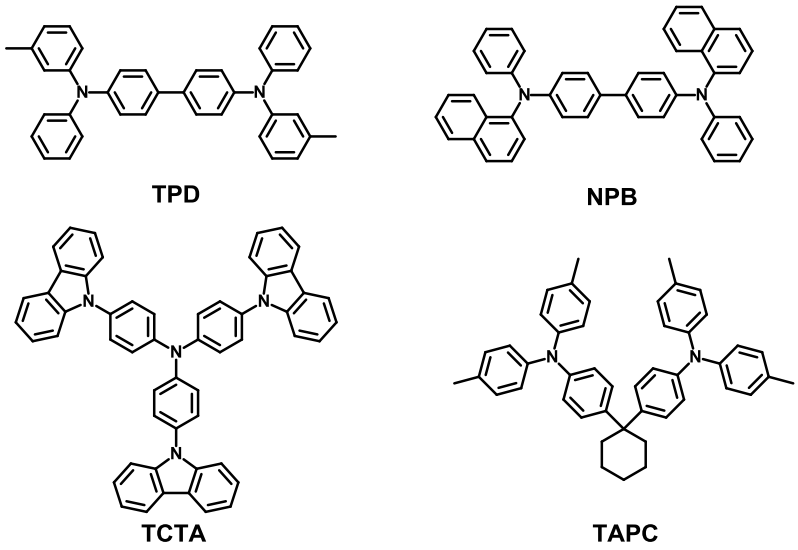


**Figure 17.** Typical hole transport materials containing triarylamine and carbazole moieties.

### 1.2.4.2 Typical Electron Transport Materials

In contrast to hole transport materials, electron transport materials (ETM) usually contain electron-withdrawing groups in their molecular structures. Similar to hole transporting materials, an appropriate ETM in PhOLEDs should possess good electron mobility, suitable HOMO and LUMO levels to block holes and facilitate electron injection, appropriate triplet energy to confine triplet excitons and good thermal stability.[59]

A suitable electron transport host should meet some requirements: (i) it usually incorporate both electron-donating and electron-withdrawing moieties. (ii) Good thermal and morphological stabilities to ensure the device stability. (iii) Matching HOMO and LUMO energy levels with those of adjacent layers to reduce charge injection barriers and device

driving voltages. (iv) Higher triplet energy than the dopant to effectively prevent exothermic reverse energy transfer from the guest emitter to the host. However, it is difficult for a bipolar host to acquire high triplet energy, because the electron-donating and electron-withdrawing moieties in one molecule unavoidably lower the band gap of the material through intramolecular charge transfer, while the low triplet energy of the host can cause reverse energy transfer, which consequently decreases the efficiency of PhOLEDs. In this context, molecular designs (Figure 18) of bipolar host materials focus on the interruption of the p-conjugation between electron donating and electron-withdrawing moieties. There have been various methodologies to suppress the intramolecular charge transfer: by introducing a fluorene spacer[60] or methyl steric group[61] between the electron-donating (D) and electron accepting (A) unit; connecting the two D–A through meta- and/or ortho-linkage instead of para-position;[62] by incorporating the p-type group to an n-type segment through the sp3-hybridized atom;[63] by flexible non-conjugated s-bonds linkage[64] between the two D–A moieties.

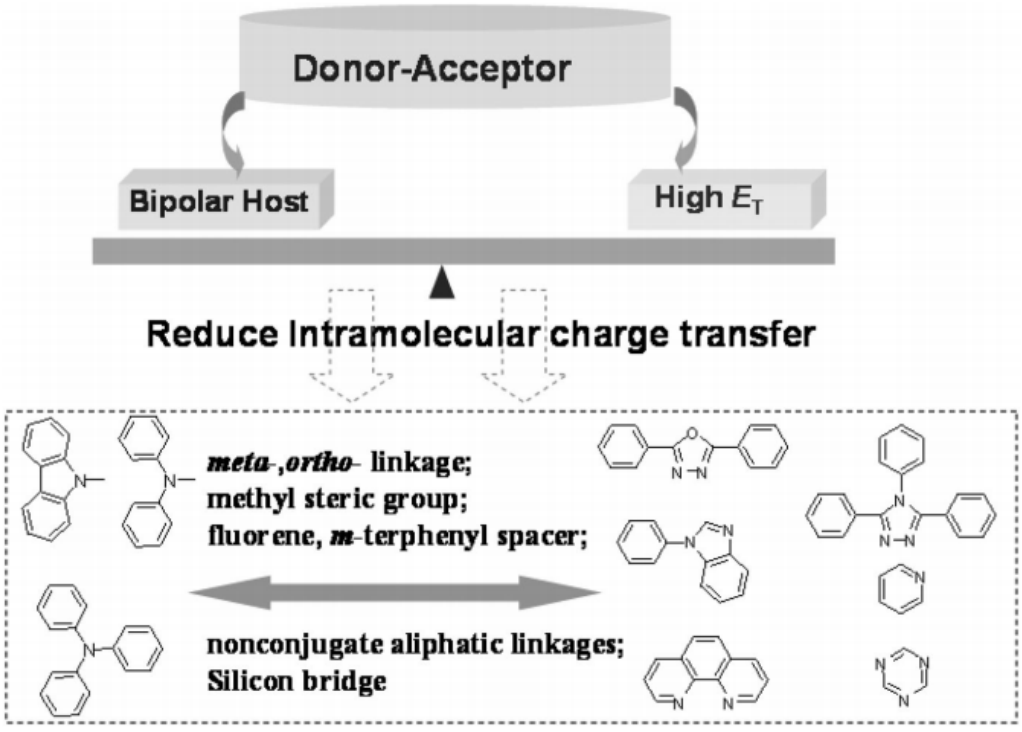


**Figure 18.** Schematic description on molecular design of bipolar host materials through various linking spacers or linking topologies between electron-donating and electron-accepting moieties to reduce intramolecular charge transfer.

## 1.2.5 The Future of OLEDs

OLED technology may usher in a new era of large-area, transparent, flexible and low-energy display and lighting products. The flexibility of OLEDs enables manufacturers to produce OLEDs using roll-to-roll manufacturing processes, and allows for the production of flexible display and lighting products. OLEDs are commercially produced on rigid glass substrates mainly. However, first applications like watches or bent displays using flexible OLEDs have entered the market lately.

Developing sufficiently durable and flexible OLEDs will require better materials and further development of manufacturing tools and processes. Flexible plastic substrates need improved barrier layers to protect OLEDs from moisture and oxygen. Thin-film encapsulation also is needed to create thin and flexible metal- and glass-based OLEDs.

These advances ultimately may lead to very flexible OLED panels for both display and lighting products, ensuring that any surface area – flat or curved – will be able to host a light source. Recent demonstrations by display and lighting companies already have hinted at the potential of flexible OLED technology. Substantial development efforts are being invested in this area and, if successful, flexible OLED panels may become commercially available as early as the last half of this decade.

**Figure 19.** Potential applications of OLED technology.

## 1.3 Working Mechanisms of Luminescence

Decipherment of the underlying mechanisms for the luminescence phenomena is of great importance to the quest for fundamental knowledge of photophysics, and just as crucial, it will guide our endeavors to design novel luminogens, explore practical applications, and promote technological innovations.

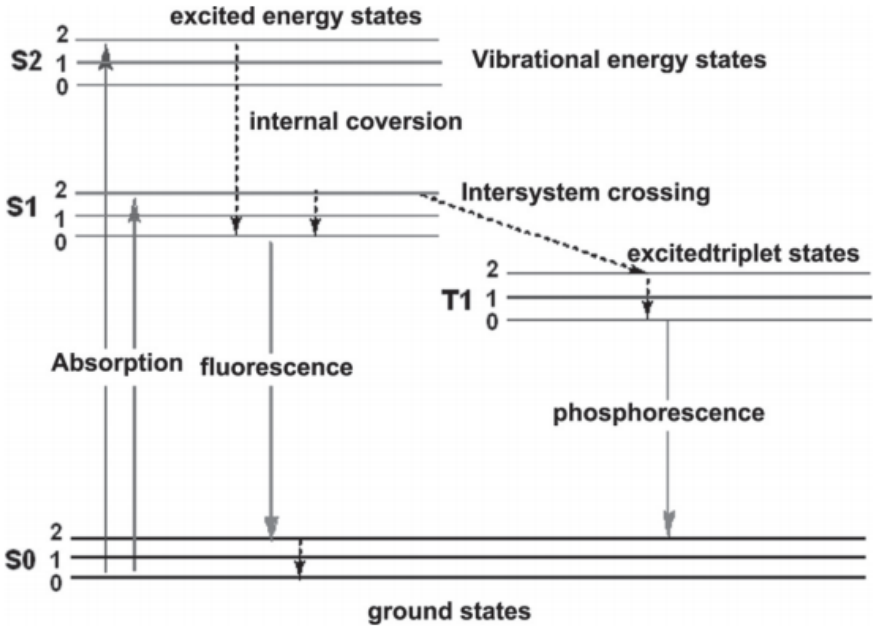


**Figure 20.** The Jablonski Energy Diagram.

Pyrenes as typical polycyclic aromatic hydrocarbons (PAHs) possess unique optoelectronic properties and features that can be readily modified, which have allowed them to be extensively explored as fluorophores, particularly in view of their additional favorable stability and high fluorescence efficiency.[65] Generally, the availability of efficient monomeric emission in the range of 370–430 nm and the excimer emission at around 480 nm,[66] combined with the charge-transfer (CT) emission possible by means of the introduction of donor/acceptor moieties at the pyrene has established their position/reputation in comparison with other polyaromatic fluorophores (see examples in Figure 21).[67] However, the mechanisms associated with multiple photoluminescence from a single molecule in pyrene chemistry remains relatively unexplored. The minimal mechanistic work to date reflects the limiting harsh prerequisites, such as the combination of multidimensional intermolecular interactions

required, not to mention the pre-determined spatial arrangements combined with appropriate donor/acceptor constituents.[68] Thus, the design and synthesis of organic molecules with multiple photoluminescence remains a challenging topic.

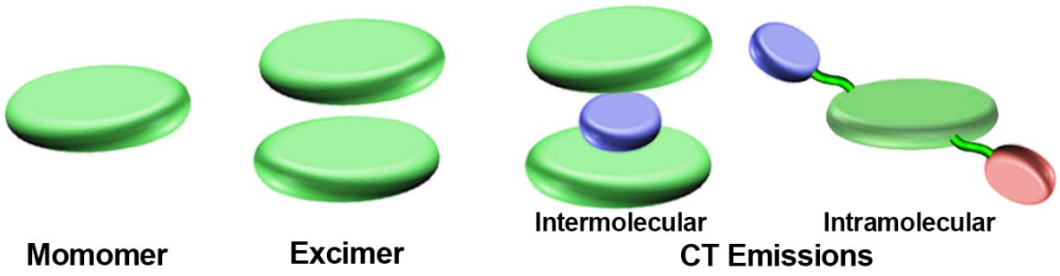


**Figure 21.** Diagrammatic sketch illustrating the typical structures giving rise to emissions in the pyrene system.

## 1.3.1 Excimer Emissions

Where aromatic rings are involved in weak interactions (such as $\pi$-stacking) which bring them within van der Waals contact distances, electronic excitation of one ring can cause an enhanced interaction with its neighbor, leading to what is termed an excited-state dimer or "excimer".[69] In other words, an excimer is a complex formed by the interaction of an excited fluorophore with another fluorophore in its ground state. Excimer emission typically provides a broad fluorescence band without vibrational structure, with the maximum shifted, in the case of most aromatic molecules,[70] by about 6000 $cm^{-1}$ to lower energies compared to that of the uncomplexed ("monomer") fluorophore emission. An excimer may also form from an excited monomer if the interaction develops within the lifetime of the latter. Thus, it is expected that excimers are more likely to be produced by relatively long-lived monomer excited states.[71] Rates of fluorophore diffusion, especially in viscous solvents, are therefore another limit on excimer formation.[72] Importantly, the separation and relative orientation of multiple fluorophore units attached to ligands can be controlled by metal ion coordination, so that recognition of a cation can be monitored by the monomer:excimer fluorescence intensity ratio.[73]

As shown in Figure 22, A new *N*-thiophosphorylated thiourea (1-pyrene)NHC(S)NHP(S)$(OiPr)_2$ (**HL**) has been synthesized. The molecular structure of **HL** was elucidated by X-ray diffraction revealing a linear intramolecular hydrogen bond. Additionally, its crystal structure is stabilized by two intermolecular hydrogen bonds, which in turn leads to a centrosymmetric $R_2^2(8)$ dimer formation. These dimers are packed into polymeric chains through $\pi\cdots\pi$ stacking interactions between the pyrene rings. The reaction of the deprotonated **HL** with $Ni^{II}$ leads to the $Ni^{II}$ complex (**[$NiL_2$]**).

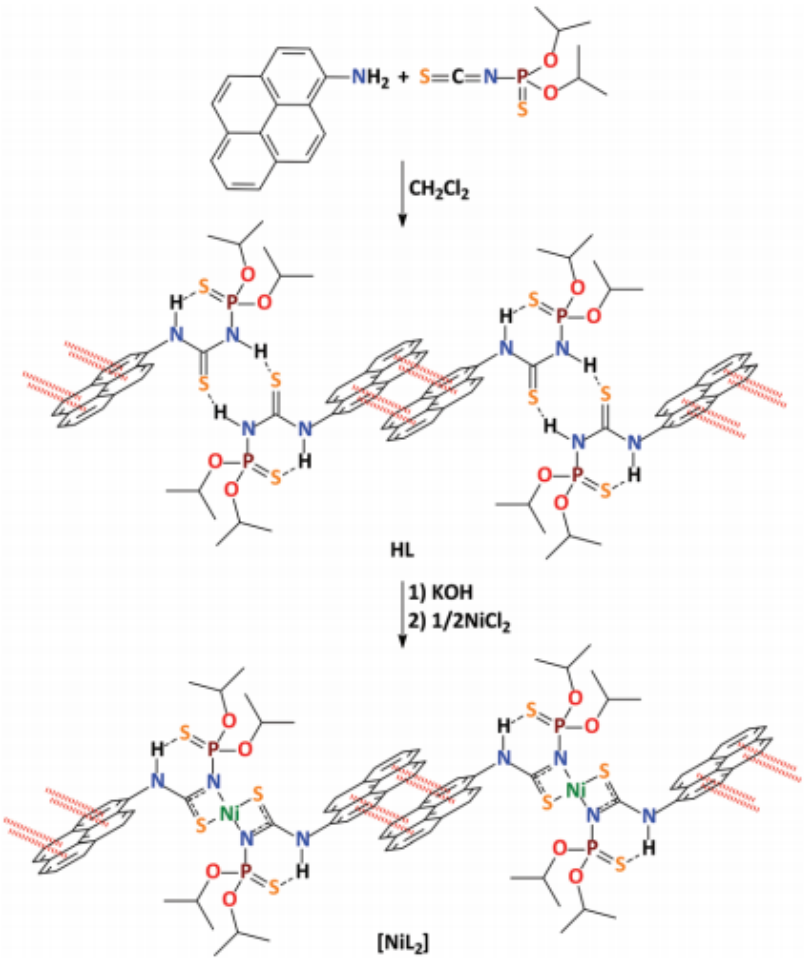


**Figure 22.** Synthetic route and strong intramolecular hydrogen bonding between the sulfur atom of the thiophosphoryl function and the hydrogen atom of the pyreneNH fragment.

The crystal structure of **[$NiL_2$]** exhibits a centrosymmetric homoleptic structure, where the $Ni^{II}$ ion is coordinated in a square-planar fashion with the ligands arranged in a trans-N2S2 configuration. The pyreneN-H protons in **[$NiL_2$]** are involved in intramolecular hydrogen

bonds of the pyreneN–H···S=P type. Molecules of **[NiL$_2$]** form $\pi\cdots\pi$ stacking interactions between the pyrene rings, yielding 1D polymeric chains similar to those observed in the structure of **HL**. These $\pi\cdots\pi$ stacked 1D polymeric chains are linked to each other through C–H···S and anagostic C–H···Ni interactions, yielding 2D sheets. Hirshfeld surface analysis showed that the structures of both HL and **[NiL$_2$]** are highly dominated by H···H, H···C, H···S and C···C contacts and also characterized by H···O and H···N contacts. The molecular surfaces of **HL** and **[NiL$_2$]** also contain O···S and H···Ni contacts, respectively. Both **HL** and **[NiL$_2$]** were found to be emissive in $CH_2Cl_2$ solution, which is due to the concentration dependent emission of the pyrene monomer and excimer (Figure 23). It was established that the latter fluorescence is due to the intermolecular excimer formation. The DFT calculations allowed us to confirm the aggregation ability of the synthesized species in solution through the numerous non-covalent interactions C–H···S, C–H···Ni and C–H···π, which, in turn, might be responsible for the concentration dependent photophysical properties.[74]

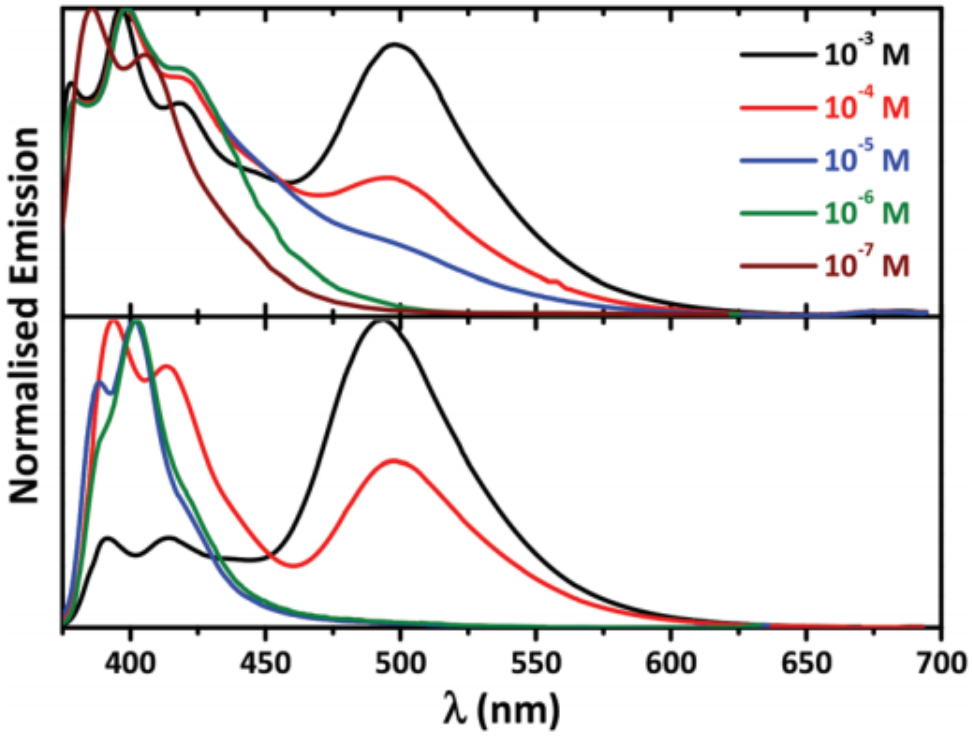


**Figure 23.** Normalized concentration dependent fluorescence spectra ($\lambda_{exc}$ = 350 nm) of HL (bottom) and **[NiL2]** (top) in $CH_2Cl_2$.

### 1.3.2 Charge-Transfer (CT) Emission

The investigation of intramolecular charge transfer (ICT) in donor−acceptor systems such as substituted benzenes reveals many interesting processes occurring in electronically excited states. For example, dual fluorescence of 4-(*N*, *N*-dimethylamino)benzonitrile (DMABN) in polar solution, consisting of an emission from the $^1L_b$ state and an "anomalous" red-shifted emission from the $^1L_a$ state[1] has attracted considerable attention. The $^1L_b$ state is usually characterized to be local excitation (LE) and the $^1L_a$ state as charge-transfer (CT) state. The position and intensity of the red-shifted band show a marked dependence on solvent polarity. This property was interpreted as an indication for a large dipole moment of the emitting state and hence for its charge-transfer character. In contrast to solution, in the gas phase, the emission spectrum of DMABN consists of a single local excitation (LE) fluorescence band $S_1(^1L_b)$, and evidence for a LE → ICT process in DMABN was not found.[75] The structural and electronic nature of the red-shifted emission band of DMABN has been explained by means of several excited-state ICT mechanisms.[76]

The systematic synthesis of five 1-, 3-, 6-, and 8-tetrasubstituted asymmetric pyrenes with electron donor and acceptor moieties is presented (Figure 24), together with an examination of their photophysical properties. Pyrene derivative **PA1**, containing one formyl and three piperidyl groups, showed bright solvatochromic fluorescence from green ($\lambda_{em}$ = 557 nm, $\Phi_{FL}$ = 0.94 in hexane) to red ($\lambda_{em}$ = 648 nm, $\Phi_{FL}$ = 0.50 in methanol), suggesting potential applications for **PA1** as an environmentally responsive probe. Although the synthesis of simple 1- and 3-disubstituted pyrene derivatives is considered difficult, **PA13**, with two formyl groups at the 1- and 3-positions and two piperidyl groups at the 6- and 8- positions, could be synthesized successfully. **PA13** exhibited less pronounced solvatochromism, but displayed a narrow fluorescent band with high $\Phi_{FL}$ in all solvents ($\Phi_{FL}$ > 0.75). Moreover, its absorption band displayed an exceptional bathochromic shift compared to the other derivatives (e.g., $\lambda_{abs}$ = 480 and 522 nm in ethanol for **PA1** and **PA13**, respectively), suggesting that such modifications of pyrene may be quite important for the modulation of its energy gap. Additionally, all compounds exhibited exceptionally high photostability, which highlights the advantage of these new dyes and provides new insights on the design of photostable fluorophores.[77]

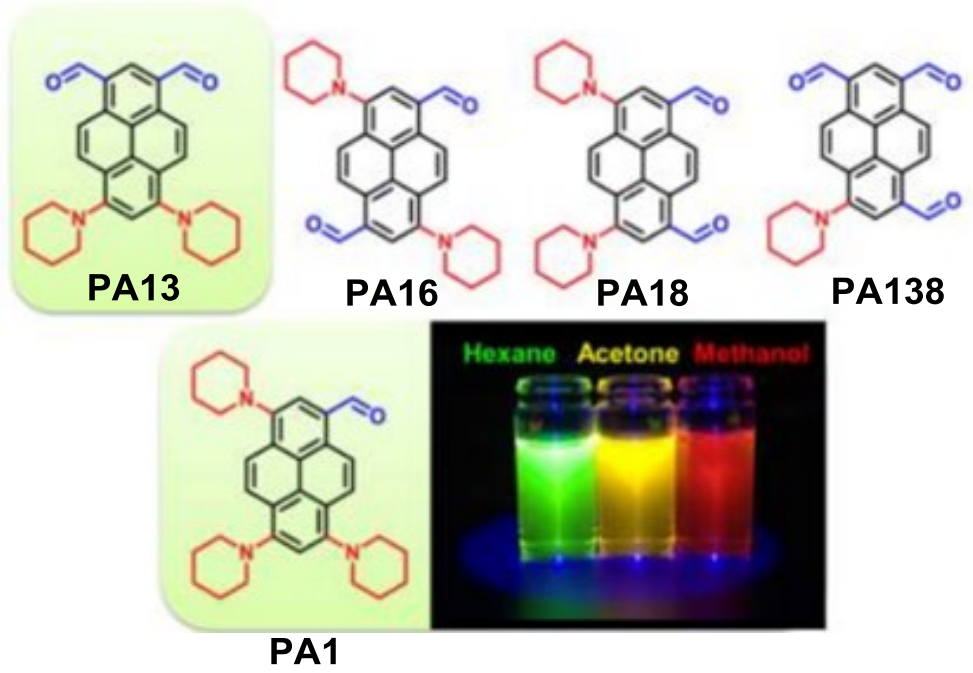


**Figure 24.** Asymmetric tetrasubstituted pyrenes with electron-donor and electron-acceptor moieties.

## 1.4 Objects and Motivation

In this work, synthetic approaches to highly functionalized pyrene derivatives will be explored. On the basis of pyrene the selective functionalization of the 1, 3- positions 1, 3, 5, 9- positions, and 1, 3, 6, 8- positions were investigated by introducing donor / acceptor groups (Figure 25).

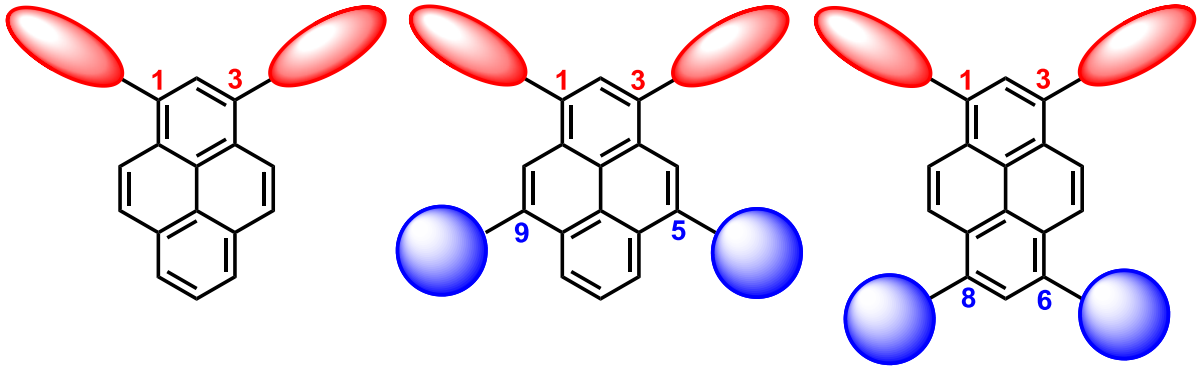


**Figure 25.** Schematic illustration of pyrene functionalization patterns investigated in this work.

From materials chemistry viewpoint two main topics are addressed in this work:

· The synthesis of strong donor / acceptor based on the pyrene scaffold by functional group modification.

· Preparation of pyrene derivatives with tunable emission properties and large two-proton absorption cross section.

The combination of chromophore design, synthesis and solid state characterization in this study allows the selection of the more promising emitter structure over the other.

## 1.5 References


1. Laurent, A. *Ann. Chim. Phys.* **1837**, *66*, 136.
2. Welham, R. D. *J. Soc. Dyers Color* **1963**, *79*, 98.
3. Siegrist, A. E.; Eckhardt, C.; Kaschig, J.; Schmidt, E. in Ullmann's Encyclopedia of Industrial Chemistry, Wiley-VCH Verlag GmbH & Co. KGaA, **2000**.
4. Tappe, H.; Helmling, W.; Mischke, P.; Rebsamen, K.; Reiher, U.; Russ, W.; Schläfer, L.; Vermehren, P.; in Ullmann's Encyclopedia of Industrial Chemistry, Wiley-VCH Verlag GmbH & Co. KGaA, **2000**.
5. Ismael, R.; Schwander, H.; Hendrix, P. In Ullmann's Encyclopedia of Industrial Chemistry, Wiley-VCH Verlag GmbH & Co. KGaA, **2000**.
6. Weitzenböock, R. *Mh. Chem.* **1913**, *34*, 193–223.
7. Casas-Solvas, J. M.; Howgego, J. D.; Davis, A. P. *Org. Biomol. Chem.* **2014**, *12*, 212–232.
8. Sato, T.; Akabori, S.; Muto, S.; Hata, K. *Tetrahedron* **1968**, *24*, 5557–5567.
9. (a) Yamato, T.; Matsumoto, J. I.; Tokuhisa, K.; Shigekuni, M.; Suehiro, K.; Tashiro, M. *J. Org. Chem.* **1992**, *57*, 395–396. (b) Yamato, T.; Ide, S.; Tokuhisa, K.; Tashirot, M. *J. Org. Chem.* **1992**, *57*, 271–275. (c) Koening, T.; Tuttle, M. *J. Org. Chem.* **1974**, *39*, 1308–1311.
10. (a) Nolan, E. M.; Lippard, S. J. *Chem. Rev.* **2008**, *108*, 3443–3480. (b) Kim, H. J.; Kim, S. K.; Lee, J. Y.; Kim, J. S. *J. Org. Chem.* **2006**, *71*, 6611–6614. (c) Li, D.; Song, J.; Yin, P. C.; Simotwo, S.; Bassler, A. J.; Aung, Y.-Y.; Roberts, J. E.; Hardcastle, K. I.; Hill, C. L.; Liu, T. *J. Am. Chem. Soc.* **2011**, *133*, 14010–14016.
11. (a) Reecht, G.; Scheurer, F.; Speisser, V.; Dappe, Y. J.; Mathevet, F.; Schull, G. *Phys. Rev. Lett.* **2014**, *112*, 047403. (b) Odoi, M. Y.; Hammer, N. I.; Rathnayake, H. P.; Lahti, P. M.; Barnes, M. D. *ChemPhysChem* **2007**, *8*, 1481–1486.
12. (a) Kim, B.; Park, Y.; Lee, J.; Yokoyama, D.; Lee, J. H.; Kido, J.; Park, J. *J. Mater. Chem. C* **2013**, *1*, 432–440. (b) Qi, H.; Chen, Y. H.; Cheng, C. H.; Bard, A. J. *J. Am. Chem. Soc.* **2013**, *135*, 9041–9049. (c) Hong, Y.; Lam, J. W. Y.; Tang, B. Z. *Chem. Soc. Rev.* **2011**, *40*, 5361–5388.

13. (a) Moulin, E.; Busseron, E.; Giuseppone, N. Published by the Royal Society of Chemistry, **2015**, 1–52. (b) Yu, C. C.; Jiang, K. J.; Huang, J. H.; Zhang, F.; Bao, X.; Wang, F. W.; Yang, L. M.; Song, Y. *Org. Electron.* **2013**, *14*, 445–450. (c) Zhang, M.; Parajuli, R. R.; Mastrogiovanni, D.; Dai, B.; Lo, P.; Cheung, W.; Brukh, R.; Chiu, P. L.; Zhou, T.; Liu, Z.; Garfunkel, E.; He, H. *Small* **2010**, *6*, 1100–1107.
14. Lambert, C.; Ehbets, J.; Rausch, D.; Steeger, M. *J. Org. Chem.* **2012**, *77*, 6147−6154.
15. (a) Dewar, M. J. J.; Dennington, R. D. *J. Am. Chem. Soc.* **1989**, *111*, 3804–3808. (b) Cerfontain, H.; Laali, K.; Lambrechts, H. J. *Rec. Trav. Chim. Pays-Bas.* **1983**, *102*, 210–214.
16. (a) Vollmann, H.; Becker, H.; Corell, M.; Streeck, H. *Liebigs Ann.* **1937**, *531*, 1–137. (b) Maeda, H.; Maeda, T.; Mizuno, K.; Fujimoto, K.; Shimizu, H.; Inouye, M. *Chem. Eur. J.* **2006**, *12*, 824–831.
17. Yang, C. H.; Guo, T. F.; Sun, I. W. *J. Luminesc.* **2007**, *124*, 93–98.
18. (a) Amann, N.; Pandurski, E.; Fiebig, T.; Wagenknecht, H. A. *Angew. Chem. Int. Ed.* **2002**, *41*, 2978–2980. (b) Amann, N.; Pandurski, E.; Fiebig, T.; Wagenknecht, H. A. *Chem. Eur. J.* **2002**, *8*, 4877–4883. (c) Suzuki, K.; Seno, A.; Tanabe, H.; Ueno, K. *Synth. Met.* **2004**, *143*, 89–96.
19. Wu, K. C.; Ku, P. J.; Lin, C. S.; Shih, H. T.; Wu, F. I.; Huang, M. J.; Lin, J. J.; Chen, I. C.; Cheng, C. H. *Adv. Funct. Mater.* **2008**, *18*, 67–75.
20. Bolm, C.; Legros, J.; Paih, J. L.; Zani, L. *Chem. Rev.* **2004**, *104*, 6217–6254.
21. (a) Chen, J. J.; Wang, I. J. *Dyes Pigm.* **1995**, *29*, 305–313. (b) Malashikhin, S.; Finney, N. S. *J. Am. Chem. Soc.* **2008**, *130*, 12846–12847.
22. Liu, F.; Tang, C.; Chen, Q. Q.; Li, S. Z.; Wu, H. B.; Xie, L. H.; Peng, B.; Wei, W.; Cao, Y.; Huang, W. *Org. Electron.* **2009**, *10*, 256–265.
23. Suzuki, H.; Kondo, A.; Inouye, M.; Ogawa, T. *Synthesis* **1986**, 121–122.
24. Radner, F. *Acta Chem. Scand.* **1989**, *43*, 481–484.
25. (a) Wang, Q.; Liu, H.; Lu, H.; Xu, Z.; Lai, G.; Li, Z.; Mack, J.; Shen, Z. *Dyes Pigments* **2013**, *99*, 771–778. (b) Liu, F.; Lai, W.-Y.; Tang, C.; Wu, H.-B.; Chen, Q.-Q.; Peng, B.; Wei, W.; Huang, W.; Cao, Y. *Macromol. Rapid Commun.* **2008**, *29*, 659–664. (c) Venkataramana, G.; Sankararaman, S. *Eur. J. Org. Chem.* **2005**, 4162–4166. (d) Bajpai, A.; Natarajan, P.; Venugopalan, P.; Moorthy, J. N. *J. Org. Chem.* **2012**, *77*, 7858–7865.

(e) Bernhardt, S.; Kastler, M.; Enkelmann, V.; Baumgarten, M.; Müllen, K. *Chem. Eur. J.* **2006**, *12*, 6117–6128. (f) Gingras, M.; Placide, V.; Raimundo, J.-M.; Bergamini, G.; Ceroni, P.; Balzani, V. *Chem. Eur. J.* **2008**, *14*, 10357–10363. (g) Moorthy, J. N.; Natarajan, P.; Venkatakrishnan, P.; Huang, D.-F.; Chow, T. *J. Org. Lett.* **2007**, *9*, 5215–5218. (h) Sonar, P.; Soh, M. S.; Cheng, Y. H.; Henssler, J. T.; Sellinger, A. *Org. Lett.* **2010**, *12*, 3292–3295. (i) Anthony, S. P. *ChemPlusChem.* **2012**, *77*, 518–531.

26. Zhang, H.-J.; Wang, Y.; Shao, K. Z.; Liu, Y. Q.; Chen, S. Y.; Qiu, W. F.; Sun, X. B.; Qi, T.; Ma, Y. Q.; Yu, G.; Su, Z. M.; Zhu, D. B. *Chem. Commun.* **2006**, 755–757.
27. Zhao, Z.; Chen, S.; Lam, J. W. Y.; Lu, P.; Zhong, Y.; Wong, K. S.; Kwok, H. S.; Tang, B. Z. *Chem. Commun.* **2010**, *46*, 2221–2223.
28. Lee, Y. O.; Pradhana, T.; Nob, K.; Kim, J. S. *Tetrahedron* **2012**, *68*, 1704–1711.
29. (a) Crawford, A. G.; Liu, Z.-Q.; Mkhalid, I. A. I.; Thibault, M-H.; Schwarz, N.; Alcaraz, G.; Steffen, A.; Collings, J. C.; Batsanov, A. S.; Howard, J. A. K.; Marder, T. B. *Chem. Eur. J.* **2012**, *18*, 5022–5035. (b) Qiao, Y.; Zhang, J.; Xua, W.; Zhu, D. *Tetrahedron* **2011**, *67*, 3395–3405. (c) Oniwa, K.; Kikuchi, H.; Shimotani, H.; Ikeda, S.; Asao, N.; Yamamoto, Y.; Tanigaki, K.; Jin, T. *Chem. Commun.* **2016**, *52*, 4800–4803. (d) Yagi, A.; Venkataramana, G.; Segawa, Y.; Itami, K. *Chem. Commun.* **2014**, *50*, 957–959. (e) Kurata, R.; Tanaka, K.; Ito, A. *J. Org. Chem.* **2016**, *81*, 137–145. (f) Ji, L.; Edkins, R. M.; Lorbach, A.; Krummenacher, I.; Brückner, C.; Eichhorn, A.; Braunschweig, H.; Engels, B.; Low, P. J.; Marder, T. B. *J. Am. Chem. Soc.* **2015**, *137*, 6750–6753. (g) Ronson, T. K.; League, A. B.; Gagliardi, L.; Cramer, C. J.; Nitschke, J. R. *J. Am. Chem. Soc.* **2014**, *136*, 15615–15624.
30. Liu, Z.; Wang, Y.; Chen, Y.; Liu, J.; Fang, Q.; Kleeberg, C.; Marder, T. B. *J. Org. Chem.* **2012**, *77*, 7124–7128.
31. Coventry, D. N.; Batsanov, A. S.; Goeta, A. E.; Howard, J. A. K.; Marder, T. B.; Perutz, R. N. *Chem. Commun.* **2005**, 2172–2174.
32. Hu, J.-Y.; Era, M.; Elsegood, M. R. J.; Yamao, T. *Eur. J. Org. Chem.* **2010**, 72–79.
33. Tan, R.; Song, D. *Tetrahedron Lett.* **2012**, *53*, 980–982.
34. Zöphel, L.; Enkelmann, V.; Rieger, R.; Müllen, K. *Org. Lett.* **2011**, *13*, 4506–4509.
35. Oberender, F. G.; Dixon, J. A. *J. Org. Chem.* **1959**, *24*, 1226–1229.

36. (a) Stille, J. K.; Mainen, E. L. *Macromolecules* **1968**, *1*, 36–42. (b) Young, E. R. R.; Funk, R. L. *J. Org. Chem.* **1998**, *63*, 9995–. (c) CHO, H.; Harvey, R. G. *Tetrahedron Lett.* **1974**, 1491–1494.
37. Hu, J.; Zhang, D.; Harris, F. W. *J. Org. Chem.* **2005**, *70*, 707–708.
38. Mateo-Alonso, A.; Kulisic, N.; Valenti, G.; Marcaccio, M.; Paolucci, F.; Prato, M. *Chem. Asian J.* **2010**, *5*, 482–485.
39. Laurent, A. *Ann. Chim. Phys.* **1837**, *66*, 136.
40. http://www. nobelprize. org/nobel_prizes/physics/laureates/2014/press. pdf
41. Miyata, S., Nalwa, H.S., Eds. Organic Electroluminescent Materials and Devices, Gordon and Breach: Amsterdam, **1997**.
42. Tang, C. W.; Van Slyke, S. A. *Appl. Phys. Lett.* **1987**, *51*, 913–915.
43. Burroughes, J. H.; Bradley, D. D. C.; Brown, A. R.; Marks, R. N.; Mackey, K.; Friend, R. H.; Burns, P. L.; Holmes, A. B. *Nature* **1990**, *347*, 539–541.
44. Baldo, M. A.; Thompson, M. E.; Forrest, S. R. *Nature* **2000**, *403*, 750–753.
45. Uoyama, H.; Goushi, K.; Shizu, K.; Nomura, H.; Adachi, C. *Nature* **2012**, *492*, 234–238.
46. Rothberg, L. J., Lovinger, A. J. *J. Mater. Res.* **1996**, *11*, 3174–3187.
47. (a) Veinot, J. G. C., Marks, T. J. *Acc. Chem. Res.* **2005**, *38*, 632-643. (b) Klauk, H., Gundlach, D. J., Nichols, J. A., Jackson, T. N. *IEEE T ELECTRON DEV.* **1999**, *46*, 1258–1263.
48. Brütting, W., Frischeisen, J., Schmidt, T. D., Scholz, B. J., Mayr, C. *Phys. Status Solidi A*, **2013**, *1*, 44–65.
49. (a) VanSlyke, S. A., Chen, C. H., Tang, C. W. *Appl. Phys. Lett.* **1996**, *69*, 2160–2162. (b) Shirota, Y., Kuwabara, Y., Inada, H., Wakimoto, T., Nakada, H., Yonemoto, Y., Kawami, S., Imai, K. *Appl. Phys. Lett.* **1994**, *65*, 807–809. (c) Deng, Z., Ding, X., Lee, S., Gambling, W. *Appl. Phys. Lett.* **1999**, *74*, 2227–2230.
50. Adamovich, V. I., Cordero, S. R., Djurovich, P. I., Tamayo, A., Thompson, M. E., D'Andrade, B. W., Forrest, S. R. *Org. Electron.* **2003**, *4*, 77–87.
51. (a) Hung, L. S., Tang, C. W., Mason, M. G. *Appl. Phys. Lett.* **1997**, *70*, 151–153. (b) Kido, J., Lizumi, Y. *Appl. Phys. Lett.* **1998**, *73*, 2721–2723.

52. (a) Fang, J.; D. Ma, *Appl. Phys. Lett.* **2003**, *83*, 4041–4043. (b) Fang, J.; You, H.; Gao, J.; Ma, D. *Chem. Phys. Lett.* **2004**, *392*, 11–16. (c) Hong, Z. R.; Lee, C. S.; Lee, S. T.; Li, W. L.; Liu, S. Y. *Appl. Phys. Lett.* **2003**, *82*, 2218–2220.

53. (a) Lee, D. H.; Liu, Y.-P.; Lee, K.-H.; Chae, H.; Cho, S. M. *Org. Electron.* **2010**, *11*, 427–433. (b) Goushi, K.; Kwong, R.; Brown, J. J.; Sasabe, H.; Adachi, C. *J. Appl. Phys.* **2004**, *95*, 7798–7802.

54. Shirota, Y. Kageyama, H. *Chem. Rev.* **2007**, *107*, 953–1010.

55. (a) Su, S.-J.; Gonmori, E.; Sasabe, H.; Kido, J. *Adv. Mater.* **2008**, *20*, 4189–4194. (b) Kim, S. H.; Jang, J.; Yook, K. S.; Lee, J. Y.; Gong, M.-S.; Ryu, S.; Chang, G.-k. Chang, H. J. *J. Appl. Phys.* **2008**, *103*, 054502. (c) Kim, S. H.; Jang, J.; Lee, J. Y. *Appl. Phys. Lett.* **2007**, *91*, 083511.

56. Lee, J.; Lee, J.-I.; Lee, J.-W.; Chu, H. Y. *Org. Electron.* **2010**, *11*, 1159–1164.

57. Lee, J.; Chopra, N.; Eom, S.-H.; Zheng, Y.; Xue, J.; So, F.; Shi, J. *Appl. Phys. Lett.* **2008**, *93*, 123306.

58. (a) Su, S.-J.; Takahashi, Y.; Chiba, T.; Takeda, T.; Kido, J. *Adv. Funct. Mater.* **2009**, *19*, 1260–. (b) Su, S.-J.; Chiba, T.; Takeda, T.; Kido, J. *Adv. Mater.* **2008**, *20*, 2125–2130.

59. (a) Kondakova, M. E.; Pawlik, T. D.; Young, R. H.; Giesen, D. J.; Kondakov, D. Y.; Brown, C. T.; Deaton, J. C.; Lenhard, J. R.; Klubek, *J. Appl. Phys.* **2008**, *104*, 094501. (b) Kim, S. H.; Jang, J.; Lee, J. Y. *Appl. Phys. Lett.* **2007**, *91*, 083511. (c) Xie, W.; Zhao, Y.; Li, C.; Liu, S. *Solid-State Electron.* **2007**, *51*, 1129–1132.

60. Lai, M.-Y.; Chen, C.-H.; Huang, W.-S.; Lin, J. T.; Ke, T.-H.; Chen, L.-Y.; Tsai, M.-H.; Wu, C.-C. *Angew. Chem., Int. Ed.* **2008**, *47*, 581–585.

61. (a) Ge, Z.; Hayakawa, T.; Ando, S.; Ueda, M.; Akiike, T.; Miyamoto, H.; Kajita, T.; Kakimoto, M.-A. *Adv. Funct. Mater.* **2008**, *18*, 584–590. (b) Ge, Z.; Hayakawa, T.; Ando, S.; Ueda, M.; Akiike, T.; Miyamoto, H.; Kajita, T.; Kakimoto, M.-A. *Chem. Mater.* **2008**, *20*, 2532–2537.

62. (a) Ge, Z.; Hayakawa, T.; Ando, S.; Ueda, M.; Akiike, T.; Miyamoto, H.; Kajita, T.; Kakimoto, M.-A. *Org. Lett.* **2008**, *10*, 421–424. (b) Tao, Y.; Wang, Q.; Yang, C.; Zhong, C.; Zhang, K.; Qin, J.; Ma, D. *Adv. Funct. Mater.* **2010**, *20*, 304–311. (c) Tao, Y.; Wang, Q.; Shang, Y.; Yang, C.; Ao, L.; Qin, J.; Ma, D.; Shuai, Z. *Chem. Commun.* **2009**, 77–79. (d) Tao, Y.; Wang, Q.; Ao, L.; Zhong, C.; Yang, C.; Qin, J.; Ma, D. *J. Phys. Chem. C* **2010**,

*114*, 601–609. (e) Tao, Y.; Ao, L. Wang, Q.; Zhong, C.; Yang, C.; Qin, J.; Ma, D. *Chem. Asian J.* **2010**, *5*, 278–284.

63. (a) Chien, C.-H.; Kung, L.-R.; Wu, C.-H.; Shu, C.-F.; Chang, S.-Y.; Chi, Y. *J. Mater. Chem.* **2008**, *18*, 3461–3466. (b) Hsu, F.-M.; Chien, C.-H.; Shih, P.-I.; Cheng, C.-H. *Chem. Mater.* **2009**, *21*, 1017–1022. (c) Hsu, F.-M.; Chien, C.-H.; Hsieh, Y.-J.; Wu, C.-H.; Shu, C.-F.; Liu, S.-W.; Chen, C.-T. *J. Mater. Chem.* **2009**, *19*, 8002–8008.
64. (a) Zeng, L.; Lee, T. Y.-H.; Merkel, P. B.; Chen, S. H. *J. Mater. Chem.* **2009**, *19*, 8772–8781. (b) Guan, M.; Chen, Z.; Bian, Z.; Liu, Z.; Gong, Z.; Baik, W.; Lee, H.; Huang, C. *Org. Electron.* **2006**, *7*, 330–336.
65. (a) Figueira-Duarte, T. M.; Müllen, K. *Chem. Rev.* **2011**, *111*, 7260–7314. (b) Feng, X.; Hu, J. Y.; Redshaw, C.; Yamato, T. *Chem. -Eur. J.* **2016**, *22*, 11898–11916.
66. Safin, D. A.; Babashkina, M. G.; Mitoraj, M. P.; Kubisiak, P.; Robeyns, K.; Bolte, M.; Garcia, Y. *Inorg. Chem. Front.* **2016**, *3*, 1419–1431.
67. (a) Förster, T. *Angew. Chem., Int. Ed.* **1969**, *8*, 333–343. (b) Ueno, A.; Suzuki, I.; Osa, T. *J. Am. Chem. Soc.* **1989**, *111*, 6391−6397. (c) Zhao, B.; Li, N.; Wang, X.; Chang, Z.; Bu, X. H. *ACS Appl. Mater. Interfaces* **2017**, *9*, 2662−2668. (d) Wang, C. Z.; Ichiyanagi, H.; Sakaguchi, K.; Feng, X.; Elsegood, M. R. J.; Redshaw, C.; Yamato, T. *J. Org. Chem.* **2017**, *82*, 7176−7182.
68. Ju, H. J.; Wang, K.; Zhang, J.; Geng, H.; Liu, Z. T.; Zhang, G. X.; Zhao, Y. S.; Zhang, D. Q. *Chem. Mater.* **2017**, *29*, 3580−3588.
69 Birks, J. B. *Photophysics of Aromatic Molecules*, Wiley-Interscience, New York, 1970.
70 Birks, J. B.; Lumb, M. D.; Munro, I. H. *Proc. R. Soc. London Series A,* 1964, *280*, 289–297.
71 (a) Winnik, F. M. *Chem. Rev*., **1993**, *93*, 587–614. (b) Kim, S. K.; Lee, S. H.; Lee, J. Y.; Lee, J. Y.; Bartsch, R. A.; Kim, J. S. *J. Am. Chem. Soc*., **2004**, *126*, 16499–16506. (c) Lee, J. Y.; Kim, S. K.; Jung, J. H.; Kim, J. S. *J. Org. Chem*., **2005**, *70*, 1463–1466.
72 (a) Wang, Y. C.; Morawetz, H. *J. Am. Chem. Soc*., **1976**, *98*, 3611–3615. (b) Goldenberg, M.; Emert, J.; Morawetz, H. *J. Am. Chem. Soc*., **1978**, *100*, 7171–7177; (c) Winnik, M. A. *Chem. Rev*., **1981**, *81*, 491–524.

73 Nohta, H.; Satozono, H.; Koiso, K.; Yoshida, H.; Ishida, J.; Yamaguchi, M. *Anal. Chem*. **2000**, *72*, 4199–4204. (b) Okamoto, A.; Ichiba, T.; Saito, I. *J. Am. Chem. Soc*., **2004**, *126*, 8364–8365.

74 Safin, D. A.; Babashkina, M. G.; Mitoraj, M. P.; Kubisiak, P.; Robeyns, K.; Boltec, M.; Garcia, Y. *Inorg. Chem. Front.* **2016**, *3*, 1419-1431.

75 (a) Daum, R.; Druzhinin, S.; Ernst, D.; Rupp, L.; Schroeder, J.; Zachariasse, K. A. *Chem. Phys. Lett.* **2001**, *341*, 272−278. (b) Zachariasse, K. A.; Grobys, M.; Tauer, E. *Chem. Phys. Lett.* **1997**, *274*, 372−382.

76 Georgieva, I. Aquino, A. J. A.;́ Plasser, F.; Trendafilova, N. Köhn, A.; Lischka, H. *J. Phys. Chem. A* **2015**, *119*, 6232−6243.

77 Niko, Y.; Sasaki, S.; Narushima, K.; Sharma, D. K.; Vacha, M.; Konishi, G.-i. *J. Org. Chem.* **2015**, *80*, 10794−10805.

# Chapter 2

# Acceptor substituted π-Conjugated Pyrene Derivatives: Structural, Photophysical and Electrochemical Properties

*A set of extended π-conjugated pyrene derivatives, namely 1,3-di(arylethynyl)-7-tert-butylpyrenes were synthesized by a Pd-catalyzed Sonogashira coupling reaction of 1,3-dibromo-7-tert-butylpyrenes with the corresponding arylethynyl group in good yields. Despite the presence of the tert-butyl group located at the 7-position of pyrene, X-ray crystallographic analyses show that the planarity of the Y-shaped molecules still exhibits strong face-to-face π-π stacking in the solid state; all of the compounds exhibit blue or green emission with high quantum yields (QYs) in dichloromethane. DFT calculations and electrochemistry revealed that this category of compound possesses hole-transporting characteristics. In addition, with strong electron-donating (-N(CH$_3$)$_2$) or electron-withdrawing (-CHO) groups in **2d** or **2f**, these molecules displayed efficient intramolecular charge-transfer (ICT) emissions with solvatochromic shifts from blue to yellow (green) on increasing the solvent polarity. Furthermore, the compounds **2d** and **2f** possess strong CT characteristics.*

## 2.1 Introduction

Large p-conjugated organic materials have attracted increasing attention in recent years, due to facile band-gap and colour control by structural modification, which makes them suitable for potential application in high performance organic electronics,[1] such as organic light emitting diodes (OLEDs),[2] liquid-crystal displays,[3] organic field effect transistors (OFETs)[4, 5] and organic photovoltaic cells (OPVs),[6] as well as optical storage devices.[7] Extension of the p-conjugation chromophores contributes to a lowering of the HOMO-LUMO gap, leading to a red-shift in absorption and emission spectra with increasing fluorescence quantum yields. In addition, molecules which possess p-conjugation with a planar structure would enhance charge carrier transport in optoelectronic applications by selfassembly via intermolecular p-p stacking.[8]

Pyrene[9] is made up of four fused aromatic rings with a large p-electron system, which exhibits good solution-processable properties with an excellent blue emission spectrum (with a long excited-state lifetime, high fluorescence intensity and quantum yield). However, the development of pyrene as a host material in blue light-emitting diodes is scarce, due to its tendency to readily aggregate in most media. Several research groups including ours have reported many new types of pyrene derivatives, and various substituent groups have been attached to the pyrene core by -C-C-, -C-N- or -C≡C- bonds for suppressing excitation emission.[10-15] Some ethynyl-substituted pyrene-based compounds displayed more intriguing fluorescence characteristics, for instance, Ziessel *et al.* reported a greenish luminescent 1,3,6,8-tetra-(4-ethynylphenylaminoacyl))pyrene with stable liquid crystalline properties for the fabrication of OLED-like devices;[16] Kim and coworkers synthesized a series of 1,3,6,8-tetrakis(ethynyl)pyrenes functionalized with varying numbers of *N*,*N*-dimethyaniline and 1-(trifluoromethyl)benzene moieties as peripheral electron-donors and acceptors for chemiluminescent (ECL) active materials, that exhibited enhanced charge transfer compared with 1,3,6,8-tetra-N,N-dimethylaniline (or 1,3,6,8-tetra-trifluoromethylbenzene).[17, 18] Interestingly, Adachi et al have designed a number of inverted singlet-triplet (iST) pyrene-based derivatives,

and the electronic structures, spin-orbit couplings, transition dipole moments, and vibronic couplings have been investigated by theoretical calculations.[19]

Generally, an acetylene group is one option among other (such as ethylene) choices to extend the $\pi$-conjugation of molecular skeletons, and the advantage over an ethylene linker is better stability, in addition, it's very convenient to prepare this kind of compounds by Pd-catalyzed coupling reaction. Previously, in our laboratory, we synthesized cruciform-shaped and hand-shaped architectures incorporating $\pi$-conjugated alkynylpyrenes as highly efficient blue emissive materials by the Sonogashira cross-coupling reaction.[20, 21] The optical properties of both types of pyrene-based material exhibited pure blue fluorescence with good quantum yield, as well as similar crystal packing in the solid-state. Our recent report on the synthesis of 1,3-dibromo-7-*tert*-butylpyrene (**1**)[22] prompted us to further explore 1,3-bis(arylphenyl)pyrenes as blue emissive materials. The arylphenyl groups located at the 1,3-positions were twisted by a considerable angle relative to the pyrene core, a feature that can play a crucial role in hindering intermolecular interactions in the solid-state. In this article, a series of Y-shaped, extended p-conjugated pyrene derivatives have been synthesized by a Pd-catalyzed Sonogashira cross-coupling reaction using 1,3-dibromo-7-tert-butylpyrene and corresponding arylethynyl groups in reasonable yield. We anticipated that the extended p-conjugated pyrene derivatives would exhibit interesting topological structures, leading to attractive photophysical properties, as well being air-stable. Indeed, the designed p-conjugated molecules showed interesting CT characteristics in polar solvents as expected. Furthermore, we investigated the effect of the various substituents and substitution positions of the (arylethynyl)pyrenes for optical properties and crystal packing.

## 2.2 Results and Discussion

### 2.2.1 Synthesis and characterization

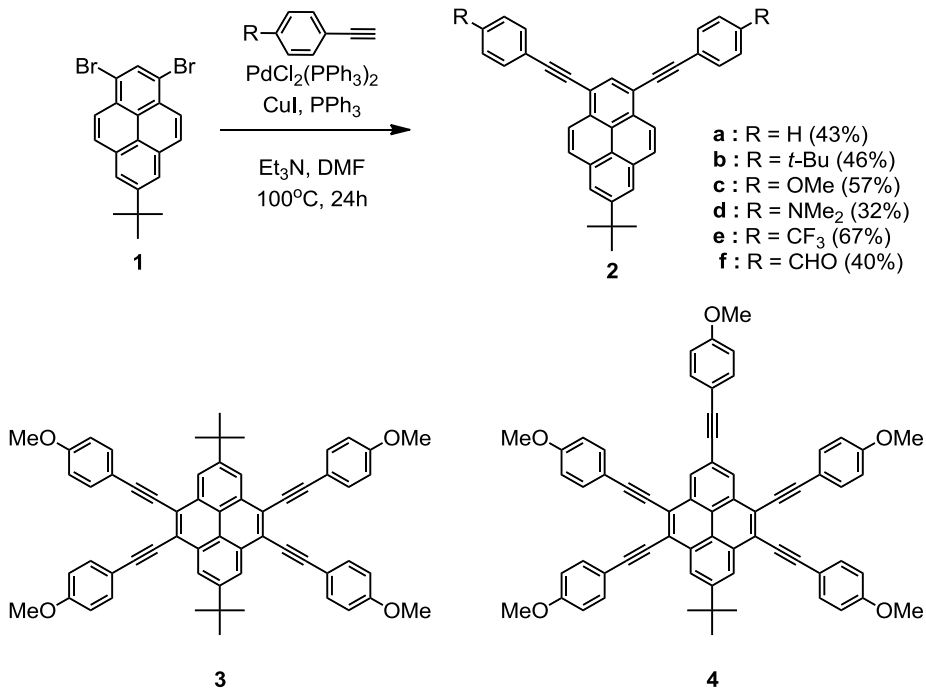


**Scheme 1**. Synthesis of pyrene-based light-emitting monomers **2**, and the cruciform-shaped and hand-shaped pyrenes **3** and **4** for comparion.

The synthesis of the Y-shaped arylethynyl-substituted pyrenes **2** are shown in Scheme 1. The target arylethynyl pyrenes **2** were obtained in 32–67 % yield through a Sonogashira coupling reaction between 1 and the corresponding arylacetylenes. All of the new pyrene derivatives **2** have been characterized by $^{1}H/^{13}C$ NMR spectroscopy, HR-MS and elemental analysis. Y-shaped compounds **2** with arylethynyl groups display good air-stability and solubility properties in common solvents, such as dichloromethane ($CH_2Cl_2$), *N*,*N*-dimethylformamide (DMF), tetrahydrofuran (THF) and methanol ($CH_3OH$). Moreover, the structures of **2c** (two polymorphs), **2d** and **2f** were further confirmed by single crystal X-ray diffraction. Very recently, compounds **2a** and **2b** have been prepared by Cooper et al as key intermediation.[23] Herein, the effect of the substituents on the crystal packing, photophysical properties and electrochemistry has been further investigated in detail; for comparison, two position-dependent

arylethynyl-functionalized pyrenes **3** and **4** are illustrated in Scheme 1. This work allows us to fully understand the effect of the various substituents and the relationship between molecular structure and optical properties.

## 2.2.2 Crystallography

Single crystals of the extended p-conjugated Y-shaped pyrene derivatives **2c** were obtained from MeOH/$CHCl_3$ or hexane/$CH_2Cl_2$, **2d·CHCl₃** from $CHCl_3$ and **2f** from $CH_2Cl_2$/benzene by slow evaporation at room temperature. All of the compounds crystallize in the triclinic crystal system with space group *P*1. Compound **2c** was obtained as two different polymorphs. A number of reports showed that pyrene derivatives with terminal methoxyphenyl moieties trends more easily to form good quality single crystals for X-ray crystallography. So this experience allows us to design pyrenes for insight into investigating the relationship between position-dependent, molecular conformation and the optical properties by using X-ray diffraction equipment. The molecular structures are shown in Figure 1 and the crystallographic data is listed in Table 1.

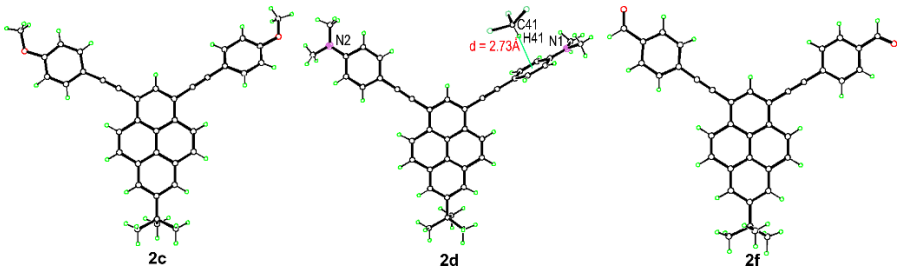


**Figure 1.** The molecular structures of **2c**, **2d**, and **2f**.

**Table 1.** Summary of crystal data for the π-conjugated molecules **2cI, 2cII, 2d·CHCl₃** and **2f.**

| Complex | 2cI | 2cII | 2d | 2f |
|---|---|---|---|---|
| Empirical formula | $C_{38}H_{30}O_2$ | $C_{38}H_{30}O_2$ | $C_{40}H_{36}N_2{\cdot}CHCl_3$ | $C_{38}H_{26}O_2$ |
| Formula weight | 518.62 | 518.62 | 664.07 | 514.59 |
| Crystal system | Triclinic | Triclinic | Triclinic | Triclinic |
| Space group | $P\bar{1}$ | $P\bar{1}$ | $P\bar{1}$ | $P\bar{1}$ |
| *a*[Å] | 8.926(2) | 8.902(2) | 10.8101(12) | 8.9354(5) |
| *b*[Å] | 12.408(3) | 12.088(3) | 11.1244(12) | 11.8785(9) |
| *c*[Å] | 13.559(3) | 27.070(8) | 14.3383(16) | 13.0754(6) |

| | | | | |
|---|---|---|---|---|
| α[°] | 99.758(9) | 101.774(18) | 91.4712(18) | 97.029(5) |
| β[°] | 100.102(9) | 93.904(19) | 91.6750(18) | 102.787(4) |
| γ[°] | 98.809(8) | 100.502(18) | 101.8031(17) | 100.349(5) |
| Volume[Å$^3$] | 1430.9(6) | 2787.1(13) | 1686.2(3) | 1312.22(14) |
| *Z* | 2 | 4 | 2 | 2 |
| λ | 0.71073 | 1.54184 | 0.71073 | 1.54184 |
| Dcalcd[Mg/m$^3$] | 1.204 | 1.236 | 1.308 | 1.302 |
| temperature [K] | 293(2) | 296(2) | 150(2) | 100(2) |
| measured reflns | 12587 | 36576 | 19720 | 7853 |
| unique reflns | 4927 | 9802 | 9976 | 5075 |
| obsd reflns | 2470 | 4722 | 7491 | 3892 |
| Parameters | 362 | 731 | 552 | 462 |
| *R*(int) | 0.0337 | 0.0548 | 0.0184 | 0.0219 |
| $R[I > 2\sigma(I)]$[a] | 0.0774 | 0.0887 | 0.0457 | 0.0545 |
| *wR2*[all data][b] | 0.2342 | 0.2725 | 0.1344 | 0.1687 |
| GOF on $F^2$ | 1.007 | 1.010 | 1.059 | 1.052 |

As shown in Figure 2, the structure of 2cI displays face-to-face π-stacking at a distance of 3.54 **Å**, which involves 14 carbons in each pyrene molecule.[24] One ethynylphenyl substituent is coplanar with the pyrene core, whilst another forms a twist angle of 28.48. A number of π···π stacking interactions between the phenyl rings and the neighbouring pyrene core were observed (3.32 **Å**). In addition, another weak but important interaction involves the methoxyl group, which has a contact with the next layer of the ethynyl fragment of pyrene via a C-H···p interaction (2.42 **Å**).

Similarly, the polymorphs of **2cII** was crystallized from hexane/$CH_2Cl_2$ solution, The X-ray structure determinations revealed that the **2cII** belongs to the same space group as **2cI**. The crystal packing analysis shows that polymorph **2cII** was arranged similar as **2cI**. There is a fine distinction between both crystals namely the asymmetric unit cell of **2cII** contained two molecules, whereas the crystals of **2cI** were found to contain one molecule in the asymmetric unit. Figure 3 reveals that the asymmetric unit contains a molecule of **2d** and a chloroform linked by a C-H···π interaction at a distance of 2.41(2) **Å**. Unlike the situation above for **2cI**, where the p-methoxylphenylethynyl

moieties and the pyrene ring are almost coplanar, here for **2d**, the torsional angle between the pyrene unit and one of the the 4-(*N*,*N*-dimethylamino)-phenylethynyl fragments is close to perpendicular with a twist angle of 87.87(3)°. Moreover, two neighbouring pyrene moieties are presented with displaced face-to-face patterns forming a starshaped architecture in the solid-state; the $\pi\cdots\pi$ stacking interactions are approximately 3.37 **Å** (Figure 3a). In addition, the terminal phenyl groups of neighbouring molecules were connected by $\pi\cdots\pi$ stacking interactions with a distace of 2.89 **Å** (Figure 3b). From the packing pattern, a two-dimensional supramolecular network was constructed by these complicated $\pi\cdots\pi$ stacking interactions, and the $CHCl_3$ molecules were captured in the molecular voids[25] by C-H$\cdots\pi$ interactions.

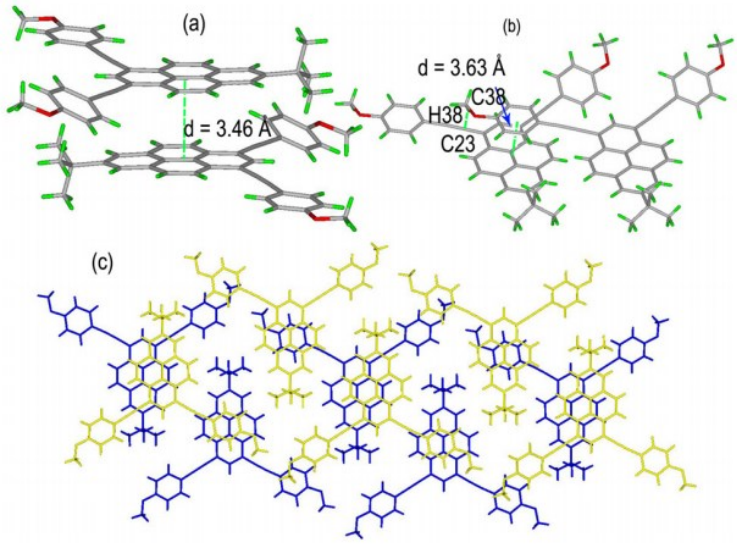


**Figure 2.** X-ray crystal structure representations of **2cI**, illustrating (a) and (b) the co-facial p-stacking structures and (c) the principal intermolecular packing interactions.

The asymmetric unit of **2f** contains one molecular with no solvent of crystallisation. As shown in Figure 4, **2f** displays a slightly curved core structure (torsional angle < 5°) with shallow twist angles of 17.57(9) and 3.03(8)° between the pyrene core and the terminal phenyl groups. Obviously, the planar molecular structure would tend to form strong co-facial $\pi\cdots\pi$ stacking, and the pairs of pyrene units arrange in head-to-tail stacking via a centre of symmetry by p$\cdots$p interactions (3.48 **Å**). In addition, the pyrene units and the adjacent phenyl rings display face-to-face $\pi\cdots\pi$ stacking at a distance of

3.32 **Å**. Interestingly, from the packing structure of **2f**, there are two key $\pi\cdots\pi$ interactions leading to a three dimensional infinite supramolecular array.

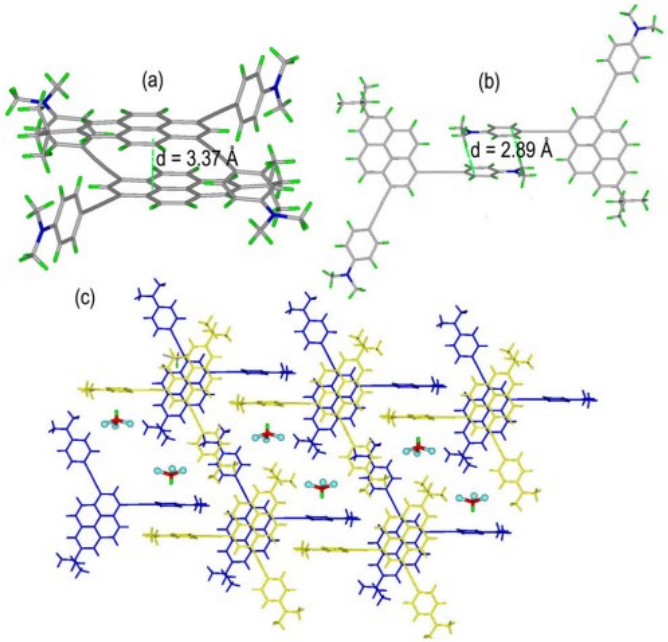


**Figure 3.** X-ray crystal structure representations of **2d·CHCl$_3$**, illustrating (a) and (b) the co-facial $\pi$-stacking structures and (c) $CHCl_3$ molecules were captured in voids supported by C-H$\cdots\pi$ interactions.

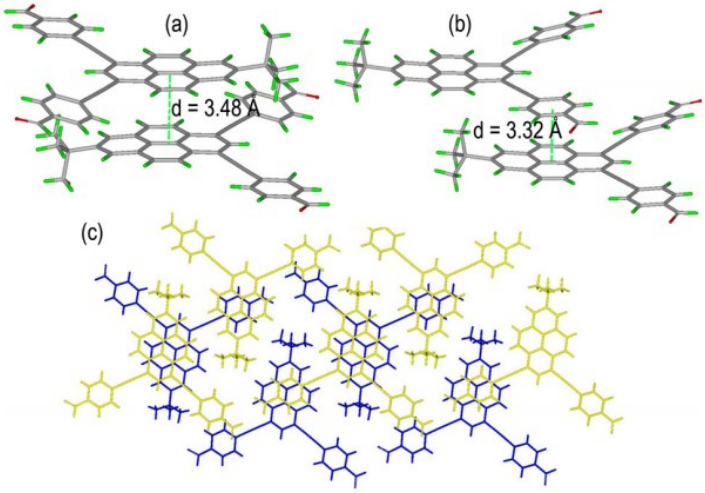


**Figure 4.** X-ray crystal structure representations of **2f**, illustrating (a) and (b) the detail of the cofacial $\pi$-stacking structures and (c) the principal intermolecular packing interactions.

Furthermore, in the packing structure of **3**, the four phenyl rings are not coplanar with the central pyrene; the two unique dihedral angles are 18.3 and 23.6°. As shown in Figure 5, two neighbouring pyrene moieties possess a centroid-to-centroid distance of 5.99 **Å**. No significant $\pi$-stacking interactions between the pyrene rings were observed and molecules adopt a herringbone packing motif. Non-covalent interactions play an important role in the stacking of the structures.

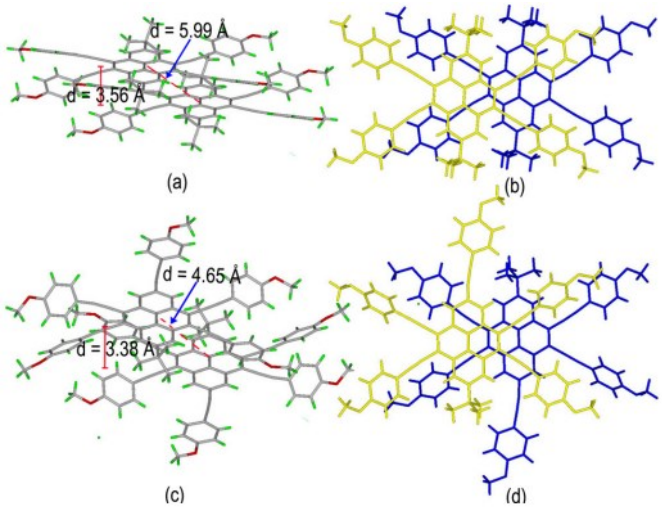


**Figure 5.** The packing structure (a) side view and (b) top view for **3** and (c) side view and (d) top view for **4**.

However, in compound **4**, when a $\pi$-methoxyphenyl moiety is located at the 7-position of pyrene, it is almost coplanar with the pyrene ring. The other four phenyl rings at the 4,5,9,10-positions of the pyrene form dihedral angles of between 6.1 and 47.3°, and two neighbouring pyrene moieties adopt a slipped face-to-face motif with off-set head-to-tail stacking with a centroid-to-centroid distance of 4.65 **Å**. Each molecule of **4** displays 24-point $\pi$-$\pi$ stacking with molecules above and below using both the pyrenyl and ethynyl carbon with intermolecular distances of 3.42–3.58 **Å**.

As mentioned above, the crystal packing is markedly different for the pyrenes **2**, **3**, and **4**. With the substituted group number increasing, the crystal packing has been transformed from face-to-face $\pi\cdots\pi$ stacking with off-set head-to-tail stacking to a herringbone arrangement on going from **2**, **3** to **4**. On the other hand, bulkier tert-butyl groups located at the 7-position of pyrene can play a more crucial role in hindering the

$\pi\cdots\pi$ stacking versus the arylethynyl-substituted group. In compound **4**, due to the nodal planes passing through the 7-position of the pyrene, the phenyl moiety attached at this position would be of limited impact for the crystal arrangement, as well as the electronic interactions.[26] The planar molecular structure of the pyrene derivatives **2**, **3** and **4** is beneficial for extending $\pi$-conjugation and improving the optical density, which can lead to special photophysical properties both in solution and in the solid state.

### 2.2.3 Photophysical Properties

The absorption spectra of the title compounds **2** in dilute dichloromethane are presented in Figure 6 and the optical data is summarized in Table 2. The maximum absorption wavelength of the ethynylpyrenes **2** is exhibited at least ca. 68 nm red-shifted compared with 2-*tert*-butylpyrene (338 nm).[15] Notably, the photophysical properties are highly dependent on the substituent units present. Y-shaped **2a**–**c** and **2e** show similar absorption behaviour and exhibit two prominent absorption bands in the regions 300–350 nm and 375–425 nm, respectively. For **2d** and **2f**, the maximum absorption wavelength has obviously red-shifted (~ 19 nm) relative to **2a**, arising from the intramolecular charge transfer (ICT) increase. Indeed, both **2d** and **2f** feature a broader and intense absorption in the long wavelength region 475–525 nm, indicating that the molecules tend to be more coplanar between the pyrene core and terminal ethynylphenyl groups by extending the p-conjugation, which is consistent with the crystallographic results. With an increased length of $\pi$-conjugation, the molar absorption coefficients (ε) of **2d** and **2f** are lower than the others observed.

**Table 2**. The photophysical and electrochemical properties of compounds **2**.

| R | $\lambda_{max\ abs}$[a] nm | $\lambda_{max\ PL}$[a] (nm) | Log ε | $\Phi_f$[a] | LUMO (eV) | HOMO (eV) | Energy gap (eV) | I ns | $T_m$[f] | $T_d$[g] |
|---|---|---|---|---|---|---|---|---|---|---|
| **2a** | 406 | 421 (325) | 4.87 | 0.93 | –2.01[b] (–2.41)[c] | –5.01[b] (–5.34)[d] | 2.99[b] (2.93)[e] | 2.89a | 198 | 479 |
| **2b** | 409 | 423 (330) | 4.88 | 0.93 | –1.93 (–2.39) | –4.93 (–5.31) | 2.99 (2.92) | 2.93 | 288 | 469 |
| **2c** | 412 | 427 (333) | 4.82 | 0.94 | –1.85 (–2.37) | –4.79 (–5.27) | 2.94 (2.90) | 2.94 | 195 | 449 |
| **2d** | 431 | 517 (380) | 4.74 | 0.86 | –1.63 (–2.61) | –4.46 (–5.27) | 2.83 (2.67) | 3.51 | 237 | 440 |
| **2e** | 411 | 427 (313) | 4.80 | 0.91 | –2.37 (–2.42) | –5.33 (–5.32) | 2.97 (2.90) | 2.48 | 220 | 469 |
| **2f** | 425 | 485 (363) | 4.77 | 0.80 | –2.56 (--) | -5.39 (--) | 2.83 (2.77) | nd | nd | nd |

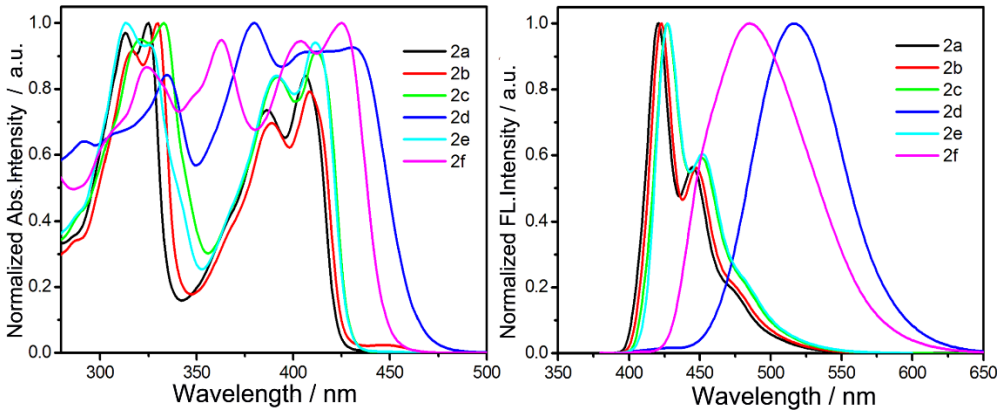


**Figure 6.** (a) Normalized UV-vis absorption and (b) fluorescence emission spectra of compounds **2** recorded in dichloromethane solutions at ~ $10^{-5}$–$10^{-6}$ M at 25°C.

In particular, the 1,3-bis(4-methoxylphenylethynyl)pyrene **2c** exhibits a more planar structure than 7-*tert*-butyl-1,3-bis(4-methoxyl-phenyl)pyrene,[22] which is beneficial to extend the conjugated pathway and increase the absorption cross-section. Indeed, the molar absorption coefficient of **2c** (log ε = 4.82) is higher than 1,3-bis(4-methoxylphenyl)pyrene (log ε = 4.51). According to the literature,[27] due to the special electronic structure of pyrene, substituents at different position would cause significant difference of electron distribution. For example, the absorption of **2a**–**c** exhibited a great differences when compared to **3**. Clearly, substitution at the K-region (4,5,9,10-positions) exerts a greater influence on the $S_2 \leftarrow S_0$ excitation than substitution at the active sites of the 1,3-position. The compounds **2a**–**c** with similar $S_2 \leftarrow S_0$ excitation coefficients (log ε =4.87 for **2a**, 4.88 for **2b** and 4.82 for **2c**) are much larger than **3** (log ε = 4.66).[20]

The fluorescence spectra of **2a**–**c** and **2e** exhibit a sharp peak at $\lambda_{em\ max}$ = 421, 423, 427 and 427 nm with a shoulder respectively. The emission spectra of **2d** and **2f** display a single broad peak at 517 nm and 485 nm, respectively, which indicates that the emission occurs from the lowest excited state with the largest oscillator strength. With the $\pi$-conjugation increasing, a gradual bathochromic shift in the $\lambda_{em\ max}$ is clearly observed in the order of **2a** ≈ **2b** ≈ **2c** ≈ **2e** < **2f** < **2d**, implying that the energy gap between ground and excited states would decrease in this order. In this process, the ICT plays an mportant role in lowering the energy gap.[28] The optical properties are consisted with Kim's reports.[29] All of compounds show strong emission from a deep blue to green

color with high PL quantum yields (QYs) in the 0.80–0.94 range. The quantum yields of the compounds herein are higher than those that we reported previously for a series of 7-*tert*-butyl-1,3-diarylpyrenes.[22] This was thought to be due to the increasing pconjugation and delocalization of the electron density can improve the optical density, leading to strong FL emission in the solid-state. Additionally, the fluorescence lifetimes were measured in dichloromethane, and the results are listed in Table 2.

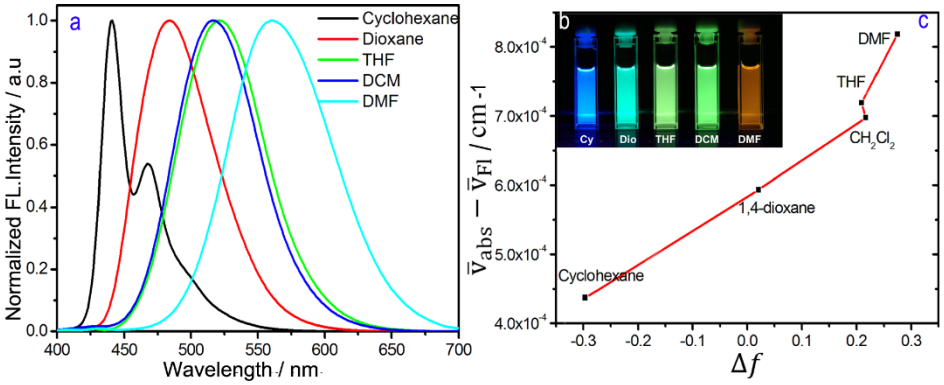


**Figure 7.** (a) Emission spectra of **2d** in cyclohexane, THF, $CH_2Cl_2$, $CH_3CN$ and DMF at 25°C. (b) the solvatochromic color change from blue to yellow, (c) Lippert-Mataga plots for compound **2d** (-$N(CH_3)_2$).

Furthermore, the effect on the optical properties of these compounds have been examined in solvents of various polarity, such as cyclohexane, 1,4-dioxane, tetrahydrofuran (THF), dichloromethane (DCM) and *N*,*N*-dimethylformamide (DMF). The solvent dependence of the absorption and fluorescene spectra of **2** are displayed in Figure 7. The fluorescence spectra of **2d** and **2f** showed an obvious intermolecular charge transfer (ICT) emission band in different solvents with different polarity; for example, in **2d**, there was a remarkable solvatochromic color change from blue (432 nm in cyclohexane) to yellow (560 nm in DMF), owing to the presence of the terminal electron-donating *N*,*N*-dimethylamino groups (–$N(CH_3)_2$) which lead to a large change in the singlet excited-state dipole moment,[30] as the polarity of the solvents increasing, the singlet excited states would decrease. The solvent effect of the absorption and fluorescence spectra was further evaluated by the Lippert-Mataga plot (Eqs. (1)–(2)),[31] which is dependent on the Stokes shift ($\Delta\nu_{st}$) and the solvent parameter $\Delta_f(\varepsilon, n)$.[32]

$$\Delta v = \frac{1}{4\pi\varepsilon_0 hc a^3} \frac{2\Delta\mu^2}{hcR^3} \Delta f + \text{const} \qquad (1)$$

Where $\Delta v = v_{abs} - v_{em}$ stands for Stokes shift, $v_{abs}$ is the wavenumber of maximum absorption, $v_{em}$ is the wavenumber of maximum emission, $\Delta_\mu = \mu_e - \mu_g$ is the difference in the dipole moment of solute molecule between excited ($\mu_e$) and ground ($\mu_g$) states, h is the Planck's constant, R is the radius of the solvent cavity in which the fluorophore resides (Onsager cavity radius), and $\Delta_f$ is the orientation polarizability given by (Eq. 2).

$$\Delta f = \frac{\varepsilon - 1}{2\varepsilon + 1} - \frac{n^2 - 1}{2n^2 + 1} \qquad (2)$$

Where ε is the static dielectric constant and n the refractive index of the solvent.

Similarly, the emission spectra of **2f** was red shifted by as much as ca. 76 nm depending on the polarity of solvents (from 432 nm in cyclohexane to 497 nm in DMF) with obvious ICT characteristics. However, the emission maxima of **2a**–**c**, with the electronic-donating groups, and **2e** were were only slightly red shifted by up to 10 nm depending on the solvent polarity even in DMF. Although the compounds **2a**–**c** and **2e** possess weak CT characteristics, they display relatively high QYs compared with the others.

### 2.2.4 Electrochemical Properties

The electrochemical properties of the title compounds **2a**–**e** were investigated by cyclic voltammetry (CV) in dichloromethane containing 0.1 M $nBu_4NPF_6$ as the supporting electrolyte, with a scan rate of 100 $mVs^{-1}$ at room temperature. As shown in Figure 8, all of the *Y*-shaped extended *π*-conjugated pyrene derivatives displayed an irreversible oxidation peak. In contrast, previous studies on similar *Y*-shaped pyrene molecules with aryl-substituted moieties have shown a quasi-reversible oxidation wave,[22] which might be due to the terminal nature of the *π*-conjugated arylethynyl

substitution effect on the electronic properties. For **2a**–**e**, the CV peaks for the positive potentials range from 1.23 to 1.28 V. According to the CVs and the UV-vis absorption, the highest occupied molecular orbital (HOMO) were estimated from the onset values of the first oxidation, and the optical energy gap ($E_g$) was derived from the UV-vis data. The HOMO energy levels for **2a**–**e** ranged from -5.28 to -5.34 eV, followed the empirical formula LUMO = HOMO-E g, the LUMO levels of **2a**–**e** are located from -2.37 to -2.61 eV. Given the considerable HOMO and LUMO energy values of the compound, it might have potential use as a luminescent hole-transporting material in OLEDs.[33]

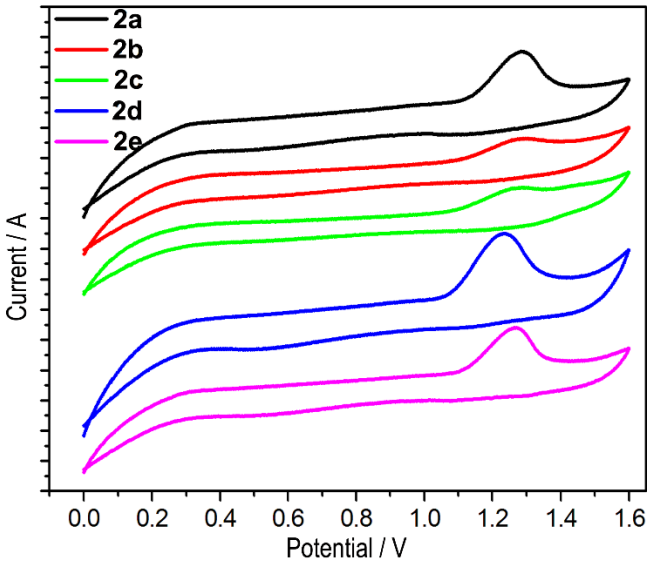


**Figure 8.** Cyclic voltammograms recorded for compounds **2a**–**e**.

## 5.2.5 Density functional theoretical calculation

To gain further insight into the electronic structures of the *Y*-shaped p-conjugated compounds **2**, DFT calculations were performed at the B3LYP/6-31G(d) level of theory using the Gaussian 2003 program. The 3D-structures and energy density of the HOMO and LUMO levels of each material are displayed in Figure 9. As the molecular geometries show, the substituent groups are almost coplanar with the pyrene core. Thus there is a close correlation between the quantum calculations and the single crystal X-ray diffraction results; minor differences of molecular geometry arise from the theoretical calculations being carried out in the "gas-phase".

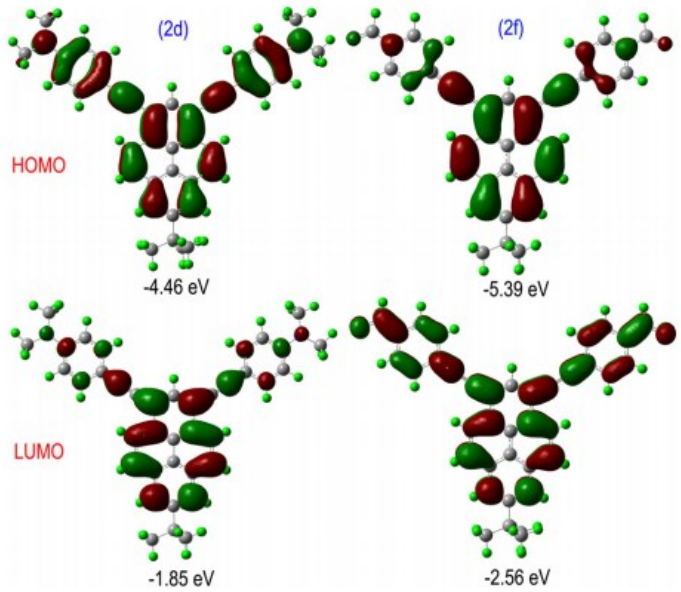


**Figure 9.** Selected computed molecular orbital plots (B3LYP/6-31G*) of the compounds **2d** and **2f**.

On the other hand, the various substituent groups play a significant role for the HOMOs and LUMOs, for example, as the electron-releasing ability increases from **2a** to **2d**, the destabilization of the HOMOs is greater than that of the LUMO, the HOMO levels are mostly located over the full molecular skeleton, whereas the LUMOs only spread in the center of pyrene rings; in contrast, with electron-withdrawing moieties, the LUMOs of **2e** and **2f** are almost fully localized on the entire molecular framework, and the HOMOs destabilized in the pyrene ring and a fragment of the phenyl groups. In addition, from the calculation data, we observed the energy gap of **2f** is close to **2d** with 2.83 eV, so both compounds exhibit similar UV spectra with a broad and strong absorption band in the 370–450 nm region. It is noteworthy that the HOMO-LUMO energy gaps of the title compounds **2** are lower than that previously reported for *Y*-shaped 1,3-bisaryl-functionalized pyrene species,[22] due to the effect of arylethynyl moieties on the energies of the molecular orbitals.

## 2.3 Conclusions

In summary, a series of Y-shaped arylethynyl-functionalized pyrenes **2** were synthesized by a Pd-catalyzed Sonogashira coupling reaction in reasonable yield. The Y-shaped, extended $\pi$-conjugated pyrene derivatives display strong face-to-face $\pi$-stacking with off-set head-to-tail stacking as compared with a *Y*-shaped carbon-carbon single bond arylsubstituted pyrene. Furthermore, the effects of the substituents and their position on the crystal packing structure and photophysical properties of the chromophores has been evaluated. Compounds **2a**–**c** and **2e** in dichloromethane exhibited deep blue fluorescence with high quantum yield, while the chromophores **2d** and **2f** exhibit intermolecular charge-transfer (ICT) leading to intense optical absorbances over a wide spectral range. Strong fluorescence spectra of **2d** and **2f** show the maximum emission at 517 nm and 485 nm, respectively, with remarkable solvatochromic effects in polar solvents. Theoretical computation and experimental CV studies on their electrochemistry verify that *Y*-shaped extended $\pi$-conjugated pyrenes **2** can be utilized in OLED devices as luminescent hole-transporting materials. In future, we will attempt to fabricate highly efficient OLED devices using these materials.

## 2.4 Experimental Section

### 2.4.1 General

All melting points (Yanagimoto MP-S1) are uncorrected. $^1$H NMR spectra (300 MHz) were recorded on a Nippon Denshi JEOL FT-300 NMR spectrometer with $SiMe_4$ as an internal reference: *J*-values are given in Hz. IR spectra were measured for samples as KBr pellets in a Nippon Denshi JIR-AQ2OM spectrophotometer. UV-vis spectra were recorded on a Perkin Elmer Lambda 19 UV/VIS/NIR spectrometer. Mass spectra were obtained on a Nippon Denshi JMS-01SA-2 spectrometer at 75 eV using a direct-inlet system.

**Materials**

Unless otherwise stated, all other reagents used were purchased from commercial sources and were used without further purification. The preparations of 7-*tert*-butyl-1,3-dibromopyrene (**1**) were described previously.[22]

### 2.4.2 Synthetic Procedures

**Synthesis,of,1,3-bisarylethynyl-7-*tert*-butylpyrenes (2)**

The series of compounds **2** was synthesized from 1,3-dibromo-7-tert-butylpyrene (**1**) with the corresponding arylethynyl compound by a Sonogashira coupling reaction.

**Synthesis of 7-*tert*-butyl-1,3-bis(4-methoxyphenylethynyl)pyrene (2c)**

To a stirred solution of 7-*tert*-butyl-1,3-dibromopyrene **1** (200 mg, 0.481 mmol), $Et_3N$ (10 mL) and DMF (10 mL), was added 4-methoxyphenyl acetylene (254 mg, 1.92 mmol) and $PPh_3$ (20.0 mg, 0.077 mmol), and the mixture was stirred at room temperature under argon. $PdCl_2(PPh_3)_2$ (24 mg, 0.034 mmol), CuI (10 mg, 0.053 mmol) were then added, and the mixture was heated to 100 °C with stirring for 24 h. After it was cooled, the mixture was diluted into $CH_2Cl_2$ (50 mL) and washed successively with saturated aqueous $NH_4Cl \cdot H_2O$ and brine. The organic extracts were dried with $MgSO_4$ and evaporated. The residue was purified by column chromatography eluting with ($CH_2Cl_2$/hexane,1:1) to give **2c** as a light yellow solid. Recrystallization from hexane gave 7-*tert*-butyl-1,3-bis(4-methoxyphenylethynyl)pyrene **2c**

(142 mg, 57 %) as a light yellow solid. M.p. 191–192°C; IR (KBr): $\nu_{max}$ = 1591, 1513, 1457, 1288, 1249, 1166, 1029, 872, 822, 714, 530 $cm^{-1}$; $^1H$ NMR (300 MHz, $CDCl_3$): $\delta_H$ = 1.60 (s, 9H, *t*Bu), 3.87 (s, 6H, OMe), 6.96 (d, *J* = 9.0 Hz, 4H, Ar-*H*), 7.66 (d, *J* = 9.0 Hz, 4H, Ar-*H*), 8.15 (d, *J* = 9.2 Hz, 2H, pyrene-*H*), 8.26 (s, 2H, pyrene-*H*), 8.36 (s, 1H, pyrene-*H*), 8.59 ppm (d, 2H, *J* = 9.0 Hz, pyrene-*H*); $^{13}C$ NMR (100 MHz, $CDCl_3$): $\delta_C$ = 31.90, 35.28, 55.38, 86.82, 95.16, 114.18, 115.61, 117.93, 122.42, 123.29, 124.48, 125.43, 128.88, 131.18, 131.27, 132.57, 133.22, 149.72, 159.86 ppm; FAB-MS: m/z calcd for $C_{38}H_{30}O_2$ 518.22 [$M^+$]; found 518.09 [$M^+$]; anal. calcd (%) for $C_{38}H_{30}O_2$ (518.64): C 88.00, H 5.83, O 6.17; found: C 87.89, H 5.63%.

A similar procedure using phenylacetylene, 4-*tert*-butylphenyl acetylene, *N,N*-dimethyl-4-ethynylaniline, 4-(trifluoromethyl)phenylacetylene and 4-ethynylbenzaldehyde was followed for the synthesis of **2a–2f**.

**7-*tert*-Butyl-1,3-bisphenylethynylpyrene (2a)** was obtained as a light green solid (recrystallized from hexane, 95 mg, 43%). M.p. 182–183°C; IR (KBr): $\nu_{max}$ = 891, 876, 813, 752, 716, 687, 534 $cm^{-1}$; $^1H$ NMR (300 MHz, $CDCl_3$): $\delta_H$ = 1.60 (s, 9H, *t*Bu), 7.37–7.47 (m, 6H, Ar-*H*), 7.71–7.74 (m, 4H, Ar-*H*), 8.18 (d, *J* = 9.2 Hz, 2H, pyrene-*H*), 8.28 (s, 2H, pyrene-*H*), 8.40 (s, 1H, pyrene-*H*), 8.61 ppm (d, *J* = 9.2 Hz, 2H, pyrene-*H*); $^{13}C$ NMR (100 MHz, $CDCl_3$): $\delta_C$ = 31.90, 35.30, 88.02, 95.13, 117.52, 122.34, 123.45, 123.52, 124.41, 125.33, 128.51, 129.21, 131.12, 131.65, 131.75, 132.88, 149.83 ppm; FAB-MS: *m/z* calcd for $C_{36}H_{26}$ 458.20 [$M^+$]; found 458.08 [$M^+$]; anal. calcd (%) for $C_{36}H_{26}$ (458.59): C 94.29, H 5.71; found: C 94.09, H 5.91%.

**7-*tert*-Butyl-1,3-bis(4-*tert*-butylphenylethynyl)pyrene (2b)** was obtained as a light green needles (recrystallized from hexane, 126 mg, 46%). M.p. 298–299 °C; IR (KBr): $\nu_{max}$ = 2959, 1515, 1464, 1360, 1225, 873, 831, 714, 557 $cm^{-1}$; $^1H$ NMR (300 MHz, $CDCl_3$): $\delta_H$ = 1.38 (s, 18H, *t*Bu), 1.60 (s, 9H, *t*Bu), 7.46 (d, *J* = 8.4 Hz, 4H, Ar-*H*), 7.66 (d, *J* = 8.6 Hz, 4H, Ar-*H*), 8.16 (d, *J* = 9.2 Hz, 2H, pyrene-*H*), 8.27 (s, 2H, pyrene-*H*), 8.38 (s, 1H, pyrene-*H*), 8.61 ppm (d, *J* = 9.0 Hz, 2H, pyrene-*H*); $^{13}C$ NMR (100 MHz, $CDCl_3$): $\delta_C$ = 31.23, 31.90, 34.90, 35.28, 87.42, 95.30, 117.79, 120.43, 122.39, 123.38, 124.44, 125.41, 125.51, 129.02, 131.16, 131.50, 132.77, 149.74, 151.84 ppm; FAB-MS: *m/z* calcd for $C_{44}H_{42}$ 570.33 [$M^+$]; found 570.19 [$M^+$]; anal. calcd (%) for $C_{44}H_{42}$ (470.80): C 92.58, H 7.42; found: C 92.79, H 7.22%.

**7-*tert*-Butyl-1,3-bis(4-*N,N*-dimethylaminophenylethynyl)pyrene (2d)** was obtained as yellow prisms (recrystallized from $CH_2Cl_2$/hexane; 3:7, 84 mg, 32%). M.p. 221–223°C; IR (KBr): $\nu_{max}$ = 2189, 1650, 1523, 1441, 1362, 1219, 1178, 1147, 812, 752 $cm^{-1}$; $^1H$ NMR (300 MHz, $CDCl_3$): $\delta_H$ = 1.59 (s, 9H, *t*Bu), 3.03 (s, 12H, $NMe_2$), 6.74 (d, *J* = 9.0 Hz, 4H, Ar-*H*), 7.59 (d, *J* = 9.0 Hz, 4H, Ar-*H*), 8.12 (d, *J* = 9.0 Hz, 2H, pyrene-*H*), 8.23 (s, 2H, pyrene-*H*), 8.33 (s, 1H, pyrene-*H*), 8.61 ppm (d, *J* = 9.0 Hz, 2H, pyrene-*H*); $^{13}C$ NMR (100 MHz, $CDCl_3$): $\delta_C$ = 31.91, 35.25, 40.26, 86.27, 96.47, 110.33, 111.97, 118.62, 122.59, 122.94, 124.58, 125.67, 128.39, 130.76, 131.30, 132.26, 132.89, 149.51, 150.28 ppm; FAB-MS: *m/z* calcd for $C_{40}H_{36}N_2$ 544.29 [$M^+$]; found 544.11 [$M^+$]; anal. calcd (%) for $C_{40}H_{36}N_2$ (544.73): C 88.20, H 6.66, N 5.14; C 88.01, found: H 6.96, N 5.03%.

**7-*tert*-Butyl-1,3-bis(4-trifluoromethylphenylethynyl)pyrene (2e)** was obtained as light green needles (recrystallized from hexane, 192 mg, 67%). M.p. 241–243°C; IR (KBr): $\nu_{max}$ = 1611, 1322, 1161, 1123, 1064, 1015, 889, 836 $cm^{-1}$; $^1H$ NMR (300 MHz, $CDCl_3$): $\delta_H$ = 1.61 (s, 9H, *t*Bu), 7.69 (d, *J* = 8.0 Hz, 4H, Ar-*H*), 7.80 (d, *J* = 7.9 Hz, 4H, Ar-*H*), 8.20 (d, *J* = 9.0 Hz, 2H, pyrene-*H*), 8.30 (s, 2H, pyrene-*H*), 8.40 (s, 1H, pyrene-*H*), 8.56 ppm (d, *J* = 8.9 Hz, 2H, pyrene-*H*); $^{13}C$ NMR (100 MHz, $CDCl_3$): $\delta_C$ = 31.88, 35.34, 90.24, 93.69, 116.66, 122.16, 122.62, 123.96, 124.31, 125.02, 125.52, 127.13, 129.80, 129.99, 130.31, 130.99, 131.83, 131.89, 131.98, 132.12, 133.16, 150.11 ppm; FAB-MS: *m/z* calcd for $C_{38}H_{24}F_6$ 594.18 [$M^+$]; found 593.65 [$M^+$]; anal. calcd (%) for $C_{38}H_{24}F_6$ (594.59): C 76.76, H 4.07; found: C 76.86, H 4.27%.

**7-*tert*-Butyl-1,3-bis(4-formylphenylethynyl)pyrene (2f)** was obtained as yellow solid (recrystallized from $CH_2Cl_2$/hexane; 3:7, 100 mg, 40%). M.p. 283–285°C; IR (KBr): $\nu_{max}$ = 1696, 1600, 1557, 1203, 1163, 873, 825 $cm^{-1}$; $^1H$ NMR (300 MHz, $CDCl_3$): $\delta_H$ = 1.61 (s, 9H, *t*Bu), 7.84 (d, *J* = 8.4 Hz, 4H, Ar-*H*), 7.93 (d, *J* = 8.4 Hz, 4H, Ar-*H*), 8.22 (d, *J* = 9.2 Hz, 2H, pyrene-*H*), 8.32 (s, 2H, pyrene-*H*), 8.41 (s, 1H, pyrene-*H*), 8.57 (d, *J* = 9.2 Hz, 2H, pyrene-*H*), 10.06 ppm (s, 2H, C*H*O); $^{13}C$ NMR (100 MHz, $CDCl_3$): $\delta_C$ = 31.88, 35.34, 91.93, 94.32, 116.61, 122.12, 124.08, 124.29, 124.99, 129.54, 129.71, 129.94, 130.96, 132.16, 132.25, 133.25, 135.56, 150.17,191.38 ppm; FAB-MS: *m/z* calcd for $C_{38}H_{26}O_2$ 514.19 [$M^+$]; found 513.71 [$M^+$]; anal. calcd (%) for $C_{38}H_{26}O_2$ (514.61): C 88.69, H 5.09, O 6.22; found: C 88.49, H 5.29%.

## 2.5 References


1. Wang, C.-L.; Dong, H.-L.; Hu, W.-P.; Liu, Y.-Q.; Zhu, D.-B. *Chem. Rev.* **2012**,*112*, 2208–2267.
2. Usta, H.; Facchetti, A.; Marks, T. *Acc. Chem. Res.* **2011**, *44*, 501–510.
3. Pietrangelo, A.; Patrick, B. O.; MacLachlan, M. J.; Wolf, M. O. *J. Org. Chem.* **2009**, *74*, 4918–4926.
4. Wu, W.; Liu, Y.-Q.; Zhu, D.-B. *Chem. Soc. Rev.* **2010**, *39*, 1489–1502.
5. Li, J.; Zhang, Q. *ACS Appl. Mater. Interfaces* **2015**, *7*, 28049–28062.
6. Cheng, Y.-J.; Yang, S.-H.; Hsu, C.-S. *Chem. Rev.* **2009**, *109*, 5868–5923.
7. (a) Murphy, A. R.; Frchet, J. M. J. *Chem. Rev.* **2007**, *107*, 1066–1096. (b) Mardanya, S.; Karmakar, S.; Mondal, D.; Baitalik, S. *Dalton Trans.* **2015**, *44*, 15994–16012.
8. Tang, M. L.; Mannsfeld, S. C. B.; Sun, Y.-S.; Becerril, H. A.; Bao, Z. *J. Am. Chem. Soc.* **2009**, *131*, 882–883.
9. Figueira-Duarte, T. M.; Mullen, K. *Chem. Rev.* **2011**, *111*, 7260–7314.
10. D. Karthik, K. R. J. Thomas, J.-H. Jou, S. Kumar, Y.-L. Chen, Y.-C. Jou, *RSC Adv.* **2015**, *5*, 8727–8738.
11. Chercka, D.; Yoo, S.-J.; Baumgarten, M.; Kim, J.-J.; Mullen, K. *J. Mater. Chem. C* **2014**, *2*, 9083–9086.
12. Salunke, J. K.; Wong, F. L.; Roy, V. A. L.; Lee, C. S.; Wadgaonkar, P. P. *Phys. Chem. Chem. Phys.* **2014**, *16*, 23320–23328.
13. Jeon, N. J.; Lee, J.; Noh, J. H.; Nazeeruddin, M. K.; Grtzel, M.; Il Seok, S. *J. Am. Chem. Soc.* **2013**, *135*, 19087–19090.
14. Hu, J.-Y.; Feng, X.; Seto, N.; Do, J.-H.; Zeng, X.; Tao, Z.; Yamato, T. *J. Mol. Struc.* **2013**, *1035*, 19–26.
15. Feng, X.; Hu, J.-Y. ; Iwanaga, F.; Seto, N.; Redshaw, C.; Elsegood, M. R. J.; Yamao, T. *Org. Lett.* **2013**, *15*, 1318–1321.
16. Diring, S.; Camerel, F.; Donnio, B.; Dintzer, T.; Toffanin, S.; Capelli, R.; Muccini, M.; Ziessel, R. *J. Am. Chem. Soc.* **2009**, *131*, 18177–18185.
17. Lee, Y. O.; Pradhana, T.; No, K.; Kim, J. S. *Tetrahedron* **2012**, *68*, 1704–1711.
18. Kim, H. M.; Lee, Y. O.; Lim, C. S.; Kim, J. S.; Cho, B. R. *J. Org. Chem.* **2008**, *73*, 5127–

5130.

19. Sato, T.; Uejima, M.; Tanaka, K.; Kaji, H.; Adachi, C. *J. Mater. Chem. C* **2015**, *3*, 870–878.
20. Hu, J.-Y.; Era, M.; Elsegood, M. R. J.; Yamato, T. *Eur. J. Org. Chem.* **2010**, 72–79.
21. Hu, J.-Y.; Ni, X.-L.; Feng, X.; Era, M.; Elsegood, M. R. J.; Teat, S. J.; Yamato, T. *Org. Biomol. Chem.* **2012**, *10*, 2255–2262.
22. Feng, X.; Hu, J.-Y.; Yi, L.; Seto, N.; Tao, Z.; Redshaw, C.; Elsegood, M. R. J.; Yamato, T. *Chem. Asian J.* **2012**, *7*, 2854–2863.
23. Cheng, G.; Bonillo, B.; Sprick, R. S.; Adams, D. J.; Hasell, T.; Cooper, A. I. *Adv. Funct. Mater.* **2014**, *24*, 5219–5224.
24. Pope, M.; C. E. Swenberg, Electronic Processes in Organic Crystals and Polymers; Oxford University Press: Oxford, **1999**. 48–53.
25. Feng, X.; Du, H.; Chen, K.; Xiao, X.; Luo, S.-X.; Xue, S.-F.; Zhang, Y.-Q.; Zhu, Q.-J.; Tao, Z.; Zhang, X.-Y.; Wei, G. *Cryst Growth Des.* **2010**, *10*, 2901–2907.
26. Wang, C.-G.; Chen, S.-Y.; Wang, K.; Zhao, S.-S.; Zhang, J.-Y.; Wang, Y. *J. Phys. Chem. C* **2012**, *116*, 17796–17806.
27. Crawford, A. G.; Dwyer, A. D.; Liu, Z.; Steffen, A.; Beeby, A.; P&lsson, L.-O.; Tozer, D. J.; Marder, T. B. *J. Am. Chem. Soc.* **2011**, *133*, 13349–13362.
28. (a) Karmakar, S.; Maity, D.; Mardanya, S.; Baitalik, S. *J Phys Chem. A* **2014**, *118*, 9397–9410. (b) Droumaguet, C. L.; Sourdon, A.; Genin, E.; Mongin, O.; Blanchard-Desce, M. *Chem. Asian J.* **2013**, *8*, 2984–3001. (c) Lartia, R.; Allain. C.; Bordeau, G.; Schmidt, F.; Fiorini-Debuisschert, C.; Charra, F.; Teulade-Fichou, M.-P. *J. Org. Chem.* **2008**, *73*, 1732–1744. (d) Chen, X.; Sang, X.; Zhang, Q. *RSC Adv.* **2015**, *5*, 53211–53219.
29. (a) Kim, H. M.; Lee, Y. O.; Lim, C. S.; Kim, J. S.; Cho, B. R. *J. Org. Chem.* **2008**, *73*, 5127–5130. (b) Lee, Y. O.; Pradhan, T.; Yoo, S.; Kim, T. H.; Kim, J.; Kim, J. S. *J. Org. Chem.* **2012**, *77*, 11007–11013. (c) Sung, J.; Kim, P.; Lee, Y. O.; Kim, J. S.; Kim, D. *J. Phys. Chem. Lett.* **2011**, *2*. 818–823.
30. (a) Sakuda, E.; Ando, Y.; Ito, A.; Kitamura, N. *J. Phys. Chem. A* **2010**, *114*, 9144–9150. (b) Ito, A.; Kawanishi, K.; Sakuda, E.; Kitamura, N. *Chem. Eur. J.* **2014**, *20*, 3940–3953.
31. (a) Han, F. Chi, L. Wu, W. Liang, X.; Fu, M.; Zhao, J.; Photochem. J. *Photobio. A: Chem.* **2008**, *196*, 10–23; b) Zhao, G.-J.; Liu, J.-Y.; Zhou, L.-C.; Han, K.-L. *J. Phys. Chem. B*

**2007**, *111*, 8940–8945.

32. Sciano, J. C. Handbook of Organic Photochemistry; CRC Press: Boca Raton, FL, **1989**.
33. (a) Duong, H. M.; Bendikov, M.; Steiger, D.; Zhang, Q.; Sonmez, G.; Yamada, J.; Wudl, F. *Org. Lett.* **2003**, *5*, 4433–4436. (b) Mardanya, S.; Karmakar, S.; Das, S.; Baitalik, S. *Sens. Actuators B Chem.* **2015**, *206*, 701–713.
34. Crosby, G. A.; Demas, J. N. *J. Phys. Chem.* **1971**, *75*, 991–1024.
35. SAINT, SMART and APEX 2 (2000 & 2008) software for CCD diffractometers. Bruker AXS Inc., Madison, USA.
36. Programs CrysAlis-CCD and -RED, Oxford Diffraction Ltd., Abingdon, UK (**2013**).
37. Palatinus, L.; Chapuis, G. *J. Appl. Cryst.* **2007**, *40*, 786–790.
38. Sheldrick, G. M. *Acta Crystallogr.* **2008**, *A64*, 112–122.

# Chapter 3

# Synthesis and tunable emission properties of 1, 3-bis(*N*, *N*-diaryl)amino substituted pyrene-based fluorophores

*The development of functionalized, luminescent, pyrene-based monomers has been and continues to be an area of great interest in terms of the design and fabrication of optical and electronic devices. Herein, a facile strategy to tune the emission color of pyrene-based chromophores has been established by simple functional group modification at the para position to the diphenylamino on the donor building block. Intriguing photophysical properties were obtained and are described both in different solutions and in the solid state. The results obtained could be explained by the Hammett method and by density functional theory (DFT) calculations. A good correlation was observed between the Hammett $\sigma_{para}$ constants of the functional groups para to the phenyl and the wavenumber ($cm^{-1}$) of the emission profile. This positive correlation, namely between the σ constants of the functional groups and the emission properties of the monomers, can be used to develop a predictive method for these types of systems.*

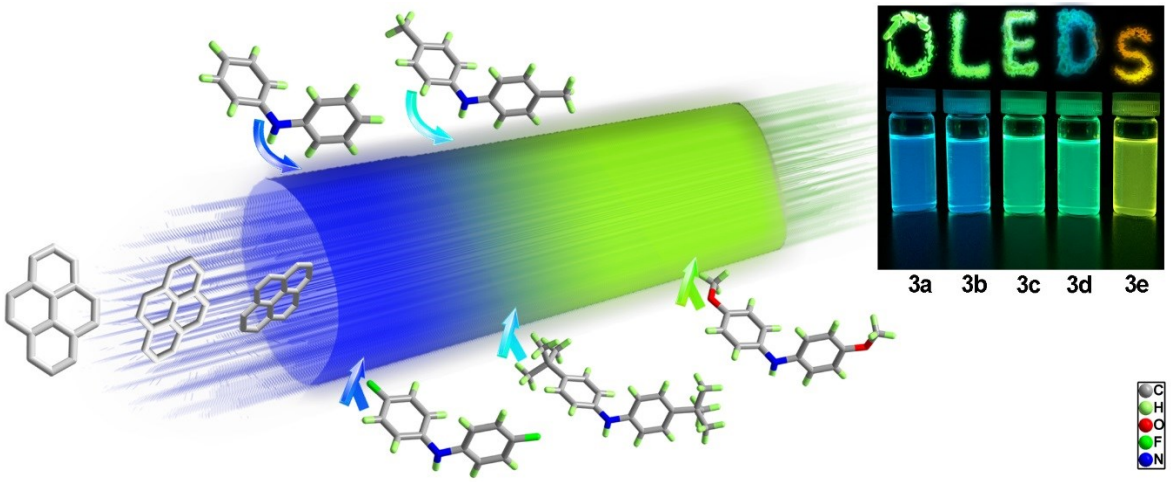

## 3.1 Introduction

Chromophores are a class of functional π-electron systems that have progressively established themselves as useful tuneable molecules in modern organic electronics and organic electronic devices.[1] Indeed, it is important to have the ability to tune the emission property of materials in a facile approach when designing light-emitting diodes,[2] bio-imaging probes,[3] and other photoelectric emitting devices,[4] particularly in the visible region. Various strategies have been established to achieve efficient full-color emitting materials which are based on underlying mechanisms, including intramolecular charge-transfer (ICT),[5] twisted intramolecular charge-transfer (TICT),[6] excimer,[7] excited-state proton transfer (ESIPT),[8] and photo-induced electron transfer (PET).[9] Such strategies provide significant guidance when designing novel luminescent molecules. In particular, it is worth noting that in recent years the introduction of donors and acceptors has played a crucial role in organic electronics based on ICT.[5, 10] Furthermore, much effort has been devoted to developing highly efficient host materials.

Among the many promising unmodified host candidates, polyaromatic pyrene have attracted attention because of their high thermal and photochemical stability, pure blue fluorescence, planar geometry, and natural high charge carrier mobility.[11] It is also possible to append electron-accepting/donor groups at the suitable positions on the pyrene core, which can result in enhanced intramolecular charge-transfer. Generally speaking, acceptors and donors provide energetically high lying occupied molecular orbitals (HOMOs) and low lying unoccupied molecular orbitals (LUMOs), respectively. The D−A unit is conducive to the fine-tuning of the electronic interactions and charge transfer efficiencies.[12] A wide variety of D−A type pyrene derivatives have been investigated by comparing experimental and theoretical results in recent years.[13] For instance, many pyrene-based chromophores, based on both covalent and acceptor-donor structures, have been found to possess differing yet distinctive emission properties by functionalization at the different positions of the pyrene core.[4a, 14] On the basis of these experimental observations, in case of a donor/acceptor substituted molecule, the band-gap of the new material can be significantly reduced when compared to the pure components.[15]

Herein, we present a facile strategy to investigate the influence of covalent donor groups. Specifically, a series of classical donor groups, which differ only by the functional group *para* to an *N*, *N*-diphenylamine core, have been studied. The groups were introduced at the 1-, and 3-positions of 7-*tert*-butylpyrene *via* a Buchwald–Hartwig amination reaction. As anticipated, we observed distinct/different emission properties both in solution and in the solid state, simply by fine-tuning of the *para* substituents of the *N*, *N*-diphenylamine core. Broad and tuneable emission, from blue to yellow wavelengths, were achieved in dilute $CH_2Cl_2$ solutions. Moreover, one of the compounds was found to emit orange light in the solid state. To decipher the underlying mechanisms responsible for these attractive properties, we further investigated the solvatochromism of the five compounds and report their absorption and emission spectra. The pronounced positive solvatochromism combined with theoretical calculations indicate that these systems have potential for the design of full-colour organic electrochromic devices.[16]

## 3.2 Results and Discussion

### 3.2.1 Synthetic procedures of monomers 3

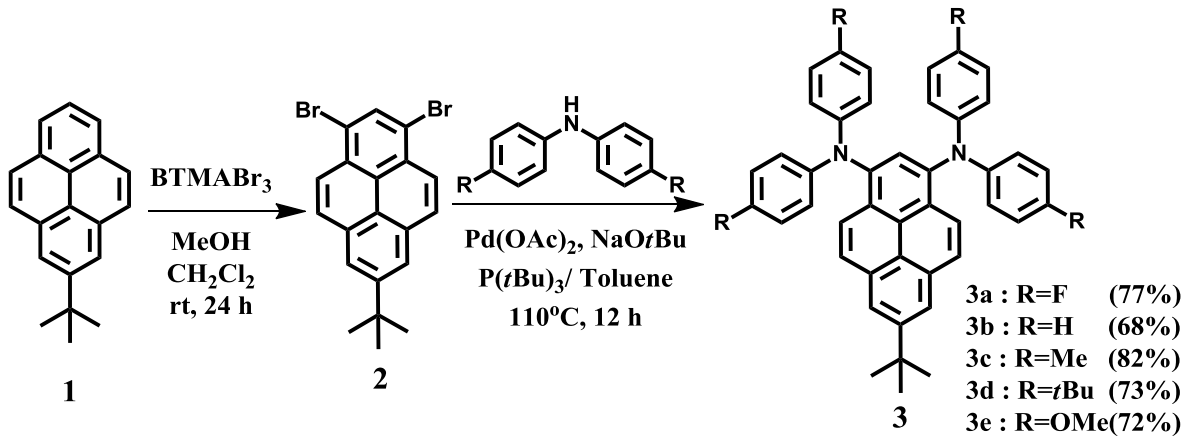


**Scheme 1**. Synthesis of pyrene-based light-emitting monomers **3**.

Shown in Scheme 1 is the synthesis of 3a-e starting from 7-*tert*-butylpyrene. This synthetic strategy was adapted from the well-known Buchwald–Hartwig amination reaction. The compounds were characterized by $^{1}H$ and $^{13}C$ NMR spectroscopy, high resolution mass spectrometry. The detailed synthetic procedures and characterization data are given in the Experimental Section. All compounds exhibited good solubility in common organic solvents with excellent thermal stability. The thermal properties of these monomers were determined by differential scanning calorimetry (DSC) and thermogravimetric analysis (TGA) under a nitrogen atmosphere and the results are shown in Table 1. Compounds of type 3 showed very high thermal stability with decomposition temperatures ($T_d$) of 348 to 392 °C and melting temperatures ($T_m$) of 198 to 262 °C. The high thermal values endow high morphologic stability of the amorphous phase in the solid state.

### 3.2.2 Crystallography

The molecular structure of 7-*tert*-butyl-1,3-bis[*N*, *N*-bis(4'-methoxyphenyl)amino]pyrene (**3e**) was unambiguously confirmed by X-ray crystallography. Shown in Figure 1 is the crystal structure of **3e**, which shows the

dihedral angles between the $C_6$ aromatic rings and the pyrene unit. Unsurprisingly, the *p*-OMe-phenyl groups point in different directions (Figure 1b). The dihedral angles between the pyrene core (C1 > C16) and the $C_6$ aromatic rings are as follows: 75.81(3)° (C21 > C26), 79.34(3)° (C28 > C33), 60.79(11)° (C35 > C40) for the major disorder component, and 81.25(3)° (C42 > C47), respectively. The aromatic rings of the diphenylamino unit exhibit a twisted geometry, which, when combined with the bulky *tert*-butyl groups, reduces the $\pi$–$\pi$ stacking interactions. By comparison, both the phenyl and pyrene units of **3e** are involved in two kinds of $\pi$ interactions between adjacent molecules, which results in the formation of a three-dimensional framework (Figure 2a).[17]

**Table 1.** The physical properties of compounds of type **3a-e**.

| R | $\lambda_{abs}$ (nm) sol[a] | $\lambda_{PL}$ (nm) sol[a]/solid[b] | log ε $M^{-1}\cdot cm^{-1}$ | $T_m$ (°C)[c] | $T_d$ (°C)[d] | $\Phi_{PL}$(%) sol[a]/solid[b] | HOMO (eV)[e] | LUMO (eV)[f] | $E_g$ (eV)[g] |
|---|---|---|---|---|---|---|---|---|---|
| **3a** | 294, 414 | 465/525 | 4.59 | 198 | 348 | 79/33 | -4.95 | -1.95 | 3.00 |
| **3b** | 299, 414 | 467/514 | 4.62 | 238 | 372 | 82/46 | -4.79 | -1.79 | 3.00 |
| **3c** | 302, 424 | 489/494 | 4.65 | 214 | 383 | 78/29 | -4.65 | -1.72 | 2.93 |
| **3d** | 302, 425 | 491/472 | 4.61 | 229 | 391 | 57/10 | -4.68 | -1.76 | 2.92 |
| **3e** | 301, 434 | 525/573 | 4.62 | 262 | 392 | 60/24 | -4.43 | -1.57 | 2.86 |

[a] Measured in dichloromethane at room temperature. [b] Measure in the solid state as powder. [c] Melting point: Obtained from DSC measurements. [d] Thermal decomposition temperature: Obtained from TGA measurements. [e] DFT/B3LYP/6-31G* using Gaussian. [f] LUMO = *E*g + HOMO, [g] Estimated from the absorption edge of UV-Vis spectra.

A detailed investigation indicated that two types of $\pi$ interactions were present, namely 1) a MeC–H···$\pi$ interaction of the methoxy group with the phenyl unit at a distance of 2.86 Å (yellow dashed lines); and 2) an edge-to-face ArC–H···$\pi$ interaction between the edge of the phenyl unit and the face of the pyrene core at a distance in the range 3.56–4.03 Å (green dashed lines). This interestingly results in a regular arrangement of alternating, anti-parallel stacks (Figure 2b). To be more exact, a compact supramolecular assembly is observed from alternating donor of phenyl groups (orange colour) and the pyrene core (blue colour) due to weak intermolecular interactions.

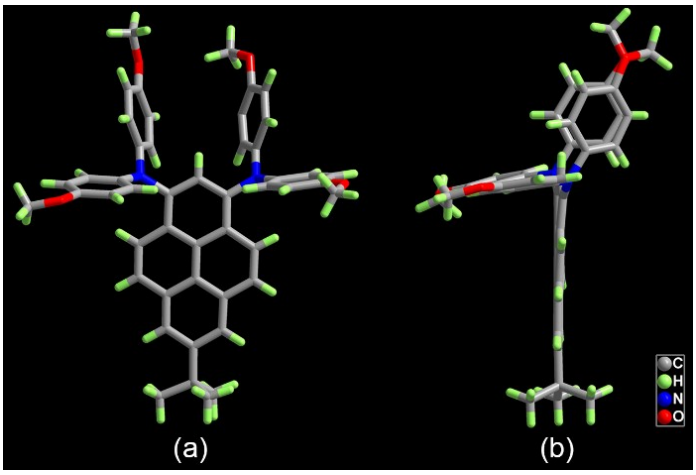


**Figure 1**. The crystal structure of compound **3e**: (a) top view and (b) side view.

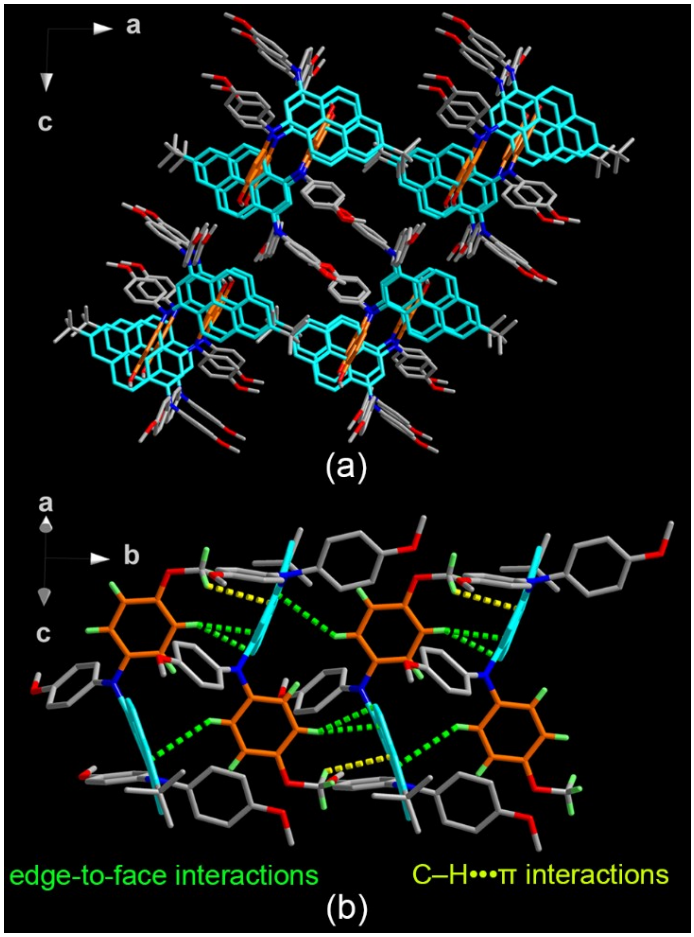


**Figure 2**. (a) The molecular packing of compound **3e** as viewed parallel to the *b* axis of the unit cell; (b) the principal intermolecular packing interactions (Most hydrogen atoms are omitted for clarity).

### 3.2.3 Density Functional Theoretical Calculation

These molecular designs were guided by density functional theory (DFT) calculations at the B3LYP/6-31g-(d)) level to examine their lowest unoccupied molecular orbital (LUMO), and highest occupied molecular orbital (HOMO). As depicted in Figure 3, the HOMOs of **3a-e** are mainly spread over the diphenylamino moiety and the pyrene core, while the LUMOs are mostly distributed on the pyrene core and slightly extended to the phenyl ring. It is noteworthy that the separated HOMOs and LUMOs are important for high luminescence efficiency of the molecule in certain circumstances, which could increases the potential of Thermally Activated Delayed Fluorescence (TADF) emitters by adjusting the energy gap.[18]

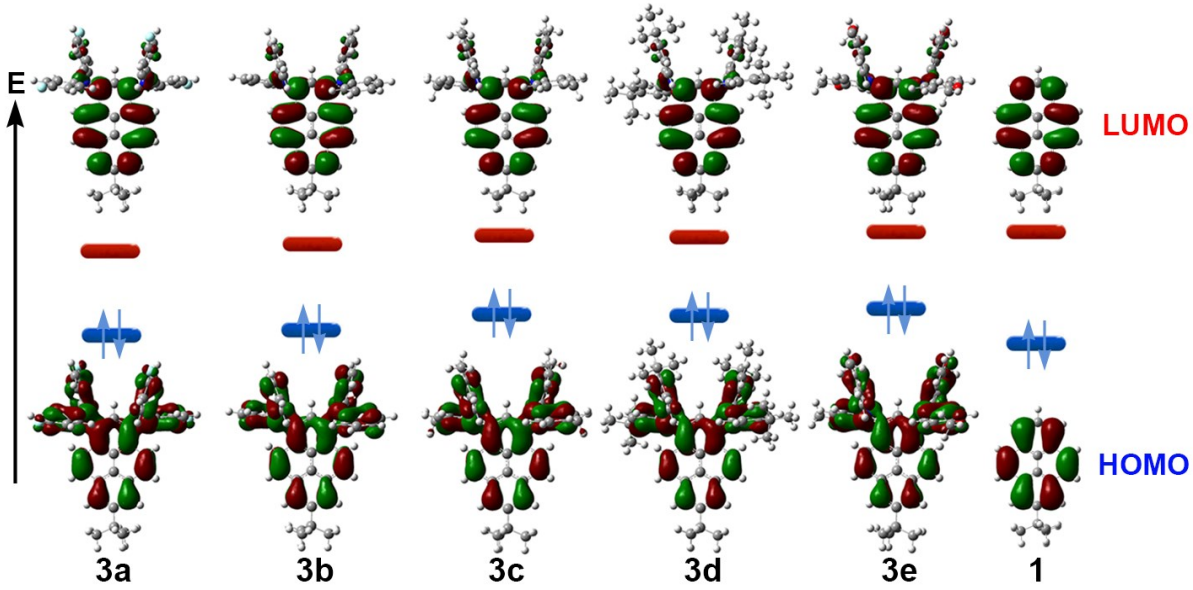


**Figure 3**. Frontier-molecular-orbital distributions and energy levels diagram of **3a-e** and **1** by DFT calculations.

More and more classical donors and acceptors are attracting interest in the field of organic electronics. Herein, donor functionalized diphenylamines were selected as the hole-transport materials.[19] The contours of the LUMO and HOMO of compounds **3a-e** revealed that the incorporation of a strong electron-donating group on the diphenylamine decreases the contribution of the pyrene core in the HOMOs. The distribution of LUMO orbitals of **3a-e** indicated the acceptor nature of the pyrene unit.

It is very likely that intramolecular charge-transfer (ICT) states would be formed for these monomers. In this case of the donor appended molecules, the energy gaps were further evaluated. As shown in Table 1 and the energy level diagram Figure 3, the energetic proximity of the low lying LUMO and high lying HOMO results in a reduced energy gap compared with compound **1**.[20] The most interesting finding from the DFT calculations is that there is a positive correlation trend between the electronegativity of the functional groups occupying the *para* position at the phenyl moiety and the HOMO−LUMO gaps, which makes it possible to predict that the monomers **3a-e** would have red-shifted absorption spectra. Based on our preliminary theoretical guidance, the steady-state absorption and emission properties were investigated both in solution and in the solid state.

### 3.2.4 Optical Properties

The absorption and emission spectra of compounds **3a-e** both in solution and in the solid state are shown in Figure 4, and summarized in Table 1. As shown in Figure 4 (top), type 3 compounds have a strong, high-energy band centered at 294−302 nm, which is mainly due to the $\pi$–$\pi^*$ transitions of the substituents and pyrene core. In this type of molecule, with classical donor groups at the terminal aromatic rings of pyrene, all of the monomers exhibited a broad absorption band with low-energy absorption (414−434 nm), indicating that their excited states possess some charge transfer (CT) absorption associated with the ICT from the *para* substituents of the *N*,*N*-diphenylamine terminal to the pyrene unit, which is attributed to the separated HOMO and LUMO distributions. It was found that the low-energy band is relatively more affected and sensitive than the high-energy band by the nature of the functional groups *para* to the phenyl moiety according to the molar absorption coefficient (Figure 4 top). Compounds **3a-e** have a high-energy band which corresponds to a molar absorption coefficient centered at 48046−50002 $cm^{-1}$ $M^{-1}$, and a low-energy band which corresponds to a molar absorption coefficient ranging from 22135 to 31614 $cm^{-1}$ $M^{-1}$. The band gap energy ($E_g$) of compounds **3a-e** calculated from the absorption edge of the UV/Vis spectra are also summarized in Table 1. The LUMO levels of **3a-e** were estimated from the $E_g$ and HOMO levels.

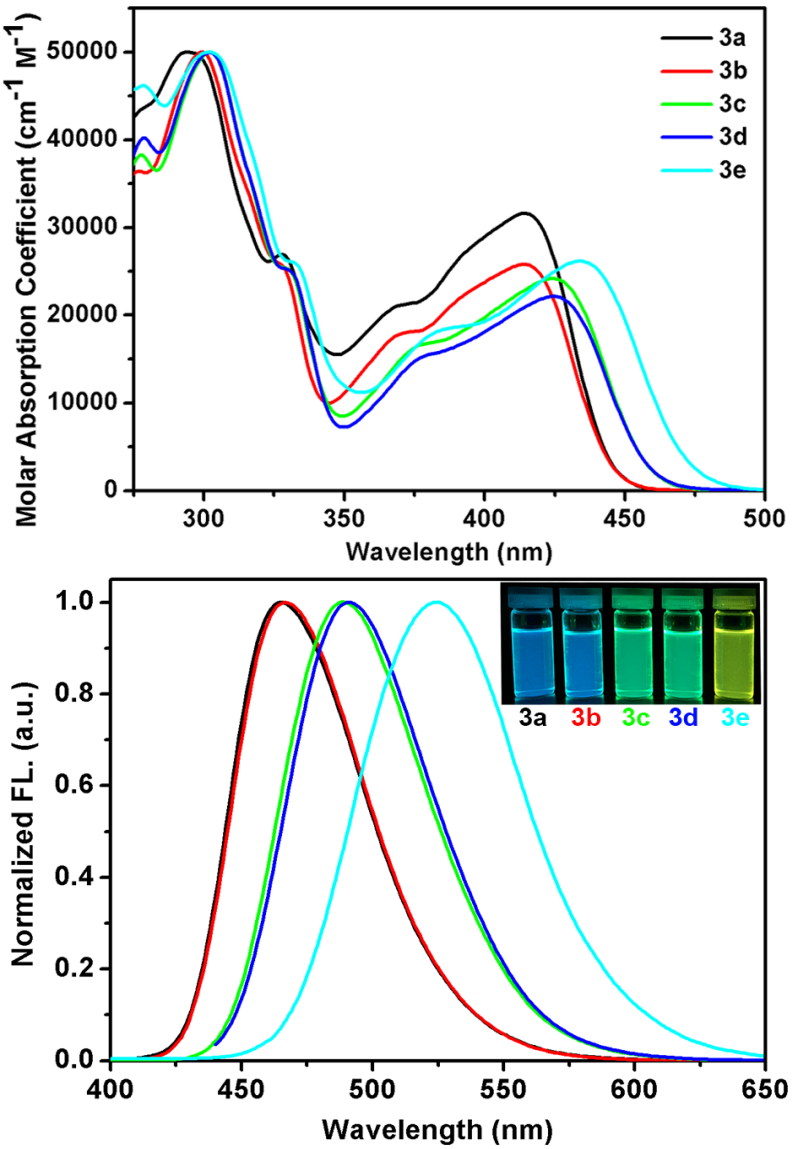


**Figure 4.** Absorption (top) and emission (bottom) profiles for compounds **3** in $CH_2Cl_2$ solution.

The emission maxima of this set of monomers **3** are in the range 465−525 nm in dilute $CH_2Cl_2$ solutions with a systematic bathochromic shift in the order **3a** < **3b** < **3c** < **3d** < **3e** (Figure 4 bottom), consistent with the electronegativity of the substituents at the *para* position of the phenyl moiety. These results, combined with the theoretical calculations, indicate that the energy gap ($E_g$) could be tuned between the group and the excited states by introducing different substituent groups. More interestingly, when the $\lambda_{em\ max}$ are converted to wavenumbers ($cm^{-1}$) and plotted *versus* the Hammett $\sigma_{para}$ constants for the functional groups *para* on the phenyl, a positive correlation was clearly observed obviously (Figure 5). This

result establishes a promising strategy for the design of pyrene-based luminophores by choosing functional groups on the basis of their Hammett $\sigma_{para}$ value.

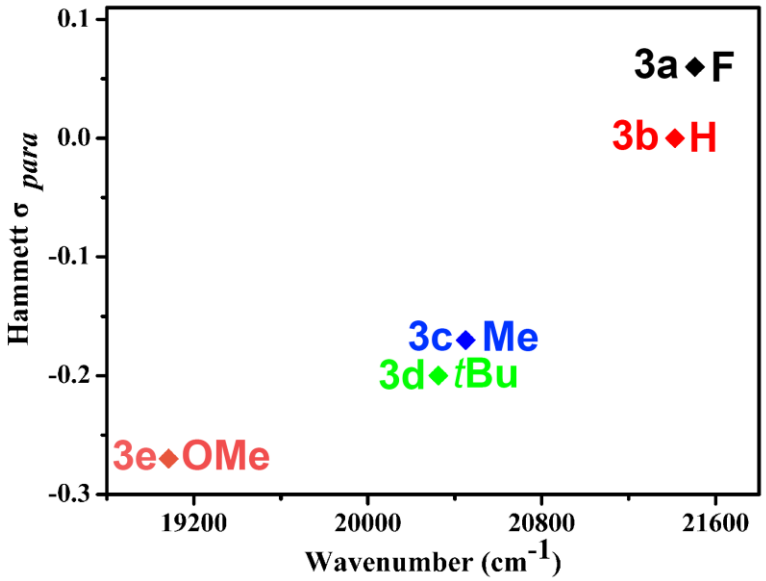


**Figure 5**. Hammett $\sigma_{para}$ constants *versus* wavenumber ($cm^{-1}$) for **3a** (black), **3b** (red), **3c** (blue), **3d** (green), and **3e** (orange).

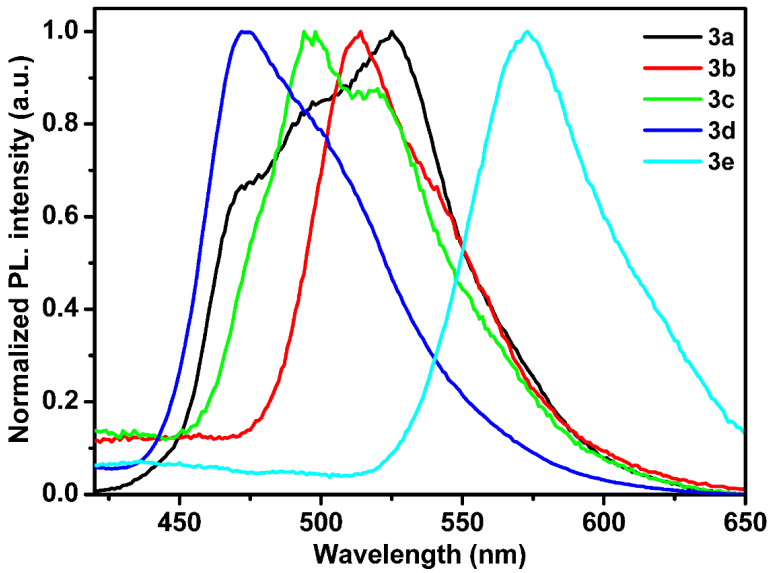


**Figure 6.** Emission spectra of compounds of type **3** in the solid state.

The emission spectra in the solid state were also recorded, and all the compounds were found to exhibit a red shift trend compared with their corresponding emission spectra in solution (Table 1, and Figure 6). However, the emission band maxima of **3d** was blue-shifted

(19 nm) relative to the results in solution, because of the introduction of the *para*-position of bulky electron donor *tert*-butyl group in phenyl ring that not only plays a role in restricting aggregation in the solid state but also affects the conformation of the electronic structures. It was observed that the quantum yields showed no trend in solution. Additionally, a decrease in the photoluminescence quantum yield of these compounds was observed in the solid state. In order to gain further insight into the pronounced difference of luminescence quantum efficiency in both these two states, additional analysis of compound **3e** using powder X-ray diffraction (PXRD) was investigated. And the PXRD pattern of **3e** shows an obvious crystalline phase (Figure 7).

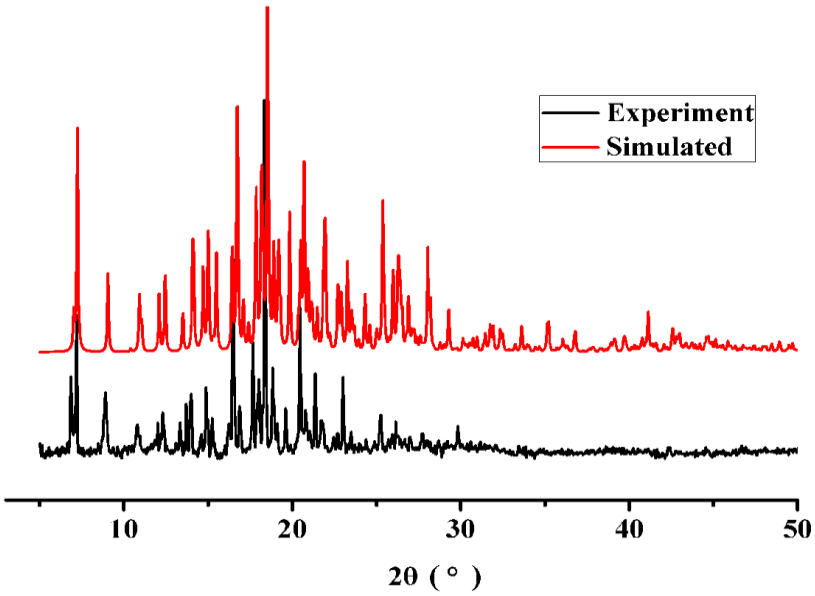


**Figure 7.** Powder X-ray diffraction (PXRD) of compound **3e** and the corresponding comparison with simulation.

Most importantly, comparison of this result of compound **3e** with corresponding simulation showed that the powder is mainly crystalline, so it can be better understandable through the guidance of stacking of X-ray structure. The *H*- and *J*-aggregates[21] were elucidated since it is generally agreed that these are the best known theoretical predictors (Figure 8). According to the optical results, we assumed that these molecules may aggregate in a parallel way (face-to-face stacking) to form a sandwich-type arrangement (*H*-dimer) with the aid of the ArC−H···π interaction between the pyrene core combine the crystallization results.[22] Further

evidence to be confirmed, the low quantum yield of compounds **3** in the solid state are also attributed to the *H*-aggregate of the dimer, as the lowest excited energy level is forbidden.

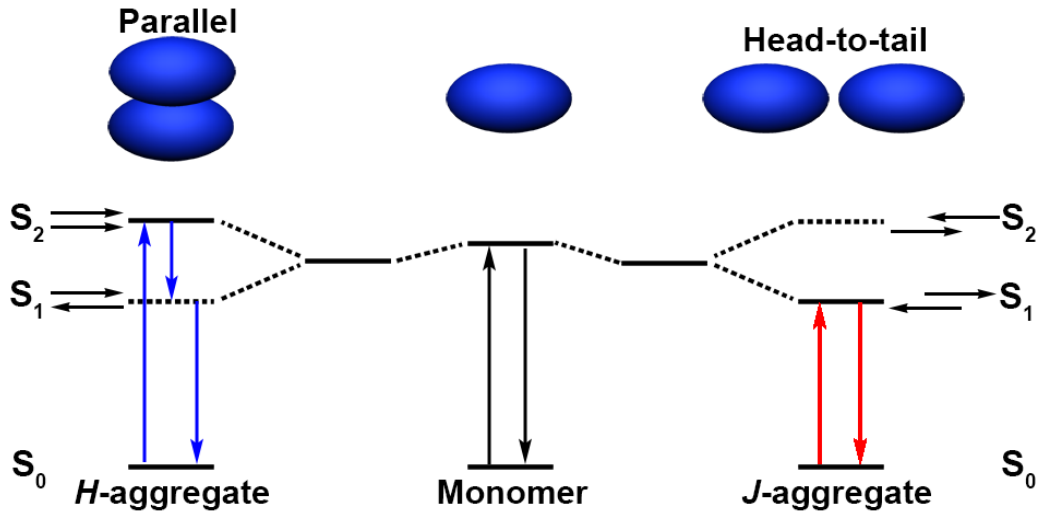


**Figure 8**. Schematic representation of the relationship between chromophore arrangement based on the molecular exciton theory.

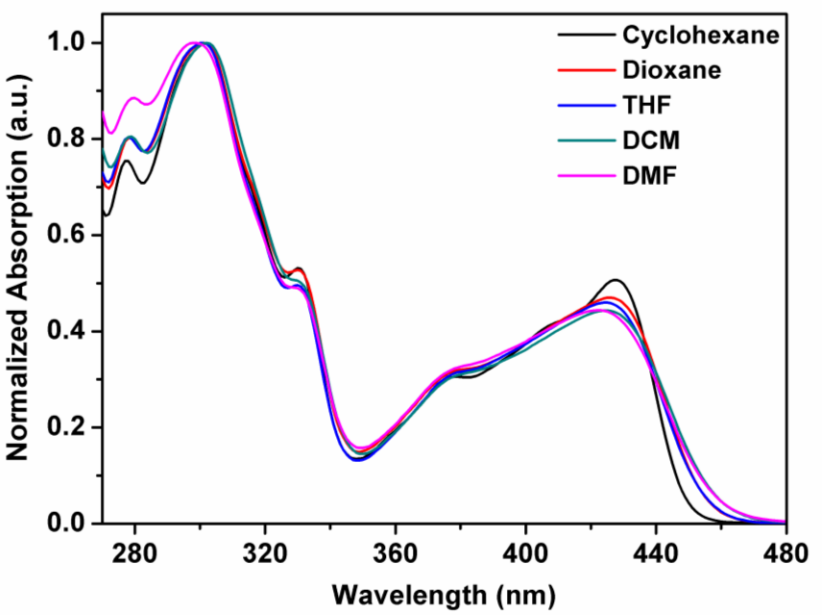


**Figure 9.** Absorption spectra of **3d** in different solvents.

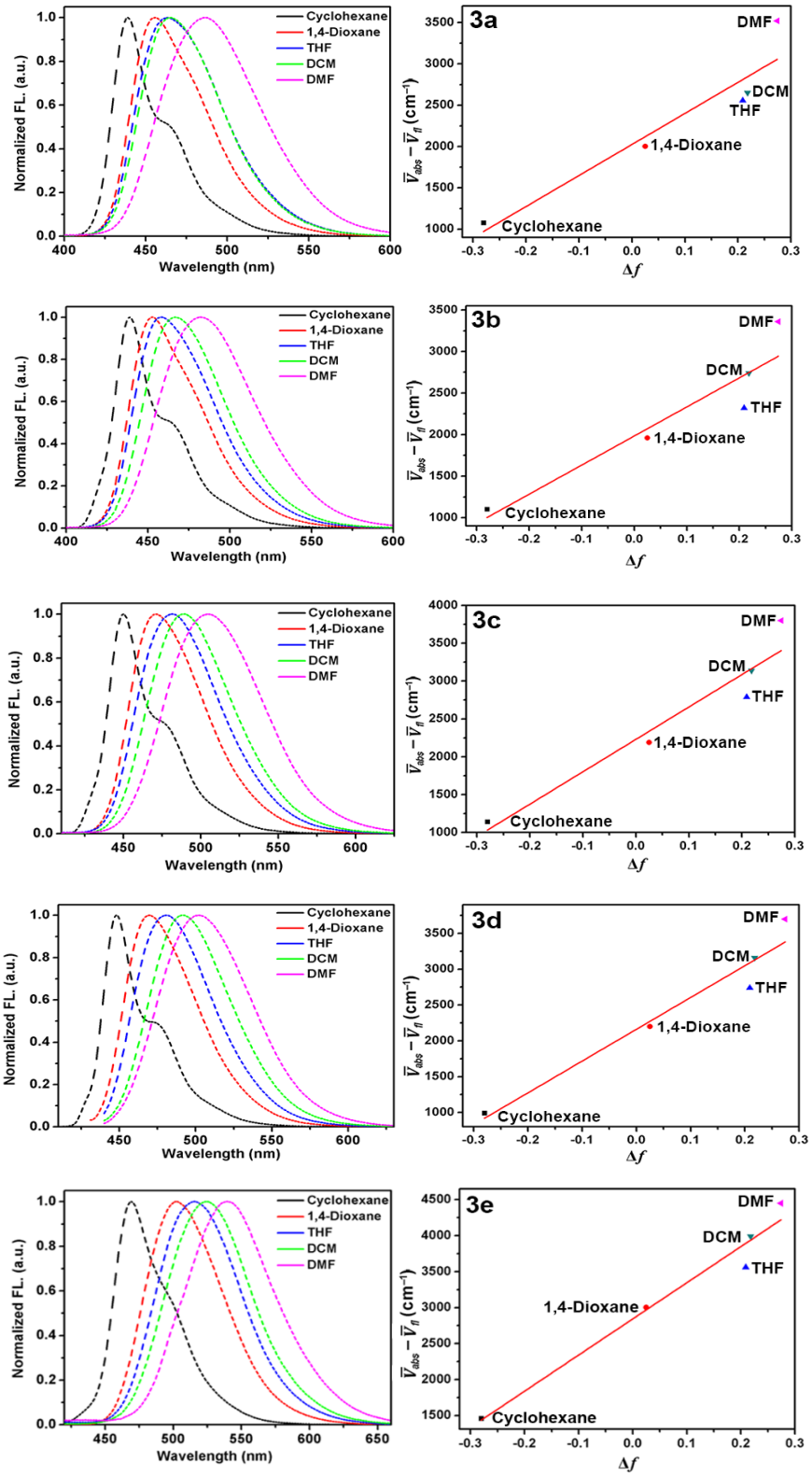


**Figure 10.** (left) Emission spectra of **3a-3e** in cyclohexane, 1,4-dioxane, THF, DCM, and DMF at room temperature. (right) Lippert-Mataga plots for compounds **3a-3e**.

The fluorescence spectra of **3a-e** are highly sensitive toward the solvent polarity, while the absorption spectra exhibit slightly shift (to see Figure 9). The spectral properties of the solvatochromism were investigated in different solvents with varying polarity (cyclohexane, 1,4-dioxane, tetrahydrofuran, dichloromethane, and dimethyl formamide), the results are shown in Figure 10. Compound **3e** is a representative example, for which Figure 10 (left) shows a significant red-shift on increasing the solvent polarity from cyclohexane to DMF (47 nm for **3a**, 43 nm for **3b**, 54 nm for **3c**, 54 nm for **3d**, 71 nm for **3e**, respectively). This phenomenon was further evaluated by the relationship between the Stokes shifts in various solvents and the Lippert equation,[23] which shows a linear correlation between these two factors (Figure 10 right). The trend in the slope of the Lippert-Mataga plots follow the order **3e** > **3d** > **3c** > **3b** ≈ **3a**, and we can find that the value of the slope of the fitting line for **3e** (5021.5) is higher than that for **3b** (3502.4), indicating the intramolecular excited state with a larger dipolar moment for the former than the latter. Also, those results reveal extraordinary sensitivity to solvent polarity. Moreover, the distinct charge separation and higher dipole moment were further confirmed in the excited state.[24]

## 3.3 Conclusions

In summary, a series of tuneable pyrene-based monomers **3a-e** were designed and synthesized by a facile strategy, and their optical properties were investigated both experimentally and computationally. It was determined that these systems exhibited predictable photophysical properties by introducing different substituents at the *para* position of the phenyl moieties. Moreover, a positive correlation between the wavelength of the $\lambda_{em\ max}$ and the Hammett $\sigma_{para}$ constants for the functional groups provided evidence that these systems may be used to tune the emission colour from blue to yellow or orange, and further investigations aimed at developing these opto-electronic materials for practical applications are ongoing in our group.

## 3.4 Experimental Section

### 3.4.1 General

All melting points (Yanagimoto MP-S1) are uncorrected. $^1$H NMR spectra (300 MHz) were recorded on a Nippon Denshi JEOL FT-300 NMR spectrometer with $SiMe_4$ as an internal reference: *J*-values are given in Hz. IR spectra were measured for samples as KBr pellets in a Nippon Denshi JIR-AQ2OM spectrophotometer. UV-vis spectra were recorded on a Perkin Elmer Lambda 19 UV/VIS/NIR spectrometer. Mass spectra were obtained on a Nippon Denshi JMS-01SA-2 spectrometer at 75 eV using a direct-inlet system.

**Materials**

Unless otherwise stated, all other reagents used were purchased from commercial sources and were used without further purification. The preparations of 2-*tert*-butylpyrene (**1**) and 7-*tert*-butyl-1,3-dibromopyrene (**2**) were described previously.[25]

### 3.4.2 Synthetic Procedures

**Synthesis of 7-*tert*-butyl-1,3-bis(*N*,*N*-bis(4'-fluorophenyl)amino)pyrene (3a)**

A mixture of 7-*tert*-butyl-1,3-dibromopyrene **2** (300 mg, 0.72 mmol), bis(4-fluorophenyl)amine (443 mg, 2.16 mmol), palladium(II) acetate (8.1 mg, 36 μmol), sodium *tert*-butoxide (416 mg, 4.33 mmol), and tri-*tert*-butylphosphine (1M in toluene, 0.07 mL, 70 μmol) in toluene (15 mL) was heated to reflux for 12 h under argon. The mixture was chilled to room temperature and quenched with water (100 mL). The mixture was extracted with dichloromethane (3 × 50 mL), and the combined extracts were washed with water and brine, dried with $MgSO_4$ and concentrated. The residue was chromatographed over silica gel (Wako C-300, 200 g) with chloroform:hexane (2:8) as eluent to give an orange solid. Recrystallization from methanol afforded 7-*tert*-butyl-1,3-bis(*N*,*N*-bis(4'-fluorophenyl)amino)pyrene **3a** (368 mg, 77%) as orange prisms. M.p. 198–200°C; $^1$H NMR (300 MHz, $CDCl_3$): $\delta_H$ = 1.53 (s, 9H, *t*Bu), 6.85–6.97 (m, 16H, Ar-*H*), 7.47 (s, 1H, pyrene-*H*), 7.88 (d, *J* = 9.2 Hz, 2H, pyrene-*H*), 8.00 (d, *J* = 9.2 Hz, 2H, pyrene-*H*), 8.13 ppm (s, 2H, pyrene-*H*); $^{13}$C NMR (100 MHz, $CDCl_3$):

$\delta_C$ = 31.8, 35.20, 115.9, 116.1, 122.8, 123.2, 123.2, 126.0, 127.7, 127.8, 128.0, 131.0, 141.6, 144.7, 144.7, 150.0, 156.9, 159.3 ppm; FAB-MS (MALDI-TOF): *m*/*z* calcd for $C_{44}H_{32}F_4N_2$ 664.2502 [$M^+$]; found 664.2526 [$M^+$].

**Synthesis of 7-*tert*-butyl-1,3-bis(*N*,*N*-diphenylamino)pyrene (3b)**

A mixture of 7-*tert*-butyl-1,3-dibromopyrene **2** (300 mg, 0.72 mmol), diphenylamine 2 (366 mg, 2.16 mmol), palladium(II) acetate (8.1 mg, 36 μmol), sodium *tert*-butoxide (416 mg, 4.33 mmol), and tri-*tert*-butylphosphine (1M in toluene, 0.07 mL, 70 μmol) in toluene (15 mL) was heated to reflux for 12 h under argon. The mixture was chilled to room temperature and quenched with water (100 mL). The mixture was extracted with dichloromethane (3 × 50 mL), and the combined extracts were washed with water and brine, dried with $MgSO_4$ and concentrated. The residue was chromatographed over silica gel (Wako C-300, 200 g) with chloroform:hexane (2:8) as eluent to give a light-yellow solid. Recrystallization from ethyl acetate afforded 7-*tert*-butyl-1,3-bis(*N*,*N*-diphenylamino)pyrene **3b** (291 mg, 68%) as light yellow prisms. M.p. 235–236°C; $^1$H NMR (300 MHz, $CDCl_3$): $\delta_H$ = 1.53 (s, 9H, *t*Bu), 6.90 (t, *J* = 7.2 Hz, 4H, Ar-*H*), 7.04 (d, *J* = 7.5 Hz, 8H, Ar-*H*), 7.16 (d, *J* = 8.0 Hz, 8H, Ar-*H*), 7.67 (s, 1H, pyrene-*H*), 7.86 (d, *J* = 9.2 Hz, 2H, pyrene-*H*), 8.06 (d, *J* = 9.2 Hz, 2H, pyrene-*H*), 8.10 ppm (s, 2H, pyrene-*H*); $^{13}$C NMR (100 MHz, $CDCl_3$): $\delta_C$ = 31.8, 35.2, 121.7, 121.8, 122.5, 123.1, 123.2, 126.8, 127.7, 127.9, 129.1, 129.2, 131.1, 141.5, 148.3, 149.8 ppm; FAB-MS (MALDI-TOF): *m*/*z* calcd for $C_{44}H_{36}N_2$ 592.2878 [$M^+$]; found 592.2865 [$M^+$].

**Synthesis of 7-*tert*-butyl-1,3-bis(*N*,*N*-bis(4'-methylphenyl)amino)pyrene (3c)**

A mixture of 7-*tert*-butyl-1,3-dibromopyrene **2** (300 mg, 0.72 mmol), bis(4-methylphenyl)amine (426 mg, 2.16 mmol), palladium(II) acetate (8.1 mg, 36 μmol), sodium *tert*-butoxide (416 mg, 4.33 mmol), and tri-*tert*-butylphosphine (1M in toluene, 0.07 mL, 70 μmol) in toluene (15 mL) was heated to reflux for 12 h under argon. The mixture was chilled to room temperature and quenched with water (100 mL). The mixture was extracted with dichloromethane (3 × 50 mL), and the combined extracts were washed with water and brine, dried with $MgSO_4$ and concentrated. The residue was chromatographed over silica gel (Wako C-300, 200 g) with chloroform:hexane (2:8) as eluent to give a light-yellow solid.

Recrystallization from ethyl acetate afforded 7-*tert*-butyl-1,3-bis(*N*,*N*-bis(4'-methylphenyl)amino)pyrene **3c** (387 mg, 82%) as light-yellow prisms. M.p. 224–225°C; $^1$H NMR (300 MHz, $CDCl_3$): $\delta_H$ = 1.52 (s, 9H, *t*Bu), 2.25 (s, 12H, Me), 6.91 (d, *J* = 8.8 Hz, 8H, Ar-*H*), 6.96 (d, *J* = 8.4 Hz, 8H, Ar-*H*), 7.60 (s, 1H, pyrene-*H*), 7.83 (d, *J* = 9.2 Hz, 2H, pyrene-*H*), 8.06 (d, *J* = 9.7 Hz, 2H, pyrene-*H*), 8.07 ppm (s, 2H, pyrene-*H*); $^{13}$C NMR (100 MHz, $CDCl_3$): $\delta_C$ = 20.7, 31.8, 35.1, 121.7, 122.3, 123.3, 126.4, 127.2, 127.9, 128.9, 129.6, 130.8, 131.1, 142.0, 146.2, 149.6 ppm; FAB-MS (MALDI-TOF): *m*/*z* calcd for $C_{48}H_{44}N_2$ 648.3504 [$M^+$]; found 648.3521 [$M^+$].

**Synthesis of 7-*tert*-butyl-1,3-bis(*N*,*N*-bis(4'-*tert*-butylphenyl)amino)pyrene (3d)**

A mixture of 7-*tert*-butyl-1,3-dibromopyrene **2** (300 mg, 0.72 mmol), bis(4-*tert*-butylphenyl)amine (607 mg, 2.16 mmol), palladium(II) acetate (8.1 mg, 36 μmol), sodium *tert*-butoxide (416 mg, 4.33 mmol), and tri-*tert*-butylphosphine (1M in toluene, 0.07 mL, 70 μmol) in toluene (15 mL) was heated to reflux for 12 h under argon. The mixture was chilled to room temperature and quenched with water (100 mL). The mixture was extracted with dichloromethane (3 × 50 mL), and the combined extracts were washed with water and brine, dried with $MgSO_4$ and concentrated. The residue was chromatographed over silica gel (Wako C-300, 200 g) with chloroform:hexane (3:7) as eluent to give an orange solid. Recrystallization from methanol afforded 7-*tert*-butyl-1,3-bis(*N*,*N*-bis(4'-*tert*-butylphenyl)amino)pyrene **3d** (588 mg, 73%) as yellow prisms. M.p. 229–230°C; $^1$H NMR (300 MHz, $CDCl_3$): $\delta_H$ = 1.27 (s, 18H, *t*Bu), 1.29 (s, 9H, *t*Bu), 6.99 (t, *J* = 8.1 Hz, 7H, Ar-*H*), 7.07 (d, *J* = 7.6 Hz, 2H, Ar-*H*), 7.18 (t, *J* = 8.1 Hz, 7H, Ar-*H*), 7.75 (d, *J* = 7.6 Hz, 1H, pyrene-*H*), 7.86 (t, *J* = 8.6 Hz, 2H, pyrene-*H*), 8.10 ppm (m, 4H, pyrene-*H*); $^{13}$C NMR (100 MHz, $CDCl_3$): $\delta_C$ = 31.4, 31.8, 34.1, 35.1, 121.0, 122.3, 123.2, 123.4, 125.8, 126.9, 127.3, 127.9, 128.9, 129.3, 131.1, 134.7, 141.7, 144.1, 145.7, 149.6 ppm; FAB-MS (MALDI-TOF): *m/z* calcd for $C_{60}H_{68}N_2$ 816.5383 [$M^+$]; found 816.5383 [$M^+$].

**Synthesis of 7-*tert*-butyl-1,3-bis(*N*,*N*-bis(4'-methoxyphenyl)amino)pyrene (3e)**

A mixture of 7-*tert*-butyl-1,3-dibromopyrene **2** (300 mg, 0.72 mmol), bis(4-methoxyphenyl)amine (495 mg, 2.16 mmol), palladium(II) acetate (8.1 mg, 36 μmol), sodium

*tert*-butoxide (416 mg, 4.33 mmol), and tri-*tert*-butylphosphine (1M in toluene, 0.07 mL, 70 μmol) in toluene (15 mL) was heated to reflux for 12 h under argon. The mixture was chilled to room temperature and quenched with water (100 mL). The mixture was extracted with dichloromethane (3 × 50 mL), and the combined extracts were washed with water and brine, dried with $MgSO_4$ and concentrated. The residue was chromatographed over silica gel (Wako C-300, 200 g) with chloroform:hexane (8:2) as eluent to give an orange solid. Recrystallization from ethyl acetate afforded 7-*tert*-butyl-1,3-bis(*N*,*N*-bis(4'-methoxyphenyl)amino)pyrene **3e** (370 mg, 72%) as orange prisms. M.p. 260–261°C; $^1$H NMR (300 MHz, $CDCl_3$): $\delta_H$ = 1.52 (s, 9H, *t*Bu), 3.74 (s, 12H, OMe), 6.72 (d, *J* = 9.2 Hz, 8H, Ar-*H*), 6.92 (d, *J* = 9.0 Hz, 8H, Ar-*H*), 7.48 (s, 1H, pyrene-*H*), 7.80 (d, *J* = 9.3 Hz, 2H, pyrene-*H*), 8.04 (d, *J* = 8.4 Hz, 2H, pyrene-*H*), 8.06 ppm (s, 2H, pyrene-*H*); $^{13}$C NMR (100 MHz, $CDCl_3$): $\delta_C$ = 31.8, 35.1, 55.5, 114.5, 122.1, 123.2, 123.3, 123.4, 125.3, 126.8, 127.6, 128.0, 131.2, 142.5, 142.7, 149.5, 154.5 ppm; FAB-MS (MALDI-TOF): *m*/*z* calcd for $C_{48}H_{44}N_2O_4$ 712.3301 [$M^+$]; found 712.3286 [$M^+$].

### 3.4.3 X-ray Crystallography

A suitable single crystal (0.87 × 0.63 × 0.43 $mm^3$) was selected and mounted on a Bruker APEX 2 CCD diffractometer equipped with graphite-monochromated Mo-Kα radiation for **3e**.[26] Data were corrected for Lorentz and polarisation effects and for absorption.[26] The structure was solved by direct methods and refined routinely except that atoms C36 > C41 & O(3) were modelled as disordered over two sets of positions with major component 51.3(3)%. Details of the crystal parameters, data collection conditions, and refinement parameters[27] for the compound **3e** are summarized in Tables S1–2. Crystallographic data for the structure in this paper have been deposited with the Cambridge Crystallographic Data Centre as supplementary publication number CCDC 1537633. Copies of the data can be obtained, free of charge, on application to CCDC, 12 Union Road, Cambridge CB2 1EZ, UK [fax: 144-1223-336033 or e-mail: deposit@ccdc.cam.ac.uk].

Unless otherwise stated, all reagents were purchased from commercial sources and used without further purification. All solvents were dried and distilled by the usual procedures before use. Melting points were determined using a Yanagimoto MP-S1. $^1$H NMR and $^{13}$C NMR spectra were recorded on a Nippon Denshi JEOL FT-300 NMR

spectrometer and a Varian-400MRvnmrs400 with $SiMe_4$ as an internal reference: *J*-values are given in Hz. UV spectra were measured by a Shimadzu UV-3150UV-vis-NIR spectrophotometer. Fluorescence spectroscopic studies of compounds in solution were performed in a semi-micro fluorescence cell (Hellma®, 104F-QS, 10 × 4 mm, 1400 μL) with a Varian Cary Eclipse spectrophotometer. Mass spectra were obtained on a Nippon Denshi JMS-01SG-2 mass spectrometer at an ionization energy of 70 eV using a direct inlet system through GLC.

## 3.5 References


1. (a) *Functional Organic Materials - Syntheses, Strategies, and Applications*, Müller, T. J. J., Bunz, U. H. F., Ed.; WileyVHC: Weinheim, **2007**. (b) Zhu, M.; Yang, C. *Chem. Soc. Rev.* **2013**, *42*, 4963–4976. (c) Maggini, L.; Bonifazi, D. *Chem. Soc. Rev.* **2012**, *41*, 211–241. (d) Reineke, S.; Rosenow, T. C.; Lüssem, B.; Leo, K. *Adv. M*eter. **2010**, *22*, 3189−3193. (e) Fan, C.; Zhu, L.; Liu, T.; Jiang, B.; Ma, D.; Qin, J.; Yang, C. *Angew. Chem., Int. Ed.* **2014**, *53*, 2147−2151.
2. (a) Kido, J.; Okamoto, Y. *Chem. Rev.* **2002**, *102*, 2357−2368. (b) Samuel, I. D. W.; Turnbull, G. A. *Chem. Rev.* **2007**, *107*, 1272−1295. (c) Grimsdale, A. C.; Leok Chan, K.; Martin, R. E.; Jokisz, P. G.; Holmes, A. B. *Chem. Rev.* **2009**, *109*, 897−1091.
3. (a) Stender, A. S.; Marchuk, K.; Liu, C.; Sander, S.; Meyer, M. W.; Smith, E. A.; Neupane, B.; Wang, G.; Li, J.; Cheng, J.-X.; Huang, B.; Fang, N. *Chem. Rev.* **2013**, *113*, 2469−2527. (b) Wang, X. H.; Guo, Z. Q.; Zhu, S. Q.; Liu, Y. J.; Shi, P.; Tian, H.; Zhu, W. H. *J. Mater. Chem. B* **2016**, *4*, 4683−4689.
4. (a) Zhang, R.; Zhao, Y.; Zhang, T. F.; Xu, L.; Ni, Z. H. Dyes Pigments **2016**, *130*, 106−115. (b) Lee, S. Y.; Yasuda, T.; Yang, Y. S.; Zhang, Q. S.; Adachi, C. *Angew. Chem., Int. Ed.* **2014**, *53*, 6402−6406. (c) Han, M. G.; Park, K. -B.; Bulliard, X.; Lee, G. H.; Yun, S.; Leem, D. -S.; Heo, C. -J.; Yagi, T.; Sakurai, R.; Ro, T.; Lim, S. -J.; Sul, S.; Na, K.; Ahn, J.; Jin, Y. W.; Lee, S. *ACS Appl. Mater. Interfaces* **2016**, *8*, 26143−26151.
5. (a) Shen, X.; Wang, Y.; Zhao, E.; Yuan, W.; Liu, Y.; Lu, P.; Qin, A.; Ma, Y.; Sun, J.; Tang, B. Z. *J. Phys. Chem. C* **2013**, *117*, 7334−7347. (b) Xue, v; Liu, W.; Qiu, X.; Gao, Y.; Yang, W. *J. Phys. Chem. C* **2014**, *118*, 18668−18675.
6. (a) Zhu, L. M.; Xu, J. C.; Sun, Z.; Fu, B. Q.; Qin, C. Q.; Zeng, L. T.; Hu, X. C. *Chem. Commun.* **2015**, *51*, 1154−1156. (b) Teran, N. B.; He, G. S.; Baev, A.; Shi, Y. R.; Swihart, M. T.; Prasad, P. N.; Marks, T. J.; Reynolds, J. R. *J. Am. Chem. Soc.* **2016**, *138*, 6975−6984.
7. Saigusa, H.; Lim, E. C. *Acc. Chem. Res.* **1996**, *29*, 171−178.
8. Hsieh, C. C.; Jiang, C. M.; Chou, P. T. *Acc. Chem. Res.* **2010**, *43*, 1364−1374.
9. Levi, L.; Müller, T. J. J. *Chem. Soc. Rev.* **2016**, *45*, 2825–2846.

10. (a) Khramov, D. M.; Bielawski, C. W. *J. Org. Chem.* **2007**, *72*, 9407−9417. (b) Feng, X.; Tomiyasu, H.; Hu, J. Y.; Wei, X. F.; Redshaw, C.; Elsegood, M. R.J.; Horsburgh, L.; Teat, S. J.; Yamato, T. *J. Org. Chem.* **2015**, *80*, 10973−10978. (c) McNamara, L. E.; Liyanage, N.; Peddapuram, A.; Murphy, J. S.; Delcamp, J. H.; Hammer, N. I. *J. Org. Chem.* **2016**, *81*, 32−42.
11. Figueira-Duarte, T. M.; Müllen, K. *Chem. Rev.* **2011**, *111*, 7260−7314.
12. Misra, R.; Gautam, P.; Mobin, S. M. *J. Org. Chem.* **2013**, *78*, 12440−12452.
13. (a) Oseki, Y.; Fujitsuka, M.; Sakamoto, M.; Majima, T. *J. Phys. Chem. A* **2007**, *111*, 9781−9788. (b) Yang, S. W.; Elangovan, A.; Hwang, K. C.; Ho, T. I. *J. Phys. Chem. B* **2005**, *109*, 16628−16635. (c) Sessler, J. L.; Karnas, E.; Kim, S. K.; Ou, Z. P.; Zhang, M.; Kadish, K. M.; Ohkubo, K.; Fukuzumi, S. *J. Am. Chem. Soc.* **2008**, *130*, 15256−15257.
14. Feng, X.; Hu, J. Y.; Redshaw, C.; Yamato, T. *Chem. Eur. J.* **2016**, *22*, 11898−11916.
15. Jérome, D.; Schulz, H. J. *Advances in Physics* **2002**, *51*, 293−479.
16. (a) Xiao, L. X.; Chen, Z. J.; Qu, B.; Luo, J. X.; Kong, S.; Gong, Q. H.; Kido, J. *Adv. Mater.* **2011**, *23*, 926–952. (b) Ying, L.; Ho, C-L.; Wu, H. B.; Cao, Y.; Wong, W-Y. *Adv. Mater.* **2014**, *26*, 2459–2473.
17. (a) Xia, H.; Liu, D. Q.; Song, K. S.; Miao, Q. *Chem. Sci.* **2011**, *2*, 2402−2406. (b) Wang, C. Z.; Kihara, R.; Feng. X.; Thuéry, P.; Redshaw, C.; Yamato, T. *ChemistrySelect* **2017**, *2*, 1436−1441.
18. (a) Shizu, K.; Tanaka, H.; Uejima, M.; Sato, T.; Tanaka, K.; Kaji, H.; Adachi, C. *J. Phys. Chem. C* **2015**, *119*, 1291−1297. (b) Rajamalli, P.; Senthilkumar, N.; Gandeepan, P.; Huang, P. Y.; Huang, M. J.; Ren-Wu, C. Z.; Yang, C. Y.; Chiu, M. J.; Chu, L. K.; Lin, H. W.; Cheng, C. H. *J. Am. Chem. Soc.* **2016**, *138*, 628−634.
19. Sasabe, H.; Kido, J. *J. Mater. Chem. C* **2013**, *1*, 1699−1707.
20. Feng, X.; Hu, J. Y.; Tomiyasu, H.; Tao, Z.; Redshaw, C.; Elsegood, M. R. J.; Horsburgh, L.; Teat, S. J.; Wei, X. F.; Yamato, T. *RSC Adv.* **2015**, *5*, 8835–8848.
21. (a) Jelley, E. E. *Nature* **1936**, *138*, 1009−1010. (b) Kasha, M.; Rawls, H. R.; Ashraf El-Bayoumi, M. *Pure Appl. Chem.* **1965**, *11*, 371−392. (c) Lanzani, G. *Photophysics Behind Photovoltaics and Photonics Wiley*, **2002**. (d) Heyne, B. *Photochem. Photobiol. Sci.* **2016**, *15*, 1103–1114.

22. Snow, A. W. *The Porphyrin Handbook*, **2003**,*17*. 129–176.
23. (a) Lippert, V. E.; *Z. Naturforsch. A: Phys. Sci.* **1955**, *10*, 541–545. (b) Mataga, N.; Kaifu, Y.; Koizumi, M. *Bull. Chem. Soc. Jpn.* **1956**, *29*, 465–470.
24. (a) Jadhav, T.; Dhokale, B.; Patil, Y.; Mobin, S. M.; Misra, R. *J. Phys. Chem. C* **2016**, *120*, 24030−24040. (b) Tayade, R. P.; Sekar, N. *J. Lumin.* **2016**, *176*, 298−308. (c) Lim, C-H.; Ryan, M. D.; McCarthy, B. G.; Theriot, J. C.; Sartor, S. M.; Damrauer, N. H.; Musgrave, C. B.; Miyake, G. M. *J. Am. Chem. Soc.* **2017**, *139*, 348−355.
25. Feng, X.; Hu, J. Y.; Yi, L.; Seto, N.; Tao, Z.; Redshaw, C.; Elsegood, M. R. J.; Yamato, T. *Chem. - Asian J.* **2012**, *7*, 2854−2863.
26. APEX 2 & SAINT. Software for CCD Diffractometers. Madison, USA: Bruker AXS Inc; **2012**.
27. Sheldrick, G. M. *Acta Crystallogr.* **2015**, *C71*, 3−8.

# Chapter 4

# Synthesis and photophysical properties of regioselective substituted pyrene-based fluorophores

*In this chapter, a controllable regioselective approach to achieve dipolar functionalization at the active sites (1,3-positions) and K-region (5,9-positions) of pyrene is demonstrated. Following this strategy, a set of dipo-lar 1,3-diphenyl-5,9-di(4-R-phenylethynyl)pyrenes were successful synthesized and systematically inves-tigated by 1H/13C NMR spectroscopy, X-ray crystallography, electronic spectra, as well as by theoretical calculations. Further, by adjusting the substituents at the 5,9-positions of pyrene, the pyrene-based dipo-lar molecules 4 exhibit wide tunable emission from blue (474 nm) to orange-red (566 nm).*

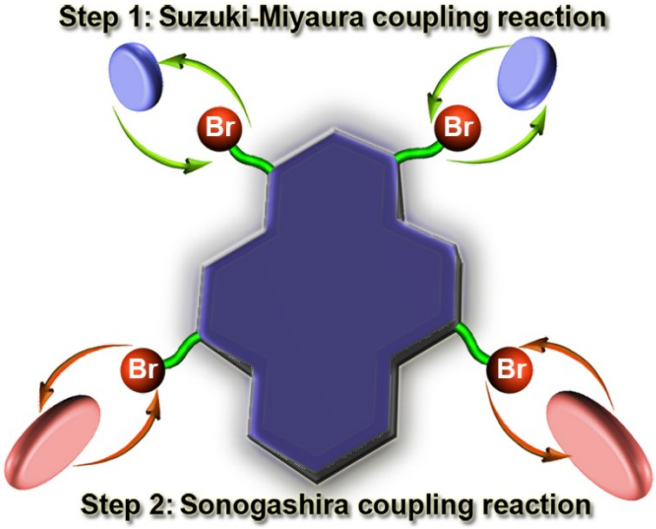


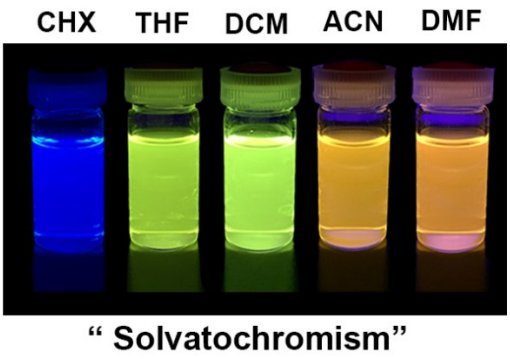

## 4.1 Introduction

The design and synthesis of tuneable emission materials has been an attractive research topic in both academic and commercial arenas, for example, multicolored emission materials have an extremely wide range of potential applications in light emitting displays,[1] multicolor lasers,[2] and organic light emitting diodes (OLEDs).[3] On the other hand, the construction of novel fluorophores with tuneable emission colors is achieved by adjusting the structure and thereby altering the transition-energy levels as evidenced by chemical/physical methods.[4] Generally, most strategies have relied on fine-tuning of the host materials for the wide-range altering of the emission colors, which involves the introduction of various electron donating or withdrawing groups to the host compounds,[5,6] tuning the particle size[7] or molecular weight (for polymers)[8] or by voltage-controlled electroluminescence (EL) technology.[9] Nevertheless, to achieve a tuneable emission material with satisfactory properties for high-performance devices remains a challenge. Moreover, understanding of the underlying structure-property relationship of such systems is still a topic of on-going interest. For conventional organic synthetic approaches, push-pull chromophores play a significant role in constructing tuneable emission molecules which can exhibit a wide emission range from deep blue to red, and even to the near infrared (NIR) region.[7,10]

The chemistry of pyrene exhibits strong positional dependence along the long axis (active site of 1-, 3-, 6- and 8- positions and plane node of 2,7-positions) and the short axis (K-region of 4-, 5-, 9- and 10-positions). Theory and experimental studies show that the substitution position can affect the intramolecular electron-transfer process.[11] For example, the uridine ring exhibited a weak electronic interaction between uridine and the pyrene core, which directly attached at the 2-position of pyrene compared with the 1-position.[12] Meanwhile, given the $S_1 \leftarrow S_0$ and $S_3 \leftarrow S_0$ transitions are polarized along the short axis of pyrene, introducing appropriate moieties into the K-region of pyrene may lead to a distinct change of the energy of the $S_1 \leftarrow S_0$ and $S_3 \leftarrow S_0$ excitations.[11] Based on previously theories, it seems that the pyrene-based push-pull molecules would exhibit interesting optical properties when functionalization of pyrene both at long axis and K-regions has occurred.

However, there are challenging issues regarding regioselectivity for modifying the pyrene core. In an effort to conquer these difficulties, a number of reliable strategies were established to modify the active sites of pyrene.[13] By contrast, functionalization at the K-region of pyrene is attractive but difficult to carry out. To date, several attempts have been made to exploit this region, including oxidation,[14] bromination,[15] nitration,[16] and formylation[17] reactions. However, multistep routes, low selectivity, and harsh conditions have driven us to explore more effective strategies for regioselective substitution at the K-region of pyrene.

## 4.2 Results and Discussion

### 4.2.1 Synthesis and Characterization

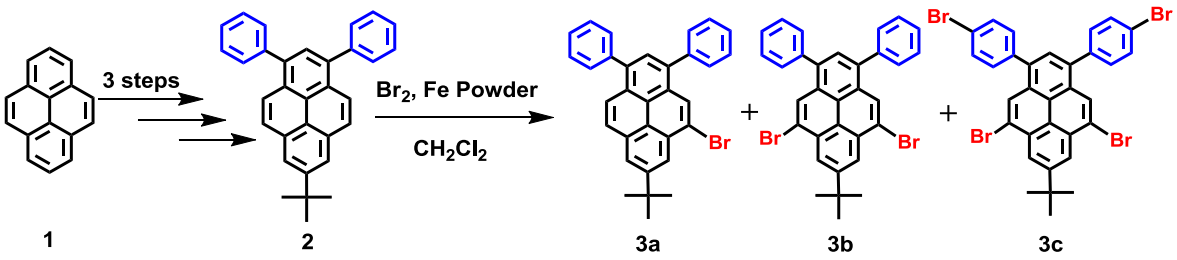


**Scheme 1.** Synthetic route of precursor molecules **3.**

To fulfil these requirements, we present herein an innovative and direct strategy to eliminate the problematic issues discussed above, see Scheme 1, by constructing a new push-pull structure (dipolar molecules) to achieve functionalization at the active sites (1,3-positions) and K-region (5,9-positions) of pyrene based on the activity of the bromination reaction. Using 7-*tert*-butyl-1,3-diphenylpyrene (**2**)[18] as the key starting material, 7-*tert*-butyl-1,3-diphenyl-5,9-dibromopyrene **3b** was then prepared from **2** with 3.0 equiv. bromine in $CH_2Cl_2$ in the presence of iron-powder in high yield (up to 83%).It is worth noting that this type of reaction did not occur in the absence of iron powder and only a trace amount of **3a** was detected (entry 1). Moreover, in order to optimize and improve this practical strategy, we carried out this reaction under different conditions, and an efficient, controllable bromination strategies were established. These optimized conditions and results are summarized in Table 1. Generally, for the selectivity of functionalization at the K-region and *para* position of phenyl ring depends on the activity in different sites by adjusting the amount of bromine and iron powder. This is the first reported example of the controllable, regioselective, and highly efficient bromination of pyrene at the K-region positions, and this highlighting methodology indeed exhibited the significance to stimulate new fundamental and theoretical studies, which is helpful to understand the mechanism of the molecular structure and photophysical properties. A set of dipolar fluorophores **4**, based on this intermediate bromopyrene **3b**, were then obtained, in considerable yields, by a Sonogashira coupling reaction (Scheme 2). The detailed synthetic procedures are described in Experimental Section; all the new compounds **3**, **4**, were fully

characterized by $^{1}H/^{13}C$ NMR spectroscopy and high resolution mass spectrometry. The thermal properties of **4a–f** were studied using thermogravimetric analysis (TGA) under a nitrogen atmosphere at a heating rate of 10 °C $min^{-1}$, as shown in Table 2 and Figure 1. It can be seen that fluorophores **4** showed very high thermal stability with decomposition temperatures ($T_d$) of 356 to 527 °C and melting temperatures ($T_m$) of 256 to 352 °C. These results revealed that the fluorophores **4** showed high thermal stabilities, which suggest great potential application in organic electronics applications.

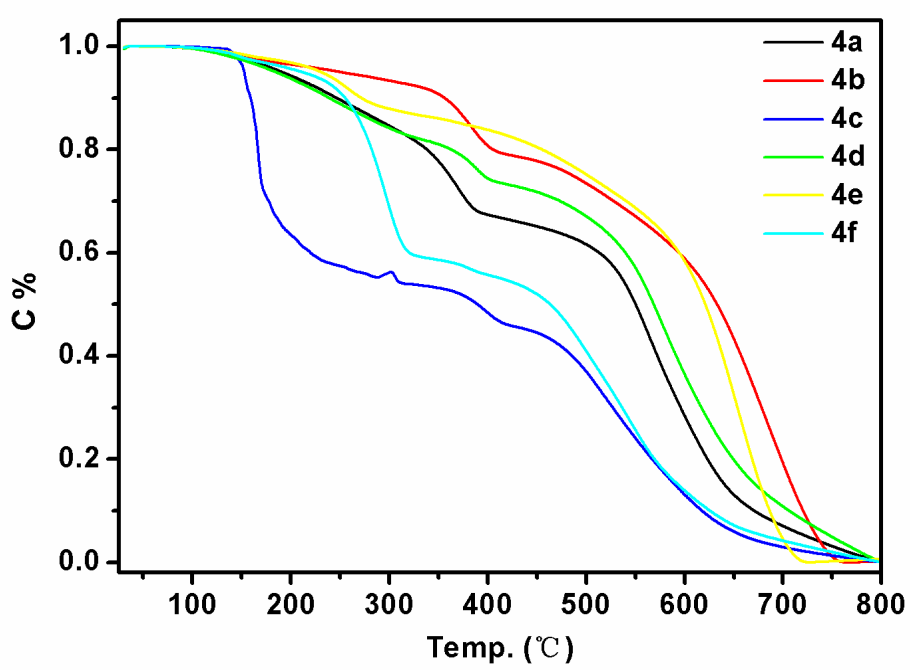


**Figure 1** TGA thermograms of compounds **4**.

**Table 1.** Optimization of reaction conditions to precursors **3.**

| Entry | Substrate **1** (equiv) | $Br_2$ (equiv) | Fe (equiv) | Products [%][a] |
|---|---|---|---|---|
| 1 | 1.0 | 1.5 | -- | **3a** [<5][b] |
| 2 | 1.0 | 1.5 | 1.5 | **3a** [65] |
| 3 | 1.0 | 3.0 | 3.0 | **3b** [83] |
| 4 | 1.0 | 6.0 | 6.0 | **3c** [71] |

[a] The isolated yields are shown in bracket.

[b] Yield was determined by $^{1}H$ NMR analysis.

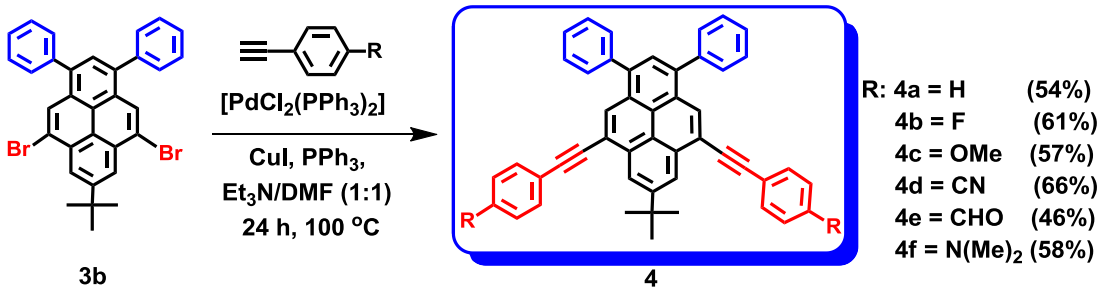


**Scheme 2.** Synthetic route of dipolar molecules **4.**

## 4.2.2 Crystallography

After numerous attempts, a crystal suitable for single crystal X-ray diffraction of the fluorophore **4c** was cultivated from a $CHCl_3$/hexane solution, and the exact conformation was unambiguously established (Figure 2a). The crystal structure of **4c** reveals that the molecular displays a more planar conformation with a tightly layered arrangement, which was attributed to the twist angles between the central pyrene (C1 > C 16) and terminal phenyl moieties at the 1,3-positions (61.09(8)°, 48.83(7)°), and the $C_6$ aromatic rings at the 5,9-positions (27.78(7)°, 24.65(6)°); the latter is less than previously reported between the pyrene core and substituents at the 1,3,5,9-positions.[18,19] Pairs of short π···π interactions were observed (3.25−3.35 Å) from the pyrene core to both $C_6H_4OMe$ rings (shown in blue dashed lines). The intermolecular π···π interactions combined with weak intermolecular hydrogen bonded interactions (green dashed lines) result in sheet-like stacks (Figure 2b).

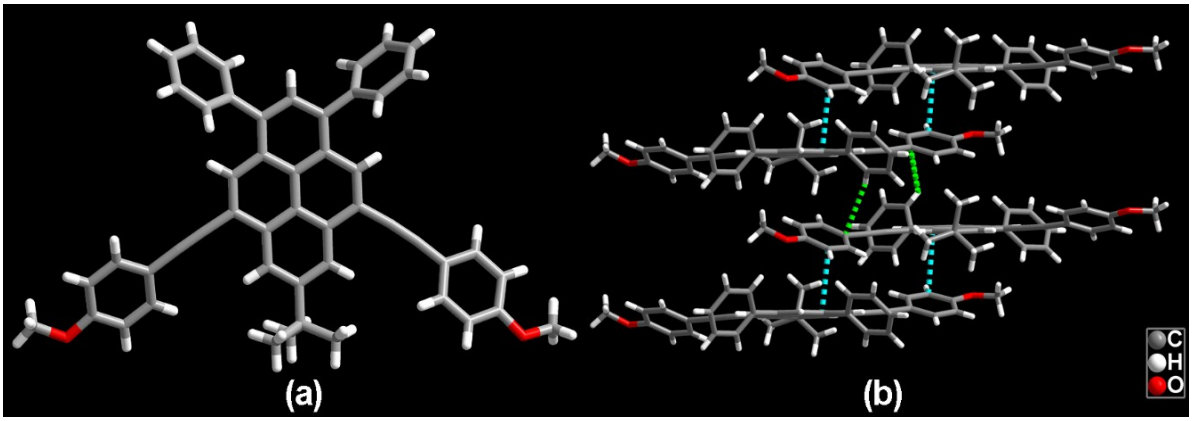


**Figure 2.** (a)The crystal structure of fluorophore **4c**; (b) the principal intermolecular packing interactions.

### 4.2.3 Density functional theoretical calculation

Density functional theory (DFT) calculations (B3LYP/6-31 g*) were performed in order to gain a deeper insight into the relationship between the structures and properties. The value and contours of the highest occupied molecular orbitals (HOMOs) and the lowest unoccupied molecular orbitals (LUMOs) of **4** are provided in Table 2 and Figure 3. As depicted in Figure 4, the contours of the HOMOs and LUMOs of **4** present a reasonable difference. The HOMOs of **4a**–**e** are mainly distributed on the pyrene core, which resulted from the weak electron-donating ability of the phenyl moiety, while the HOMOs of **4f** are spread over the arylethynyl moiety and the pyrene core, which was attributed to the strong electron-donating nature of the *N*,*N*-dimethylamino groups. The LUMOs are mostly localized on the pyrene core and alkynyl moiety, especially for **4d**, **4e**, because of the strong electron-withdrawing ability of the -CN and -CHO moieties. The theoretical results demonstrate that the ability for intramolecular charge transfer of **4d**–**f** allows them to exhibit enhanced ICT character versus **4a**–**c**. In other words, the emission behavior is sensitive to environmental change, which impacts on the separation of the HOMOs and LUMOs, particularly polarity.[20]

**Table 2.** The physical properties of compounds of type **4a**–**f**.

| R | $\lambda_{abs}$ (nm) sol[a] [$\varepsilon$ ($M^{-1}$ $cm^{-1}$ L)] | $\lambda_{PL}$ (nm) sol[a]/film[b] | $T_d$ (°C)[c] | HOMO (eV)[d] | LUMO (eV)[d] | $E_g$ (eV)[d] | HOMO (eV)[e] | LUMO (eV)[f] | $E_g$ (eV)[g] | $\Phi_{PL}$(%) sol[a]/film[b] |
|---|---|---|---|---|---|---|---|---|---|---|
| **4a** | 335 (34481), 392 (34066) | 427/566 | 525 | –5.00 | –1.93 | 3.07 | –5.55 | –2.39 | 2.78 | 89/9 |
| **4b** | 334 (38933), 393 (38486) | 426/504 | 356 | –5.06 | –2.01 | 3.05 | –5.57 | –2.41 | 2.77 | 94/7 |
| **4c** | 354 (51366), 395 (42182) | 431/511 | 477 | –4.84 | –1.79 | 3.05 | –5.52 | –2.38 | 2.87 | 98/6 |
| **4d** | 336 (44478), 375 (49021) | 452/474 | 527 | –5.41 | –2.47 | 2.94 | –5.64 | –2.33 | 2.78 | 95/23 |
| **4e** | 339 (55292), 378 (54779) | 504/521 | 356 | –5.33 | –2.42 | 2.91 | –5.61 | –2.33 | 2.58 | 71/4 |
| **4f** | 354 (73883), 381 (81269) | 520/513 | 460 | –4.54 | –1.63 | 2.91 | –5.15 | –1.90 | 2.64 | 54/3 |

[a] Measured in dichloromethane at room temperature. [b] As a thin film. [c] Obtained from TGA measurements. [d] DFT/B3LYP/6-31G* using Gaussian. [e] Measured from the oxidation potential in $CH_2Cl_2$ solution by cyclic voltammetry. [f] Calculated from HOMO + $E_g$. [g] Estimated from the absorption edge of UV-Vis spectra.

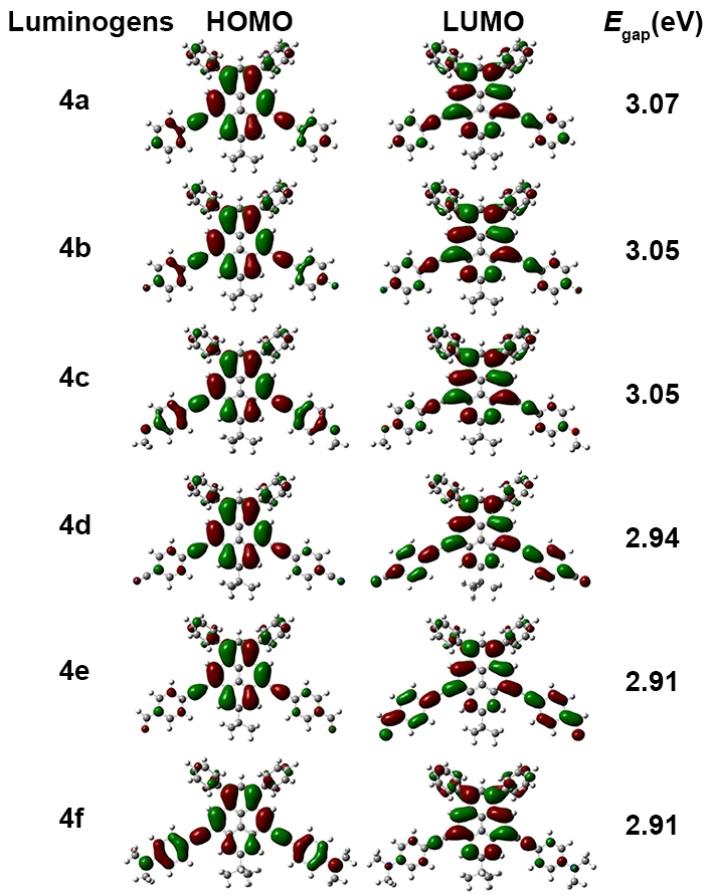


**Figure 3.** Frontier molecular orbitals HOMOs and LUMOs of **4a**–**4f**.

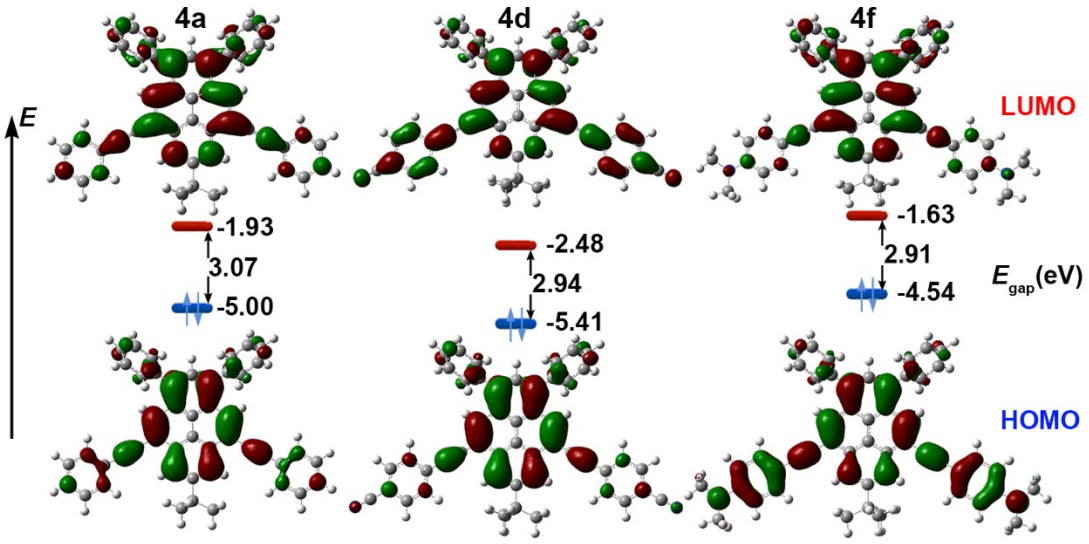


**Figure 4.** Frontier-molecular-orbital distributions and energy levels diagram of **4a**, **4d** and **4f** by DFT calculations.

### 4.2.4 Optical properties

Further investigations of the photophysical properties were carried out both in solution and in the solid state based on our preliminary theoretical guidance. As depicted in Figure 5 and Table 2, two sets of pronounced absorption bands were observed for fluorophores **4**, mainly centered at 334–354 nm (high-energy band), and 375–395 nm (low-energy band). More specifically, the high-energy band is mainly associated with the $S_2 \leftarrow S_0$ and $S_1 \leftarrow S_0$ absorption transitions of the arylethynyl and pyrene core with high molar absorption coefficients (34481−73883 $cm^{-1}$ $M^{-1}$). The values exhibit an increasing trend following the order from **4a** to **4f**, while the molar absorption coefficient of low-energy (34066−81269 $cm^{-1}$ $M^{-1}$) also follow this trend. Further, a weak band in the high-energy absorption region (299−308 nm) can be ascribed to the $S_3 \leftarrow S_0$ transitions of the phenyl and pyrene core with low molar absorption coefficients (31608−55690 $cm^{-1}$ $M^{-1}$).[11] This low-energy absorption band for **4** indicates that their excited states possess significant charge transfer (CT) absorption associated with the ICT from the 1,3-diphenyl to the 5,9-diarylethynyl terminal substituents via the pyrene core, which is also consistent with the separation of the HOMO and LUMO distributions as determined by the DFT calculations.

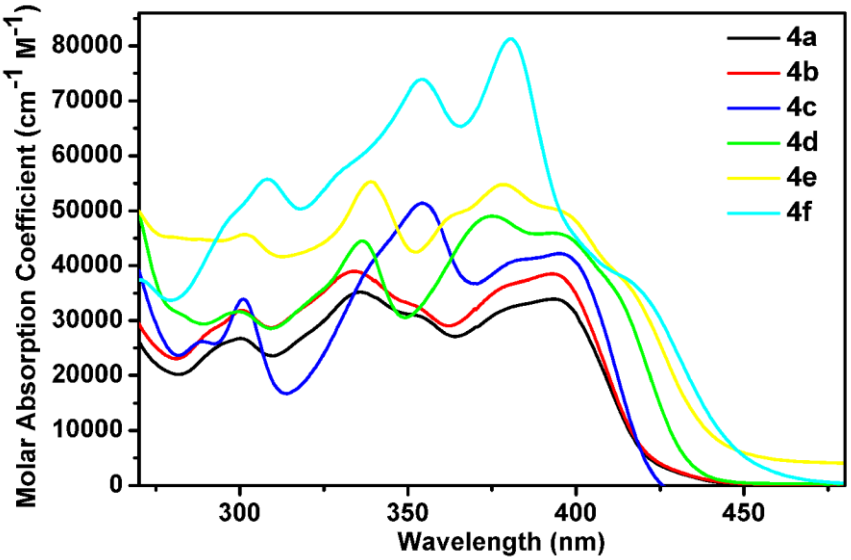


**Figure 5.** Normalized UV–vis absorption spectra of compounds **4** recorded in dichloromethane solutions at ~$10^{-5}$ M at 25 °C.

Enough interest was aroused to investigate the emission properties because of their sensitive molar absorption coefficients, arising from the small differences in their substituents at the para position of the arylethynyl group. For example, these six fluorophores **4** exhibit distinct emission properties and solvatochromic effects between fluorophores **4a–c** and fluorophores **4d–f**. The fluorescence profiles in dilute dichloromethane solution exhibit a tuneable emission wavelength in the range 426−520 nm. There was no observable bathochromic shift trend (< 5 nm) between **4a–c**, while **4d–f** exhibited a distinct bathochromic shift (26−94 nm) compared with the former. The emission maxima of this set of fluorophores follows the order **4a** ≈ **4b** ≈ **4c** < **4d** < **4e** < **4f** (Figure 6a). To further verify the tuneable wide visible emission of this system, their emission properties in the solid state were also investigated (Figure 6b). The emissions of **4a–c** are drastically red-shifted by more than 78 nm (139 nm for **4a**, 78 nm for **4b** and 80 nm for **4c**), these distinctions in solution and in the solid state are mainly due to enhanced electronic coupling with the restriction of the intramolecular rotation and the π···π interaction between the phenyl rings and the pyrene core in the solid state. On the other hand, the emissions of **4d–f** present minor red- or blue-shifts compared with those in $CH_2Cl_2$ solution (red-shift 22 nm for **4d**, 17 nm for **4e** and blue-shift –7 nm for **4f**), presumably, which is ascribed to the formation of J-aggregates.[21] As evidenced by the reasonably quantum yield both in solution and in the solid state. By comparison, this type of dipolar molecules exhibited more tuneable and sensitive emission properties than do the 1,3,5,9-tetraarylpyrenes both in solution and in the solid state.[19]

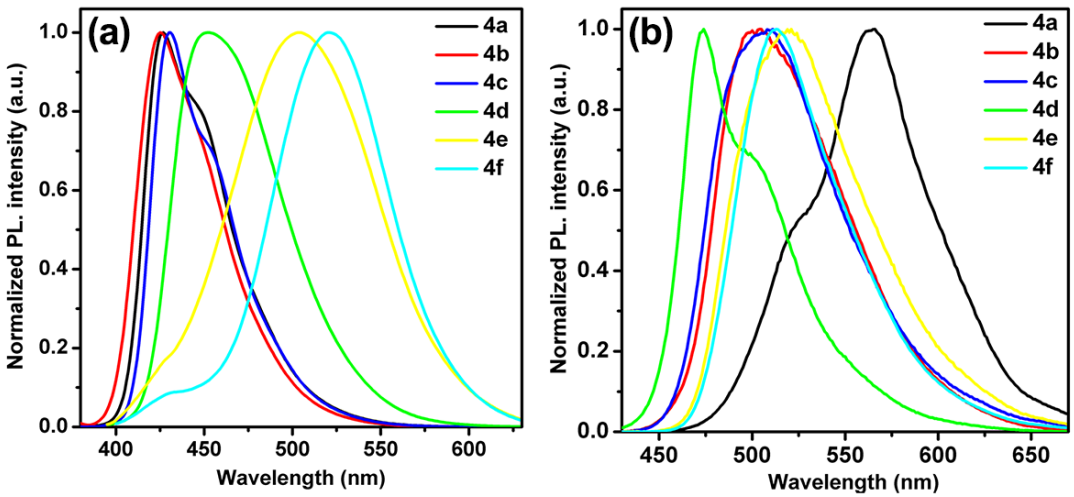


**Figure 6.** Emission spectra of fluorophores **4** in $CH_2Cl_2$ solution (a) and in the solid state (b).

In order to study the solvatochromism of these systems, solvents of various polarities, namely cyclohexane (CHX), tetrahydrofuran (THF), dichloromethane (DCM), acetonitrile (ACN), and dimethyl formamide (DMF), were selected, and the emission spectra were recorded (Figure 7a, and Figure 8). The absorption spectra of **4** manifest none or minimum solvent dependence. On the contrary, the solvatochromism could also be divided into two groups. For **4a**–**c**, there was little effect on the $\lambda_{max}$ for the emission profiles from CHX to DMF (7 nm for **4a**, 7 nm for **4b** and 11 nm for **4c**). In sharp contrast, the emission profiles of **4d**–**f** exhibited a significant red-shift as large as 134 nm for **4f**. Take **4f** as example, the fluorophore **4f** exhibited distinct color change from deep blue in cyclohexane to green, yellow, or even orange-red in DMF, which was observed under a UV light (365 nm), as shown in Figure 7b. This further indicates that fluorophores **4** are favorable, tuneable fluorescent materials. This phenomenon of solvatochromism was further confirmed by the relationship between the Stokes shifts in various solvents and the Lippert equation,[22] which revealed a linear correlation between these two factors (Figure 9). The value of the slope for **4f** (16681) is far larger than that for **4a** (1046). Moreover, the twisted intramolecular charge transfer (TICT) plays an important role in the solution state.[23] In nonpolar solvent, the more planar conformation of **4** is stabilized by electronic conjugation, which results in a sharp fluorescence spectrum on its locally excited (LE) state. The trend for intramolecular twisting in the polar solvent, however, transforms **4** from the LE state to the TICT state. The twisted conformation of **4** is stabilized due to the solvating effect of the polar solvent. Furthermore, this generates a smaller energy gap, hence bathochromically shifting its PL spectrum, especially for compounds **4d**–**f**, due to the substituents at the para position of the arylethynyl group. This is now the highest tuneable system bearing of 1,3-diphenyl-5,9-di-substituents at pyrene. As a control, more distinct charge separations and higher tuneability were observed versus the 1,3-diphenyl-6,8-di-substituents pyrene systems.[11b]

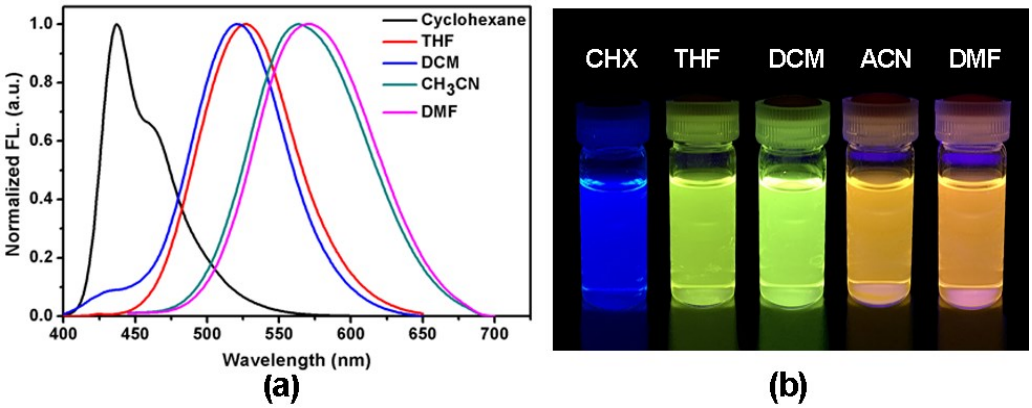


**Figure 7.** (a) Emission spectra of **4f** in solvents with varying polarity; (b) color of **4f** in different solvents under 365 nm UV illumination.

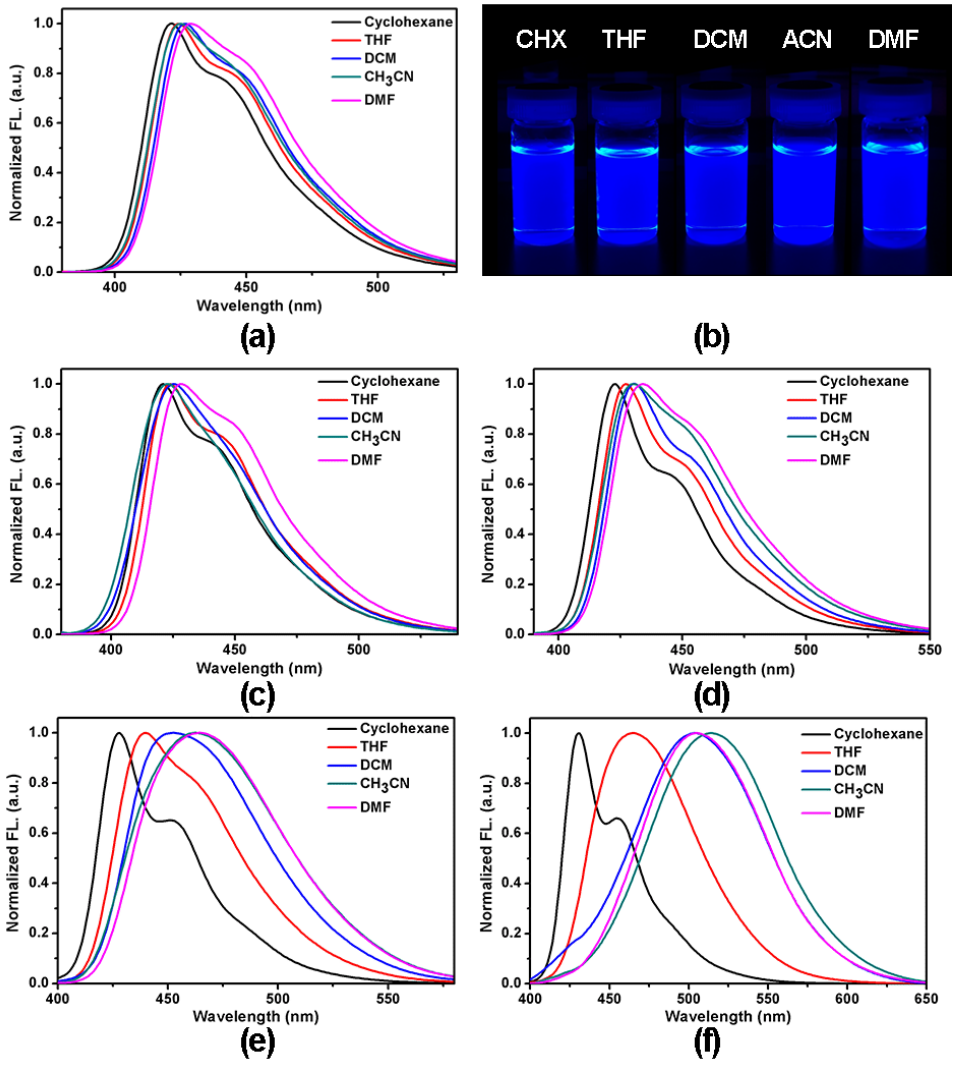


**Figure 8.** PL spectra of **4a–e** recorded in different solvents.

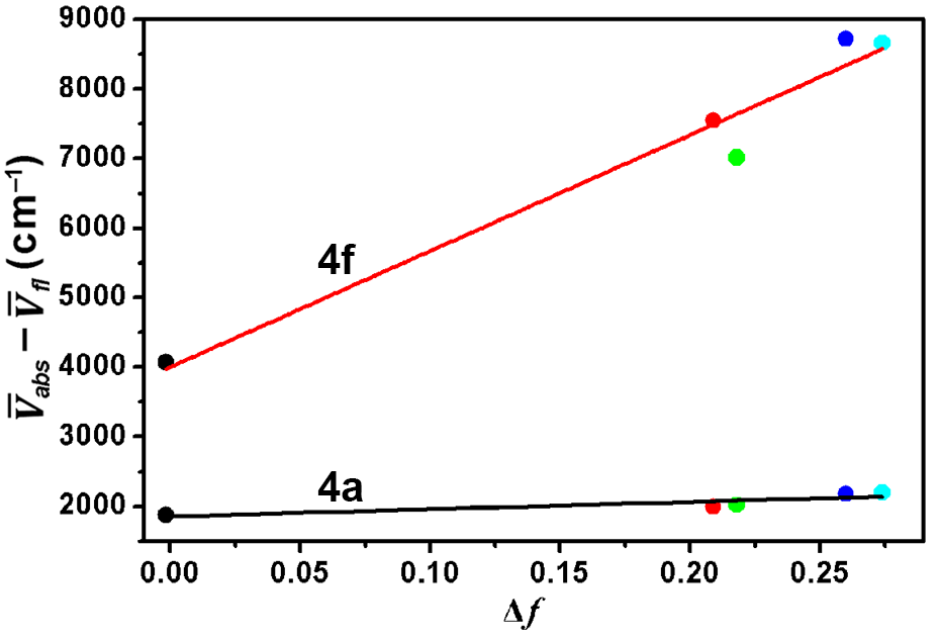


**Figure 9.** Lippert-Mataga plots for compounds **4a** and **4f**.

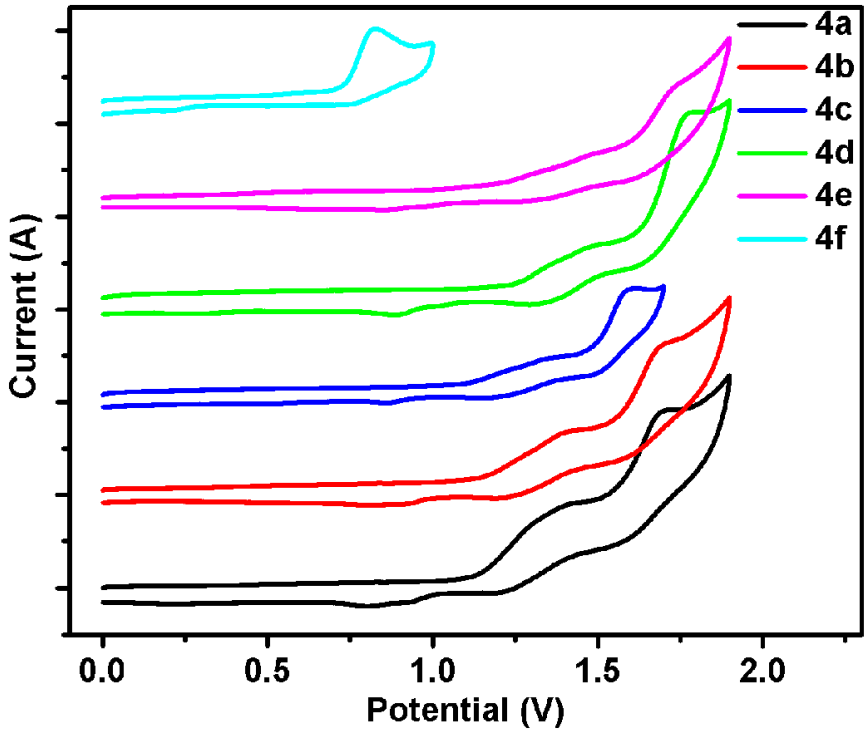


**Figure 10.** Cyclic voltammograms of fluorophores **4** in ferrocene in $CH_2Cl_2$ solution, scan rate is 0.1 V/s.

The oxidative electrochemical behavior of fluorophores **4** was investigated by cyclic voltammetry (CV) using ferrocene as the internal standard. All of the fluorophores **4** displayed irreversible oxidation processes with distinct positive potentials ranging from 0.73 to 1.22 V in $CH_2Cl_2$ solution, as shown in Figure 10, and Table 2. This can be associated with the terminal nature of the functional groups. The HOMOs of fluorophores **4a**–**f** were estimated to be −5.55, −5.57 eV, −5.52 eV, −5.64 eV, −5.61 eV, −5.15eV, respectively. The trend in the values is in good agreement with the DFT calculation results. The LUMOs were also evaluated from CVs and the UV-vis absorption to be in the range −1.90 eV to −2.41 eV. These results suggest that these dipolar molecules possess good hole- and electron-transporting properties.[24]

## 4.3 Conclusions

In conclusion, we present an innovative, facile, and promising, controllable regioselective strategy for the functionalization at the active sites (1,3-positions) and K-region (5,9-positions) of pyrene. The resulting dipolar molecules, namely 1,3-diphenyl-5,9-diarylethynyl)pyrenes, exhibit thermal stability, and tuneable emission over the entire visible region. The combined experimental and computational results provide an increasing understanding of the emission mechanism for introducing substitution at the K-region of pyrene. This work opens up new avenues to explore strategy to functionalize pyrene and to greatly expand the scope for developing highly efficient pyrene-based photoelectric materials.

## 4.4 Experimental Section

### 4.4.1 General

Synthetic routes for compounds **4** are shown in Scheme 1 and 2. All reactions were carried out under a dry $N_2$ atmosphere. Solvents were Guaranteed reagent (GR) for cyclohexane, tetrahydrofuran (THF), dichloromethane ($CH_2Cl_2$), acetonitrile ($CH_3CN$), and dimethylformamide (DMF), and stored over molecular sieves. Other reagents were obtained commercially and used without further purification. Reactions were monitored using thin layer chromatography (TLC). Commercial TLC plates (Merck Co.) were developed and the spots were identified under UV light at 254 and 365 nm. Column chromatography was performed on silica gel 60 (0.063-0.200 mm). All synthesized compounds were characterized using $^1$H-NMR and $^{13}$C-NMR spectroscopy, and by HRMS (FAB) mass analysis.

### 4.4.2 Synthetic Procedures

#### Synthesis of compounds 3

A series of precursors **3a**, **3b**, **3c** were synthesized from 7-*tert*-butyl-1,3-diphenylpyrene **2**[25] with the corresponding equiv. of $Br_2$ in the presence of iron-powder. $^1$H NMR spectra of these three precursors were investigated. We also carried out this type of reaction in the absence of iron powder, and only a trace amount of precursor **3a** was detected. In this work, preferred candidate **3b** was fully characterized by $^1$H NMR spectroscopy and mass analysis.

#### Synthesis of 7-*tert*-butyl-1,3-diphenyl-5-bromopyrene 3a

A mixture of 7-*tert*-butyl-1,3-diphenylpyrene **2** (0.5 g, 1.2 mmol), and Fe powder (0.1 g, 1.8 mmol) were added in $CH_2Cl_2$ (5 mL), and the mixture was stirred at room temperature for 15 minutes under an argon atmosphere. A solution of $Br_2$ (0.09 mL, 1.8 mmol) in $CH_2Cl_2$ (6 mL) was slowly added dropwise with stirring, and the mixture was continuously stirred for 24 h at room temperature. Then the mixture was quenched with a 10% aqueous solution of $Na_2S_2O_3$. The mixture solution was extracted with $CH_2Cl_2$ (2 × 20 mL), the organic layer was washed with water (2 × 10 mL) and brine (30 mL), and then the solution was dried ($MgSO_4$),

and the solvents were evaporated. The crude compound was washed with hot hexane to obtained **3a** as a light-yellow solid (381 mg, 65%). $^1$H NMR (400 MHz, $CDCl_3$): $\delta_H$ = 1.63 (s, 9H, *t*Bu), 7.48–7.53 (m, 2H, Ar-*H*), 7.57 (d, *J* = 7.7 Hz, 4H, Ar-*H*), 7.65–7.69 (m, 4H, Ar-*H*), 7.96 (s, 1H, pyrene-*H*), 8.03 (d, *J* = 9.2 Hz, 1H, pyrene-*H*), 8.19 (d, *J* = 9.2 Hz, 1H, pyrene-*H*), 8.27 (s, 1H, pyrene-*H*), 8.54 (s, 1H, pyrene-*H*), 8.66 (s, 1H, pyrene-*H*) ppm. Due to poor solubility in organic solvents it was not further characterized by $^{13}$C NMR spectroscopy. FAB-MS: m/z calcd for $C_{32}H_{25}Br$ 488.1140 [$M^+$]; found 488.1140 [$M^+$].

**Synthesis of 7-*tert*-butyl-1,3-diphenyl-5,9-dibromopyrene 3b**

A mixture of 7-*tert*-butyl-1,3-diphenylpyrene **2** (2.0 g, 4.8 mmol), and Fe powder (0.82 g, 14.4 mmol) were added in $CH_2Cl_2$ (30 mL), and the mixture was stirred at room temperature for 15 minutes under an argon atmosphere. A solution of $Br_2$ (0.75 mL, 14.4 mmol) in $CH_2Cl_2$ (50 mL) was slowly added dropwise with stirring, and the mixture was continuously stirred for 24 h at room temperature. Then the mixture was quenched with a 10% aqueous solution of $Na_2S_2O_3$. The mixture solution was extracted with $CH_2Cl_2$ (2 × 100 mL), the organic layer was washed with water (2 × 50 mL) and brine (50 mL), and then the solution was dried ($MgSO_4$), and the solvents were evaporated. The crude compound was washed with hot hexane to obtained **3b** as a yellow solid, which was recrystallized from hexane:$CHCl_3$ (v/v=8:1) to afford **3b** as a light yellow solid (2.3 g, 83%). M.p. 115–116°C; $^1$H NMR (400 MHz, $CDCl_3$): $\delta_H$ = 1.64 (s, 9H, *t*Bu), 7.51–7.54 (m, 2H, Ar-*H*), 7.58 (t, *J* = 7.3 Hz, 4H, Ar-*H*), 7.64 (d, *J* = 7.4 Hz, 4H, Ar-*H*), 7.96 (s, 1H, pyrene-*H*), 8.53 (s, 2H, pyrene-*H*), 8.73 (s, 2H, pyrene-*H*) ppm. Due to poor solubility in organic solvents it was not further characterized by $^{13}$C NMR spectroscopy. FAB-MS: m/z calcd for $C_{32}H_{24}Br_2$ 568.0224 [$M^+$]; found 568.0227 [$M^+$].

**Synthesis of 7-*tert*-butyl-1,3-di-(*para*-bromophenyl)-5,9-dibromopyrene 3c**

A mixture of 7-*tert*-butyl-1,3-diphenylpyrene **2** (0.5 g, 1.2 mmol), and Fe powder (0.4 g, 7.2 mmol) were added in $CH_2Cl_2$ (10 mL), and the mixture was stirred at room temperature for 15 minutes under an argon atmosphere. A solution of $Br_2$ (0.55 mL, 11.1 mmol) in $CH_2Cl_2$ (30 mL) was slowly added dropwise with stirring, and the mixture was continuously stirred for 24 h at room temperature. Then the mixture was quenched with a 10% aqueous solution of

$Na_2S_2O_3$. The mixture solution was extracted with $CH_2Cl_2$ (2 × 30 mL), the organic layer was washed with water (2 × 15 mL) and brine (50 mL), and then the solution was dried ($MgSO_4$), and the solvents were evaporated. The crude compound was purified by column chromatography eluting with a 1:6 $CH_2Cl_2$/hexane mixture to obtained **3c** as a yellow solid (653 mg, 71%). M.p. 202–203°C; $^1$H NMR (400 MHz, $CDCl_3$): $\delta_H$ = 1.64 (s, 9H, *t*Bu), 7.50 (d, *J* = 8.1 Hz, 4H, Ar-*H*), 7.72 (d, *J* = 8.2 Hz, 4H, Ar-*H*), 7.86 (s, 1H, pyrene-*H*), 8.45 (s, 2H, pyrene-*H*), 8.75 (s, 2H, pyrene-*H*) ppm. Due to poor solubility in organic solvents it was not further characterized by $^{13}$C NMR spectroscopy. FAB-MS: m/z calcd for $C_{32}H_{22}Br_4$ 725.8414 [$M^+$]; found 725.8414 [$M^+$].

**Synthesis of 7-*tert*-butyl-1,3-diphenyl-5,9-diarylethynylpyrenes (4a–f)**

A series of compounds **4a–f** were synthesized from 7-*tert*-butyl-1,3-diphenyl-5,9-dibromopyrene **3** with the corresponding aryl alkyne by a Sonogashira coupling reaction.

**7-*tert*-Butyl-1,3-diphenyl-5,9-bis-(4'-cyanophenylethynyl)pyrene (4d)**

A mixture of 7-*tert*-butyl-1,3-diphenyl-5,9-dibromopyrene **3** (150 mg, 0.26 mmol), 4-cyanophenyl acetylene (100 mg, 0.79 mmol), $PdCl_2(PPh_3)_3$ (18 mg, 0.03 mmol), CuI (10 mg, 0.52 mmol), $PPh_3$ (8 mg, 0.03 mmol) were added to a degassed solution of $Et_3N$ (6 mL) and DMF (6 mL). The resulting mixture was stirred at 100 °C for 24 h. After it was cooled to room temperature, the reaction was quenched with water. The mixture was extracted with $CH_2Cl_2$ (2 × 500 mL), the organic layer was washed with water (2 × 30 mL) and brine (30 mL), and then the solution was dried ($MgSO_4$), and evaporated. The residue was purified by column chromatography eluting with a 1:2 $CH_2Cl_2$/hexane mixture to give **4d** as a yellow floccule (115 mg, 66%). M.p. 351–353°C; $^1$H NMR (400 MHz, $CDCl_3$): $\delta_H$ = 1.68 (s, 9H, *t*Bu), 7.52–7.56 (m, 2H, Ar-*H*), 7.62 (t, *J* = 7.5 Hz, 4H, Ar-*H*), 7.66–7.73 (m, 8H, Ar-*H*), 7.77 (d, *J* = 8.2 Hz, 4H, Ar-*H*), 8.00 (s, 1H, pyrene-*H*), 8.53 (s, 2H, pyrene-*H*), 8.86 (s, 2H, pyrene-*H*) ppm; $^{13}$C NMR (100 MHz, $CDCl_3$): $\delta_C$ = 31.05, 34.76, 91.66, 92.13, 110.14, 110.81, 117.61, 117.98, 118.73, 120.75, 122.20, 124.22, 125.77, 126.03, 126.93, 127.26, 127.78, 128.57, 129.13, 129.26, 129.69, 129.81, 130.87, 131.20, 131.33, 131.61, 131.79, 132.12, 138.24, 139.30, 140.28, 149.23 ppm; FAB-MS: m/z calcd for $C_{50}H_{32}N_2$ 660.2565 [$M^+$]; found 660.2565 [$M^+$].

A similar procedure using phenylacetylene, 4-fluorophenyl acetylene, 4-methoxyphenyl acetylene, 4-formylphenyl acetylene, 4-*N,N*-dimethylphenyl acetylene, was followed for the synthesis of **4a–c**, and **4e**, **4f**.

**7-*tert*-Butyl-1,3-diphenyl-5,9-bis-(phenylethynyl)pyrene 4a** was obtained as an orange solid (recrystallized from hexane:$CH_2Cl_2$=3:1, 87 mg, 54%). M.p. 352–353°C; $^1$H NMR (400 MHz, $CDCl_3$): $\delta_H$ = 1.68 (s, 9H, *t*Bu), 7.42 (t, *J* = 7.7 Hz, 6H, Ar-*H*), 7.53 (d, *J* = 6.7 Hz, 2H, Ar-*H*), 7.61 (t, *J* = 7.5 Hz, 4H, Ar-*H*), 7.70 (d, *J* = 7.3 Hz, 8H, Ar-*H*), 7.95 (s, 1H, pyrene-*H*), 8.48 (s, 2H, pyrene-*H*), 8.93 (s, 2H, pyrene-*H*) ppm; $^{13}$C NMR (100 MHz, $CDCl_3$): $\delta_C$ = 31.97, 35.64, 88.31, 94.69, 120.62, 121.80, 123.42, 124.67, 126.91, 127.57, 128.40, 128.48, 128.53, 128.56, 129.59, 129.79, 130.43, 130.65, 131.71, 138.30, 140.58, 149.87 ppm; FAB-MS: *m/z* calcd for $C_{48}H_{34}$ 610.2661 [$M^+$]; found 610.2661 [$M^+$].

**7-*tert*-Butyl-1,3-diphenyl-5,9-bis-(4'-fluorophenylethynyl)pyrene 4b** was obtained as a pale-yellow solid (recrystallized from hexane:$CH_2Cl_2$=3:1, 104 mg, 61%). M.p. 286–287°C; $^1$H NMR (400 MHz, $CDCl_3$): $\delta_H$ = 1.68 (s, 9H, *t*Bu), 7.13 (t, *J* = 8.6 Hz, 4H, Ar-*H*), 7.53 (t, *J* = 7.5 Hz, 2H, Ar-*H*), 7.60 (t, *J* = 7.4 Hz, 4H, Ar-*H*), 7.68 (d, *J* = 7.3 Hz, 8H, Ar-*H*), 7.96 (s, 1H, pyrene-*H*), 8.47 (s, 2H, pyrene-*H*), 8.89 (s, 2H, pyrene-*H*) ppm; $^{13}$C NMR (100 MHz, $CDCl_3$): $\delta_C$ = 32.02, 35.82, 88.02, 93.64, 110.02, 115.82, 116.04, 120.50, 121.77, 126.94, 127.67, 128.64, 129.70, 130.44, 130.69, 133.59, 133.68, 138.44, 140.59, 149.79, 161.44 ppm; FAB-MS: *m/z* calcd for $C_{48}H_{32}F_2$ 646.2472 [$M^+$]; found 646.2472 [$M^+$].

**7-*tert*-Butyl-1,3-diphenyl-5,9-bis-(4'-methoxyphenylethynyl)pyrene 4c** was obtained as a yellow solid (recrystallized from hexane:$CH_2Cl_2$=4:1, 101 mg, 57%). M.p. 335–336°C; $^1$H NMR (400 MHz, $CDCl_3$): $\delta_H$ = 1.68 (s, 9H, *t*Bu), 3.87 (s, 6H, OMe), 6,92–6.98 (m, 4H, Ar-*H*), 7.51 (t, *J* = 7.3 Hz, 2H, Ar-*H*), 7.57–7.66 (m, 8H, Ar-*H*), 7.70 (d, *J* = 7.3 Hz, 4H, Ar-*H*), 7.94 (s, 1H, pyrene-*H*), 8.45 (s, 2H, pyrene-*H*), 8.92 (s, 2H, pyrene-*H*) ppm; $^{13}$C NMR (100 MHz, $CDCl_3$): $\delta_C$ = 31.94, 35.59, 87.03, 94.71, 114.16, 115.47, 120.86, 121.74, 123.11, 124.39, 126.93, 127.47, 128.51, 129.02, 129.71, 130.40, 130.63, 133.14, 137.94, 140.62, 149.66, 159.79 ppm; FAB-MS: *m/z* calcd for $C_{50}H_{38}O_2$ 670.2872 [$M^+$]; found 670.2872 [$M^+$].

**7-*tert*-Butyl-1,3-diphenyl-5,9-bis-(4'-formylphenylethynyl)pyrene 4e** was obtained as an orange solid (recrystallized from hexane:$CH_2Cl_2$=2:1, 81 mg, 46%). M.p. 256–257°C; $^1$H NMR (400 MHz, $CDCl_3$): $\delta_H$ = 1.70 (s, 9H, *t*Bu), 7.06 (s, 2H, Ar-*H*), 7.55 (d, *J* = 6.3 Hz, 2H, Ar-*H*), 7.61 (t, *J* = 6.8 Hz, 4H, Ar-*H*), 7.70 (d, *J* = 7.4 Hz, 4H, Ar-*H*), 7.80 (d, *J* = 7.9 Hz, 4H, Ar-*H*), 7.90 (d, *J* = 7.0 Hz, 4H, Ar-*H*), 7.98 (s, 1H, pyrene-*H*), 8.50 (s, 2H, pyrene-*H*), 8.88 (s, 2H, pyrene-*H*), 10.03 (s, 2H, CHO) ppm; $^{13}$C NMR (100 MHz, $CDCl_3$): $\delta_C$ = 31.80, 35.53, 92.16, 93.71, 121.53, 126.51, 127.62, 128.50, 128.74, 129.37, 129.56, 129.84, 130.02, 130.34, 130.46, 131.95, 135.37, 138.77, 149.71, 191.16 ppm; FAB-MS: *m/z* calcd for $C_{50}H_{34}O_2$ 666.2559 [$M^+$]; found 666.2559 [$M^+$].

**7-*tert*-Butyl-1,3-diphenyl-5,9-bis-(4'-*N*,*N*-dimethylphenylethynyl)pyrene 4f** was obtained as a yellow solid (recrystallized from hexane:$CH_2Cl_2$=4:1, 107 mg, 58%). M.p. 346–347°C; $^1$H NMR (400 MHz, $CDCl_3$): $\delta_H$ = 1.68 (s, 9H, *t*Bu), 3.03 (s, 12H, Me), 6.74 (d, *J* = 8.4 Hz, 4H, Ar-*H*), 7.50 (t, *J* = 6.9 Hz, 2H, Ar-*H*), 7.59 (t, *J* = 7.7 Hz, 8H, Ar-*H*), 7.70 (d, *J* = 7.7 Hz, 4H, Ar-*H*), 7.92 (s, 1H, pyrene-*H*), 8.42 (s, 2H, pyrene-*H*), 8.94 (s, 2H, pyrene-*H*) ppm; $^{13}$C NMR (100 MHz, $CDCl_3$): $\delta_C$ = 32.35, 35.97, 40.43, 40.55, 73.01, 82.73, 86.82, 96.51, 108.93, 110.44, 112.02, 112.28, 121.78, 122.18, 123.51, 124.46, 127.45, 127.74, 128.64, 128.85, 130.02, 130.86, 131.04, 133.19, 133.95, 137.86, 141.16, 149.84, 150.56, 150.65 ppm; FAB-MS: *m/z* calcd for $C_{52}H_{44}N_2$ 696.3504 [$M^+$]; found 696.3504 [$M^+$].

## 4.4.3 X-ray Crystallography

One suitable single crystals of **4c** was obtained in mixture solution, sealed in glass capillaries under argon, and mounted on a diffractometer. The preliminary examination and data collection was performed using a Bruker APEX 2 CCD detector system single-crystal X-ray diffractometer equipped with a sealed-tube X-ray source (50 kV × 30 mA) using graphitemonochromated Mo Kα radiation. Data were corrected for Lorentz and polarisation effects and for absorption.[26] The structure was solved by charge flipping or direct methods algorithms and refined by full-matrix least-squares methods, on $F^2$.[27] All esds (except the esd in the dihedral angle between two l.s. planes) are estimated using the full covariance matrix. The cell esds are taken into account individually in the estimation of esds in distances, angles and torsion angles; correlations between esds in cell parameters are only used when they are

defined by crystal symmetry. An approximate (isotropic) treatment of cell esds is used for estimating esds involving l.s. planes. The final cell constants were determined through global refinement of the xyz centroids of the reflections harvested from the entire data set. Structure solution and refinement were carried out using the SHELXTL-PLUS software package.[28] CCDC-1547621 (**4c**) contain supplementary crystallographic data for this paper. Copies of the data can be obtained, free of charge, on application to CCDC, 12 Union Road, Cambridge CB2 1EZ, UK [fax: 144-1223-336033 or e-mail: deposit@ccdc.cam.ac.uk].

## 4.5 References


1. (a) Wu, K. C.; Ku, P. J.; Lin, C. S.; Shih, H. T.; Wu, F. I.; Huang, M. J.; Lin, J. J.; Chen I. C.; Cheng, C. H. *Adv. Funct. Mater.* **2008**, *18*, 67–75. (b) Wong, W. Y.; Ho, C. L.; Gao, Z. Q.; Mi, B. X.; Chen, C. H.; Cheah K. W.; Lin, Z. Y. *Angew. Chem., Int. Ed.* **2006**, *45*, 7800–7803.
2. Liu, Z. C.; Yin, L. J.; Ning, H.; Yang, Z. Y.; Tong, L. M.; Ning, C.-Z. *Nano Lett.* **2013**, *13*, 4945−4950.
3. (a) Lin, Y. Z.; Zhao, F. W.; He, Q.; Wu, L. J.; Parker, T. C.; Ma, W.; Sun, Y. M.; Wang, C. R; Zhu, D. B. *J. Am. Chem. Soc.* **2016**, *138*, 4955–4961. (b) Liang, X. Y.; Bai, S.; Wang, X.; Dai, X. L.; Gao, F.; Sun, B. Q.; Ning, Z. J.; Ye. Z. Z.; Jin, Y. Z. *Chem. Soc. Rev.* **2017**, *46*, 1730–1759. (c) Mei, J.; Leung, N. L. C.; Kwok, R. T. K.; Lam, J. W. Y.; Tang, B. Z. *Chem. Rev.* **2015**, *115*, 11718–11940.
4. (a) Winkler, J. R.; Gray, H. B. *J. Am. Chem. Soc.* **2014**, *136*, 2930−2939. (b) Bilici, A.; Doğan, F.; Yildirim, M.; Kaya, I. *J. Phys. Chem. C* **2012**, *116*, 19934−19940.
5. (a) Tu, Z.; Liu, M.; Qian, Y.; Yang, G.; Cai, M.; Wang, L.; Huang, W. *RSC Adv.* **2015**, *5*, 7789–7793. (b) Yang, Z. Y., Mao, Z.; Xie, Z. L.; Zhang, Y.; Liu, S. W.; Zhao, J.; Xu, J. R.; Chi, Z. G. Aldred, M. P. *Chem. Soc. Rev.* **2017**, *46*, 915–1016.
6. Milián-Medina, B.; Gierschner, J. *J. Phys. Chem. Lett.* **2017**, *8*, 91−101.
7. (a) Hazarika, A.; Pandey, A.; Sarma, D. D. *J. Phys. Chem. Lett.* **2014**, *5*, 2208−2213. (b) Wang, F.; Liu, X. G. *J. Am. Chem. Soc.* **2008**, *130*, 5642–5643.
8. Yang, W.; Pan, C. Y.; Luo, M. D.; Zhang, H. B. *Biomacromolecules* **2010**, *11*, 1840−1846.
9. Wang, J.; Tang, S.; Sandström, A.; Edman, L. *ACS Appl. Mater. Interfaces* **2015**, *7*, 2784−2789.
10. (a) Mizoshita, N.; Goto, Y.; Maegawa, Y.; Tani, T.; Inagaki, S. *Chem. Mater.* **2010**, *22*, 2548–2554. (b) Zhang, Z. Y.; Wu, Y. S.; Tang, K. C.; Chen, C. L.; Ho, J. W.; Su, J. H.; Tian, H.; Chou, P. T. *J. Am. Chem. Soc.* **2015**, *137*, 8509−8520.
11. Crawford, A. G.; Dwyer, A. D.; Liu, Z. Q.; Steffen, A.; Beeby, A.; David, L.-O.; Tozer, J.; Marder, T. B. *J. Am. Chem. Soc.* **2011**, *133*, 13349−13362.
12. Wanninger-Weiß, C.; Wagenknecht, H.-A. *Eur. J. Org. Chem*. **2008**, 64−71.

13. (a) Figueira-Duarte, T. M.; Müllen, K. *Chem. Rev.* **2011**, *111*, 7260−7314. (b) Mateo-Alonso, A. *Chem. Soc. Rev.* **2014**, *43*, 6311−6324. (c) Feng, X.; Hu, J.-Y.; Redshaw, C.; Yamato, T. *Chem. -Eur. J.* **2016**, *22*, 11898–11916. (d) Feng, X.; Tomiyasu, H.; Hu, J.-Y.; Wei, X. F.; Redshaw, C.; Elsegood, M. R. J.; Horsburgh, L.; Teat, S. J.; Yamato, T. *J. Org. Chem.* **2015**, *80*, 10973−10978. (e) Wang, C. Z.; Ichiyanagi, H.; Sakaguchi, K.; Feng, X.; Elsegood, M. R. J.; Redshaw, C.; Yamato, T. *J. Org. Chem.* **2017**, *82*, 7176−7182.
14. Hu, J.; Zhang, D.; Harris, F. W. *J. Org. Chem.* **2005**, *70*, 707–708.
15. Yamato, T.; Fujimoto, M.; Miyazawa, A.; Matsuo, K. *J. Chem. Soc. Perkin Trans.* **1997**, 1201–1207.
16. Mikroyannidis, J. A.; Stylianakis, M. M.; Roy, M. S.; Suresh, P.; Sharma, G. D. *J. Power Sources* **2009**, *194*, 1171–1179.
17. Miyazawa, A.; Tsuge, A.; Yamato, T.; Tashiro, M. *J. Org. Chem.* **1991**, *56*, 4312–4314.
18. Feng, X.; Hu, J.-Y.; Yi, L.; Seto, N.; Tao, Z.; Redshaw, C.; Elsegood, M. R. J.; Yamato, T. *Chem.–Asian J.* **2012**, *7*, 2854–2863.
19. Feng, X.; Hu, J. Y.; Iwanaga, F.; Seto, N.; Redshaw, C.; Elsegood, M. R. J.; Yamato, T. *Org. Lett.* **2013**, *15*, 1318–1321.
20. Sasaki, S.; Drummen, G. P. C.; Konishi, G.-i. *J. Mater. Chem. C* **2016**, 4, 2731–2743.
21. Würthner, F.; Kaiser, T. E.; Saha-Möller, C. R. *Angew. Chem., Int. Ed.* **2011**, *50*, 3376–3410.
22. (a) Lippert, V. E. *Z. Naturforsch. A: Phys. Sci.* **1955**, *10*, 541–545. (b) Mataga, N.; Kaifu, Y.; Koizumi, M. *Bull. Chem. Soc. Jpn.* **1956**, *29*, 465–470.
23. (a) Fang, H. H.; Chen, Q. D.; Yang, J.; Xia, H.; Gao, B. R.; Feng, J.; Ma, Y. G.; Sun, H. B. *J. Phys. Chem. C* **2010**, *114*, 11958−11961. (b) Yan, Z. Q.; Yang, Z. Y.; Wang, H.; Li, A. W.; Wang, L. P.; Yang, H.; Gao, B. R. *Spectrochim. Acta A: Mol. Biomol. Spectr.* **2011**, *78*, 1640−1645.
24. (a) Zhang, Q.; Li, B.; Huang, S.; Nomura, H.; Tanaka, H.; Adachi, C. *Nat. Photonics* **2014**, *8*, 326–332. (b) Reddy, S. S.; Sree, V. G.; Gunasekar, K.; Cho, W.; Gal, Y.-S.; Song, M.; Kang, J.-W.; Jin, S.-H. *Adv. Optical Mater.* **2016**, *4*, 1236–124.

25. Feng, X.; Hu, J. Y.; Tomiyasu, H.; Tao, Z.; Redshaw, C.; Elsegood, M. R. J.; Horsburgh, L.; Teat, S. J.; Wei, X. F.; Yamato, T. *RSC Adv.* **2015**, *5*, 8835–8848.
26. APEX 2 & SAINT (**2012**), software for CCD diffractometers. Bruker AXS Inc., Madison, USA.
27. (a) G. M. Sheldrick, *Acta Crystallogr*. **2008**, *A64*, 112–122. (b) G. M. Sheldrick, *Acta Cryst.* **2015**, *A71*, 3–8. (c) G. M. Sheldrick, *Acta Cryst.* **2015**, *C71*, 3–8.
28. S. P. Westrip, *J. Apply. Cryst.* **2000**, *43*, 920–925.

# Chapter 5

# Regioselective substituted at 1, 3- and 6, 8-positions to achieve pyrene-based dipolar molecules: synthesis and large two-photon absorption cross sections

*Herein, we present a set of pyrene-based bipolar D–π–A fluorophors* ***2*** *with wide-range color tuning and large TPA cross-sections (up to 2200 GM at 780 nm) by regioselective at the 1,3- and 6.8-positions under the perspective of theoretical analysis. The linear and nonlinear optical properties of these compounds* ***2*** *were studied detailedly. The nearly identical emission wavelength between the two-photon excited fluorescence (TPEF) and one-photon excited fluorescence (OPEF) indicated that they generated from the same fluorescent excited state by either one- or two-photon excitations, except for the strong donor [–N(CH₃)₂] appended fluorophor* ***2e****, the TPEF exhibited large red-shift compared with the OPEF spectra due to the complicated working mechanisms, including intramolecular charge transfer (ICT), and twisted intramolecular charge transfer (TICT). All fluorophors exhibit high two-photon cross section (or two-photon brightness, δΦ ), especially for* ***2d*** *(1348 GM) and* ***2e*** *(641GM), which indicated that these* materials can be used as colorant for probe and bioimaging applications.

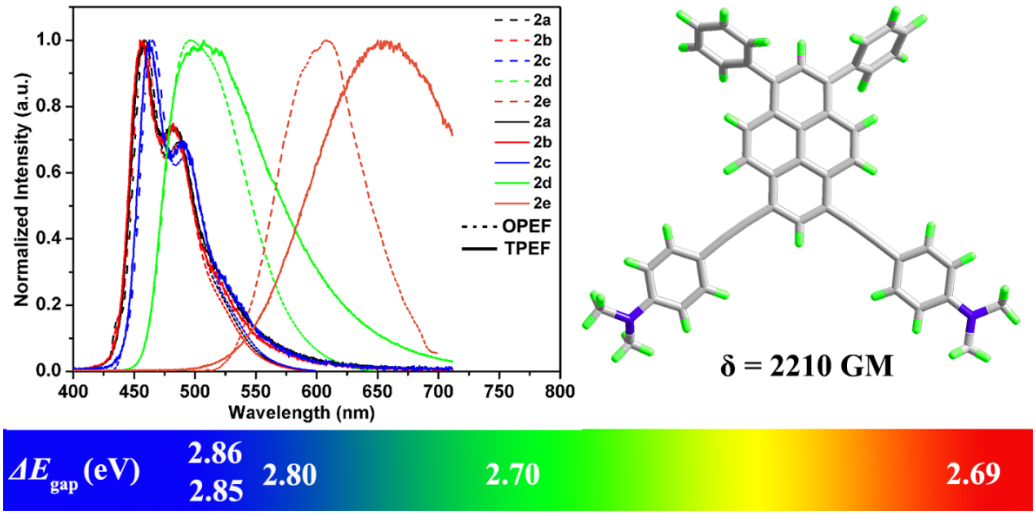

## 5.1 Introduction

Light-emitting organic conjugated molecules with large two-photon absorption (TPA) cross-sections ($\delta$) have attracted growing attention in recent decades, both at the theoretical and experimental level. This interest stems from their numerous potential applications in biologically-oriented research,[1] photodynamic therapy,[2] three-dimensional lithography/data storage,[3] and in the design of various other types of materials.[4] Within this context, developing rational strategies for the design and synthesis of molecules possessing large $\delta$ have led the trend in this field over recent years. Three basic structural motifs, namely dipolar,[5] quadrupolar,[6] and octupolar,[7] have been established, and are generalized by the construction of donor–acceptor–donor (D–A–D) type, donor–$\pi$-bridge–acceptor (D–$\pi$–A) type, donor–$\pi$-bridge–donor (D–$\pi$–D) type structures. Factors such as the geometrical parameters, including the extended π-conjugated system, the charge-transfer (CT) ability, and strength and position of donor/acceptor groups influence the adoption of such motifs.[8] As well as the rapid progress on TPA, an active strategy for tuning the CT ability of prepared molecules with a desired TPA activity has been sought. In general, the high sensitivity of various vibrations to electronic density plays a crucial role on their TPA properties.[8c] Thus, a facile approach to prepare new charge-transfer complexes with tailored band gaps ($\Delta E_g$) by introducing donor and acceptor groups was developed. Donors can provide a significant contribution to the high lying occupied molecular orbitals because they are prone to donate electrons. Acceptors on the other hand have an effect on the low lying unoccupied molecular orbitals because they are prone to accept electrons (Scheme 1).[9] In the case of donor-acceptor (D-A) structures, the energy gap of the new materials can be significantly tuned compared with the parent components.

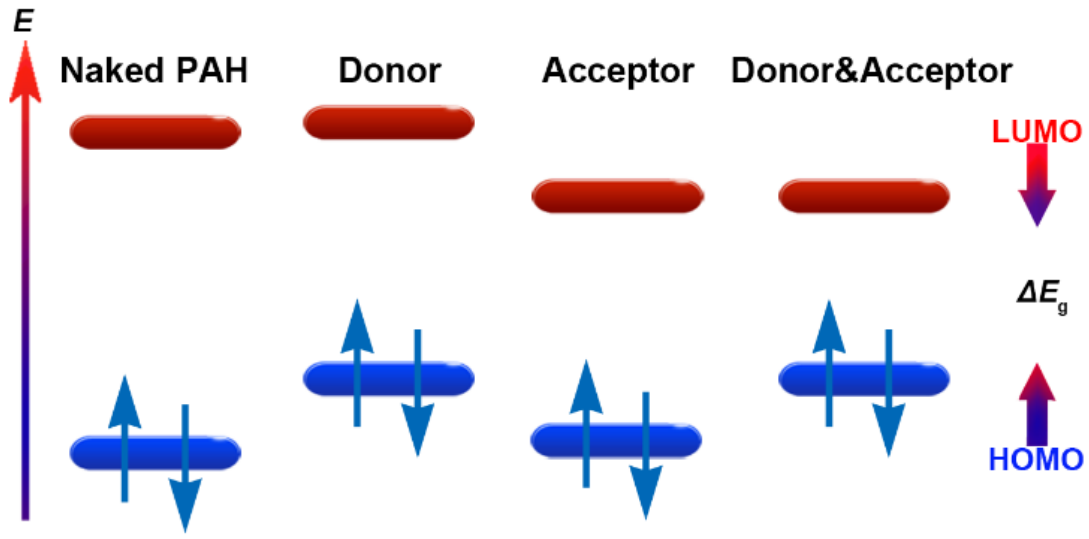


**Scheme 1** Schematic energy level diagram of PAHs.

One class of polycyclic aromatic hydrocarbons (PAHs) with a large π-conjugated core (four fused phenyl rings), excellent photoluminescence efficiency and deserving of particular attention is pyrene.[10] To date, pyrene-based fluorophors with TPA properties remain rare; examples include dipolar/quadrupolar molecules,[11] and multi-branch structural molecules.[12] Given this, the construction of pyrene-based D-$\pi$-A TPA materials with considerable $\delta$ values is a promising strategy when pyrene is employed as the $\pi$-core. Our previous studies have shown that donor/acceptor substituted pyrene-based derivatives can exhibit novel and tunable photophysical properties.[10b,13] On the other hand, we also predicted that asymmetrical D-$\pi$-A pyrene-based derivatives will possess efficient TPA properties. Taking account of the above considerations, by introducing different electron-donating/withdrawing substituents, a series of pyrene-based dipolar molecules, with tunable LUMO and HOMO levels and large $\delta$ value are reported (Scheme 2). Insight into the structure-property relationships of one-photon absorption and TPA of the five molecules reported herein was obtained by combining experimental and theoretical results, and evaluating the influence of donor and acceptor groups.

## 5.2 Results and Discussion

### 5.2.1 Synthetic procedures of 2

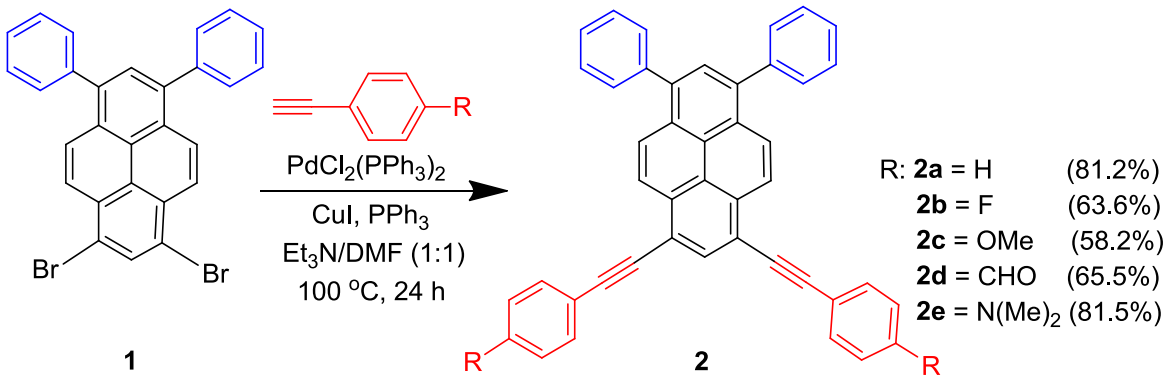


**Scheme 2** Synthetic route to dipolar molecules **2**

The synthetic procedure for **2** is outlined in Scheme 2, and was designed to gradually modulate the energy levels by changing the substituents. Thus, a set of pyrene-based dipolar molecules **2** were synthesized in high yield by the Pd-catalyzed coupling reaction of the precursor 1,3-diphenyl-6,8-dibromopyrene **1**.[13a] The structures and high purity were unambiguously confirmed by $^{1}H/^{13}C$ NMR spectroscopy, high-resolution mass spectrometry (HRMS) and X-ray crystallography. The detailed synthetic procedures and characterization data are given in Experimental Section.. All compounds exhibited good solubility in common organic solvents and exhibited excellent thermal stability.

### 5.2.2 Crystallography

Single crystals of **2b**, **2c** and **2e** were obtained from chloroform/hexane mixtures by the slow solvent evaporation method, and were analyzed by single crystal X-ray diffraction crystallography using synchrotron radiation. As depicted in Figure 1, in case of **2b** and **2e**, the two *para*-substituted rings are almost co-planar with the pyrene moiety, while the two phenyl groups are more substantially twisted in all three X-ray structures. The dihedral angles between the *para*-substituted rings and the pyrene core (C1 > C16) are 17.03(6)° (C39 > C44), 7.97(6)° (C31 > C36) for **2b**, 9.51(9)° (C41 > C46), 9.07(9)° (C31 > C36) for **2e**. The twist angles between the pyrene core and the following phenyl groups are 47.18(4)° (C17 > C22), 62.78(3)°

(C23 >C28) for **2b**, and 55.13(6)° (C17 > C22), 58.93(6)° (C23 > C28) for **2c**. It is worth noting that the $NMe_2$ *para* substituents of **2e** effectively weaken the *π–π* stacking interaction due to the twist angles between the $C_6$ aromatic ring and the $NMe_2$ groups, 15.0(3)° (C31 > C36 and N1/C37/C38), 34.8(2)° (C41 > C46 and N2/C47/C48). For **2c**, there are four molecules of the pyrene plus one molecule of chloroform in the asymmetric unit. The twist angles (°) between the pyrene core and phenyl groups and $C_6H_4$ rings beyond the alkyne linkage are summarized in Table 1. In summary, the dihedral angles between the *para*-substituted rings beyond the alkyne linkage exhibit one shallow angle (range 0.16-8.61(19)° and one more twisted angle (range 42.38-49.55(11)°) with respect to the pyrene core, while the phenyl rings are all significantly twisted (range 41.23-58.54(14)°. A detailed investigation indicated that the molecular packing of **2b**, **2c**, and **2e** displayed marked differences. For **2b**, molecules pack in layers with zones of interdigitated phenyl groups and a separate zone of interdigitated F-substituted aromatic rings (Figure 2a). Molecules form off-set face-to-face *π···π* stacks with the centre of the pyrene overlaying the alkyne group C(29)/C(30) in a neighbouring molecule at a distance in the range 3.339–3.355 Å (depicted as orange dashed lines), and edge-to-face ArC–H*···π* interactions between the edge of the phenyl groups and the pyrene core at distances of 2.704 and 2.880 Å (Figure 2b bottom, depicted as blue dashed lines). For **2c**, as shown in Figure 2c, 2d, the chloroform molecule either forms a C–H···π interaction with ring C(17) > C(22) or with a symmetry generated ring C(23B) > C(28B). Meanwhile, the molecules stack in slipped columns parallel to *a* with pyrene cores only just overlapping. Similar *π···π* stacks with the centre of the pyrene or $C_6H_4$ rings overlaying the alkyne group at a distance in the range 3.346–3.390 Å were observed. On the other hand, for **2e**, the more twisted conformations associated with the *para*-substituents can alleviate the intermolecular π–π stacking interactions to some degree, and instead they overlay with one of the alkyne groups C(39)/C(40) of a neighbouring molecule. This off-set stacking occurs parallel to *b*. The closest C···C interactions are *ca*. 3.42 Å. There are also rather distorted centro-symmetric pairs of ArC(24)–H(24)···π {centroid of ring C(41) > C(46)} interactions with a short distance of 2.59 Å (Figure 2f, blue dashed lines). These results demonstrate that compared with the F-substituted analog **2b**, the π–π stacking interactions between the $NMe_2$-substituted molecules are substantially weakened due to the bulky *para* substituent, which should favour tunable emission properties in solution with more substantially twisted structures.

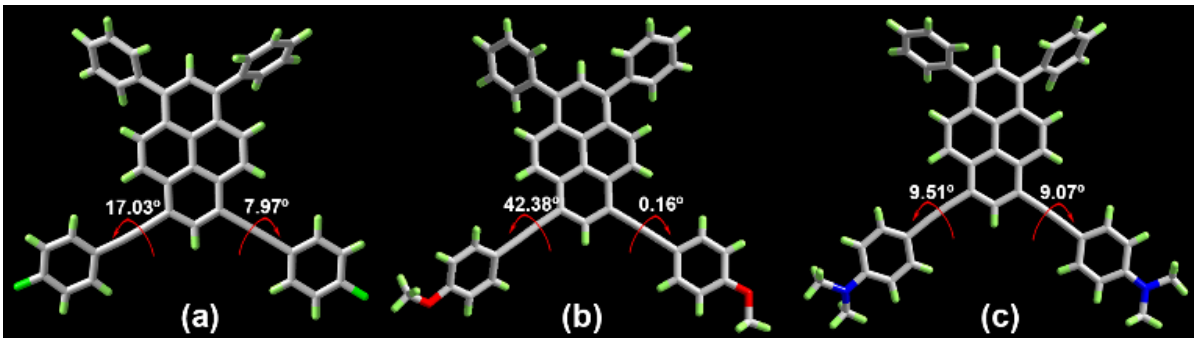


**Figure 1.** Crystal structures of **2b** (a), **2c** (b) and **2e** (c).

**Table S2.** Twist angles[a] /° between the pyrene core and phenyl groups and $C_6H_4$ rings for **2c**.

| **Molecule** | **Angle 1** | **Angle 2** | **Angle 3** | **Angle 4** |
|---|---|---|---|---|
| **No suffix** | 44.62(13) | 41.23(14) | 42.38(11) | 0.16(19) |
| **Suffix A** | 56.69(10) | 48.39(13) | 49.55(10) | 8.61(19) |
| **Suffix B** | 45.59(13) | 42.54(11) | 5.07(19) | 47.95(10) |
| **Suffix C** | 45.72(14) | 58.54(9) | 6.51(18) | 42.48(11) |

[a] Angle 1 between pyrene core and C(17) > C(22)

Angle 2 between pyrene core and C(23) > C(28)

Angle 3 between pyrene core and C(31) > C(36)

Angle 4 between pyrene core and C(40) > C(45)

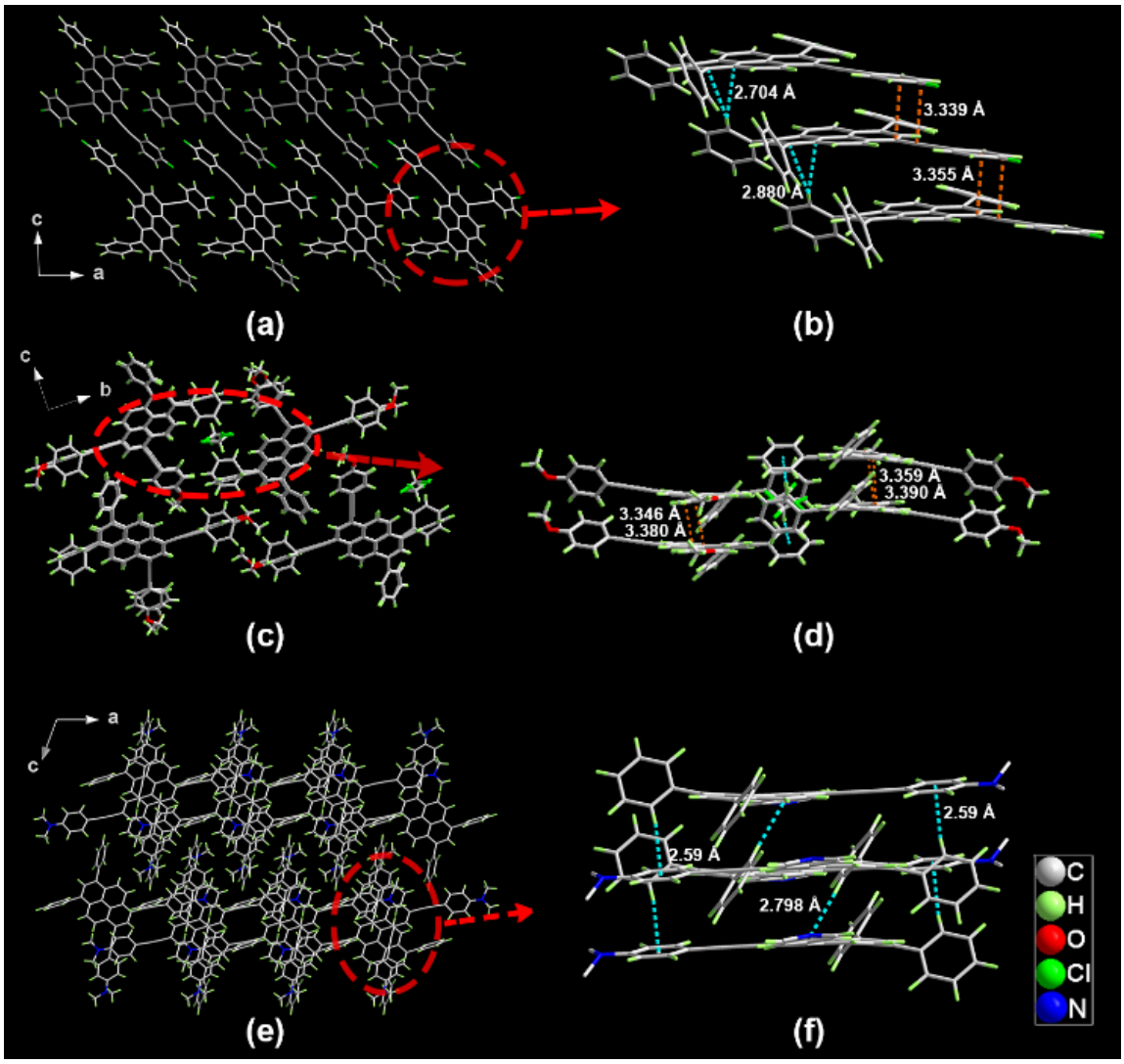


**Figure 2.** Crystal structures of **2b** (a) & (b), **2c** (c) & (d), and **2e** (e) & (f); Illustration of crystal packing and intermolecular interactions. The hydrogen atoms are omitted for clarity.

## 5.2.3 Density functional theoretical calculation

Initially, density functional theory (DFT) calculations were performed to evaluate the energy levels of this type of dipolar molecule at the B3LYP/6-31G* level. As depicted in Figure 3, the energy gaps gradually reduce from **2a** to **2e**, which further indicated that this strategy to tune the LUMO and HOMO levels is an efficient process. Compared with the compound 1,3-diphenylpyrene (3.58 eV), compounds **2** exhibited distinctly lower energy gaps, which is due to the introduction of donor or acceptor groups at the 6-, and 8- positions. Compared with **2a**, the energy gaps of the other four compounds **2b**−**2e** also gradually reduce,

which is associated with the donating- or withdrawing-electron ability of the substituents (**R**) at the *para*-position of arylethynyl. Specifically, relative to **2a** (**R** = **H**), **2b** (**R** = **F**) and **2c** (**R** = **OMe**), the substituent groups are weakly electron-withdrawing- and donating substituents, respectively, and provide a certain degree of influence over the LUMOs and HOMOs. For compound **2d** (**R** = **CHO**), the terminal substituent is a strong electron-withdrawing group, and so it provided energetically enhanced LUMOs, which are mainly distributed over the pyrene core and arylethynyl substituents. On the contrary, the HOMOs of compound **2e** (**R** = **N(CH$_3$)$_2$**), with strong electron-donating substituents, are mostly localized on the pyrene core and arylethynyl substituents. This implies that the HOMOs and LUMOs are determined by the terminal substituents **R**.[14]

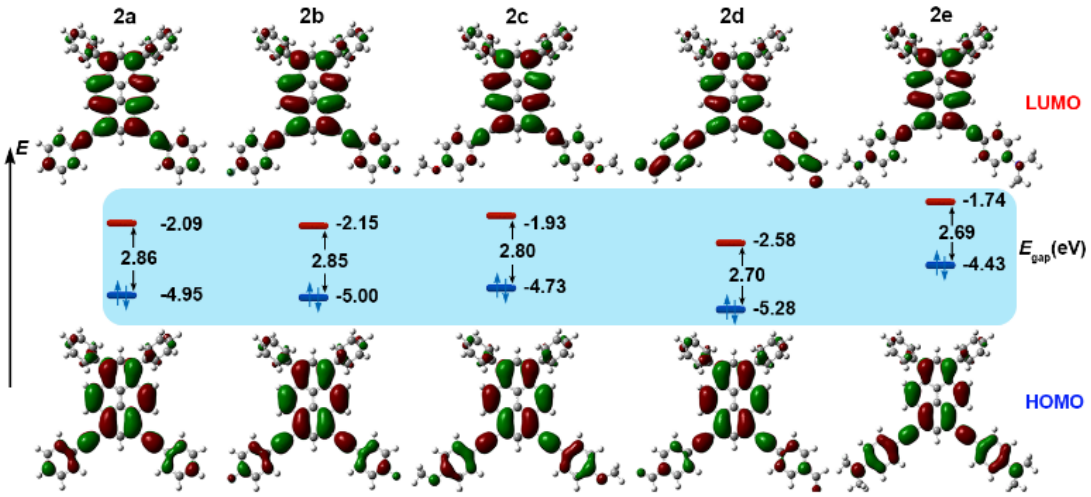


**Figure 3.** Frontier-molecular-orbital distributions and energy levels diagram of **2a**−**e** by DFT calculations.

## 5.2.4 Linear Optical Properties

Further investigations of the UV-vis absorption and emission properties were performed for compounds **2** based on our preliminary theoretical guidance, and the key spectroscopic parameters are summarized in Table 2. As shown in Figure 4a, the absorption spectra of **2** in dichloromethane are distinctive but complicated, which is attributed to the D-$\pi$-A type molecular structures and the extended $\pi$-conjugated system. A gradual bathochromic shift was observed in the order **2a** ≈ **2b** < **2c** < **2d** < **2e**, indicating the increasing tendency of

intramolecular charge transfer (ICT). On the other hand, the type of absorption profiles present obvious distinctions, especially for **2d** and **2e**, the more tuneable and sensitive absorption properties are mainly associated with the extent of ICT and twist intramolecular charge transfer (TICT). Specifically, for **2a**-**2c**, three sets of pronounced absorption bands were observed. Firstly, a short-wavelength band distributed in less than 250 nm which is mainly due to the $\pi$–$\pi$* transitions of the phenyl groups and the pyrene core. Secondly, a long-wavelength band localized in the range of 409−434 nm with high molar absorption coefficients (53081−70128 $cm^{-1}$ $M^{-1}$), and lastly an absorption band mainly centered at 318–336 nm with higher values for the molar absorption coefficients (49758−82835 $cm^{-1}$ $M^{-1}$). However, more obvious and complicated characteristic absorption bands were noted for **2d** and **2e**. In particular, new absorption bands at 367 nm with a low value of $\varepsilon$ (39806 $cm^{-1}$ $M^{-1}$) for **2d**, and at 388 nm with a low value of molar absorption coefficients (52321 $cm^{-1}$ $M^{-1}$) for **2e**, respectively. The results of the above mentioned results for compounds **2** indicate that their excited states possess significant charge transfer (CT) absorption associated with the ICT and TICT and withdrawing- or donating-electron peripheral unit at the 6,8-diarylethynyl terminal substituents in these D-$\pi$-A systems. In contrast, the fluorescence spectra of compounds **2** exhibit a clear and simple emission band, the emission maxima are in the range 452−532 nm in $CH_2Cl_2$ solution ($c = 5 \times 10^{-7}$ M) with a sequential bathochromic shift in the order **2a** ≈ **2b** < **2c** < **2d** < **2e** (Figure 4b). This is highly consistent with the energy gaps from the DFT calculation results; the energy gap ($E_g$) between the Franck-Condon and emitting state decreases in the same order. As expected, combined with the theoretical calculations, slight bathochromic shifts (< 5 nm) between **2a**–**c** were observed, while **2d**–**f** exhibited a distinct bathochromic shift (33−80 nm) compared with the former. To further elucidate the emission mechanism of this

**Table 2** Linear and nonlinear optical properties of compounds **2a**–**e**.

| Compd | $\lambda_{abs}$ [nm] sol[a] ($\varepsilon$ [$M^{-1}$ $cm^{-1}$ L]) | $\lambda_{em}$ [nm] sol[a] | $\Phi_{fl}$ [%] sol[a] | $\Phi_{fl}$ [%] sol[b] | $\lambda_{TPE}^{max}$ [nm][c] | $\delta_s$[d] [GM] | $\delta_s \times \Phi_s$[e] |
|---|---|---|---|---|---|---|---|
| **2a** | 318 (82835), 429 (70128) | 453 | 0.77 | 0.85 | 459 | 202 (780 nm) | 171 |
| **2b** | 318 (71323), 428 (60610) | 452 | 0.76 | 0.85 | 456 | 172 (780 nm) | 147 |
| **2c** | 325 (49758), 434 (53081) | 458 | 0.78 | 0.85 | 461 | 73 (800 nm) | 63 |

| | | | | | | | |
|---|---|---|---|---|---|---|---|
| **2d** | 256 (49763), 330 (48769) 367 (39806), 445 (53599) | 485 | 0.75 | 0.93 | 506 | 1450 (780 nm) | 1348 |
| **2e** | 255 (52624), 315 (50698) 388 (52321), 454 (58051) | 532 | 0.80 | 0.29 | 657 | 2210 (780 nm) | 641 |

a) Measured in dichloromethane at room temperature; b) Measured in DMSO at room temperature; c) Two-photon fluorescent maximum wavelength; d) δ is two-photon absorption cross sections determined

D-$\pi$-A system, solvatochromism was performed in solvents of different polarities (cyclohexane, CHX; 1,4-dioxane, DOA; tetrahydrofuran, THF; dichloromethane, DCM; and dimethyl formamide, DMF). As shown in Figure 5, the fluorescence spectra of this set of compounds are sensitive toward to the solvent polarity, especially for **2e**, where the emission maximum displayed a remarkable red-shift on increasing the solvent polarity (cyclohexane 470 nm, DMF 582 nm). The relationship between the Stokes shifts in various solvents and the Lippert−Mataga equation was investigated,[16] and a linear correlation between these two factors was evident (Figure 5b). The slopes of the linear fits for compounds **2a**−**e** are 16, 14, 17, 80 and 569 $cm^{-1}$, respectively, which indicates an increasing trend for the charge transfer.[17] The fluorescence quantum yields and emission decay profiles of the compounds **2** are shown in Table 1. All compounds exhibit high quantum yields (≥ 0.75) and considerably short lifetimes (≤ 15 ns) at room temperature (Figure 6). The same prompt and delayed PL emissions readily reveals the emission state resulting from the lowest singlet excited state.[18]

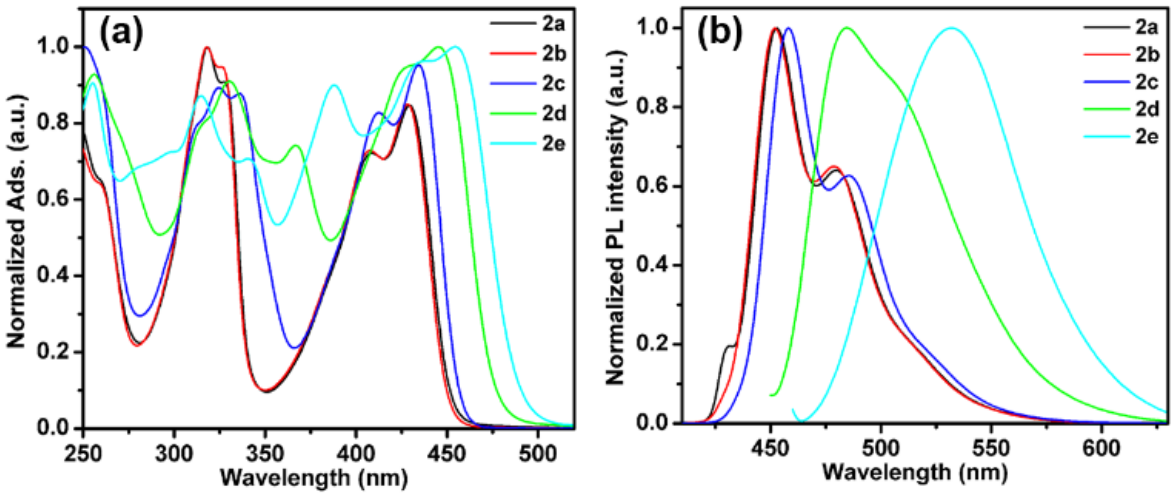


**Figure 4.** One-photon absorption (left) and emission (right) profiles for compounds **2** in $CH_2Cl_2$ solution.

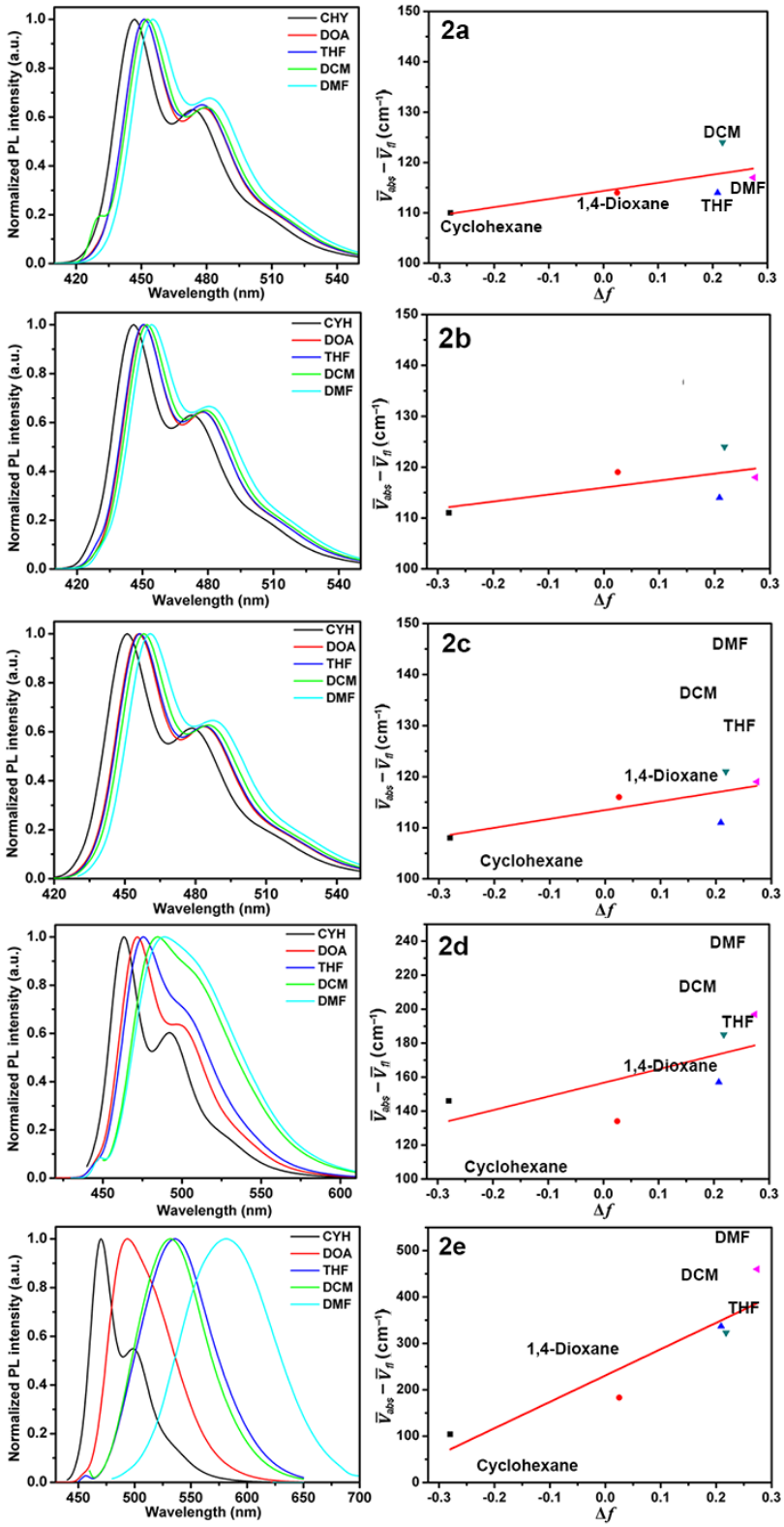


**Figure 5**. Left: PL spectra of **2** in different solvents; right: Lippert-Mataga plot for compounds **2**.

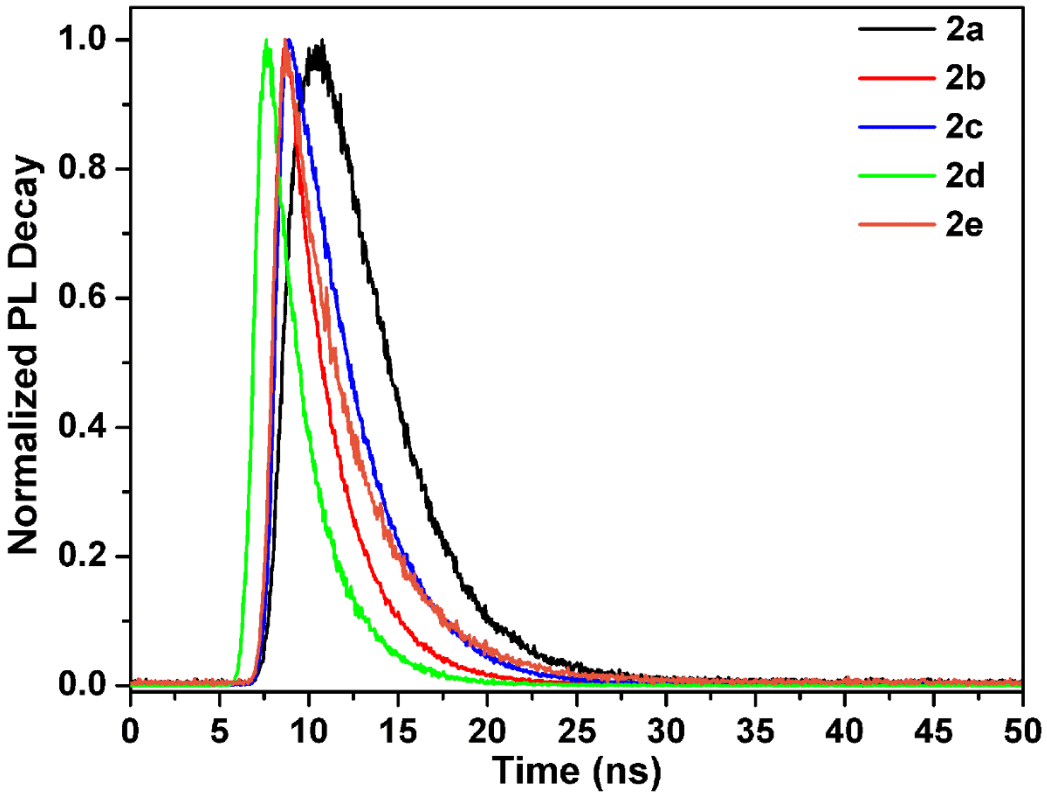


**Figure 6**. Transient PL decay profiles of compounds **2** at 25 °C.

### 5.2.5 Two-Photon Absorption (TPA) Properties

The two-photon absorption (TPA) spectra of five compounds **2** were studied using a two-photon-excited fluorescence (TPEF) technique with a femtosecond pulsed laser source.[19] According to the laser availability, the spectra were collected in the 340 nm to 700 nm range.

TPA cross sections have been measured using the two-photon induced fluorescence method,[20] and thus the cross section can be calculated by means of Eq. (1):

$$\delta_s = \delta_r \frac{\phi_r c_r n_r F_s}{\phi_s c_s n_s F_r} \qquad (1)$$

where the subscripts *s* and *r* refer to the sample and the reference materials, respectively. δ is the TPA cross section value, *c* is the concentration of the solution, *Φ* is the fluorescence quantum yield, *F* is the integrated emission intensity, and *n* is the refractive index. The relative

TPEF intensities of the molecules were measured using fluorescein in sodium hydroxide aqueous solution (pH = 13, Φ = 0.95) as the standard.[21]

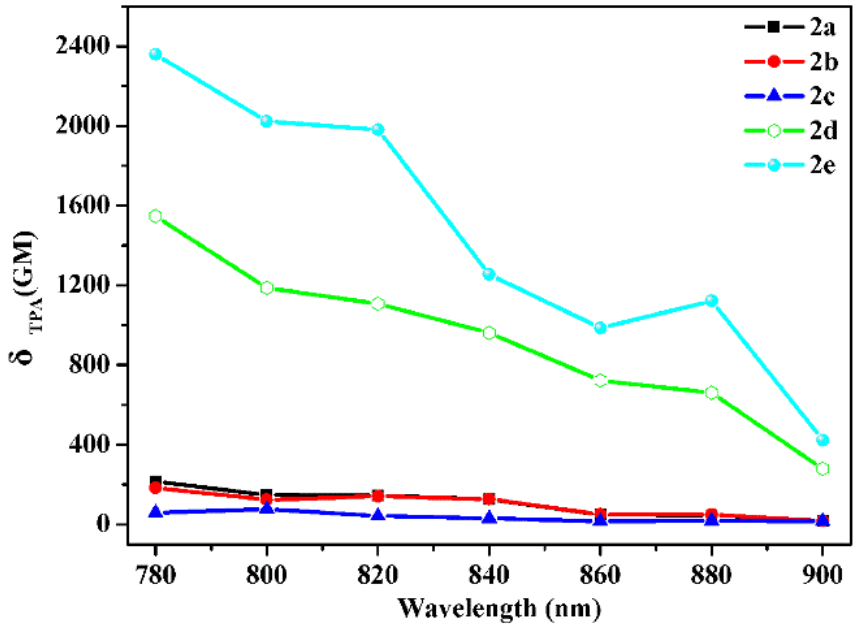


**Figure 7.** Two-photon excitation spectra of **2a**−**e** in DMSO. The values are an average of three measurements.

The TPA spectra of a series of compounds **2** were performed in DMSO solution at 20 nm intervals from 780 to 900 nm by using a femtosecond pulsed laser source. The TPA spectra of compounds **2** are presented in Figure 7. Depending on the extended $\pi$-conjugation and intermolecular charge-transfer over the entire molecule, all the compounds displayed large TPA cross-sections $\delta_s$, ($\delta$, expressed in GM = $10^{-50}$ cm$^4$ · S · photon$^{-1}$ · molecule$^{-1}$). The $\delta_s$ values, 202 GM for **2a** at 780 nm, 172 GM for **2b** at 780 nm, 73 GM for **2c** at 800 nm, 1450 GM for **2d** at 780 nm, 2210 GM for **2e** at 780 nm, are reasonable compared with other reported functionalized pyrene-based small molecules. Especially for **2d** (1450 GM) and **2e** (2210 GM), the $\delta_s$ values are large by comparison with other small pyrene-based molecules reported to-date,[11] indicating that the extended $\pi$-conjugation and increased ICT behaviour are favourable features to access high-efficiency organic molecules with large $\delta$ values. Moreover, the performance of two-photon active fluorescent molecules is generally evaluated according to the value of the two-photon action cross sections ($\delta \times \Phi$), which are an indicator of the brightness of the emission process. In this type of molecule, the $\delta\Phi$ values for **2d** (1348 GM) and **2e** (641 GM) are distinctly large compared with the values for other pyrene-based TP

active fluorescents. This result implies that pyrene as an efficient π-center may serve as a promising two-photon imaging material for various applications.[22]

Apart from TPA properties, the two-photon excited fluorescence (TPEF) of **2** was also studied under the same experimental conditions ($\lambda_{ex}$ = 800 nm). As shown in Figure 8 and Table 2, the spectral profiles for the TPEF are basically identical to the one-photon excited fluorescence (OPEF) except for **2e**. The similarities between the TPEF and OPEF indicated that they would finally relax to the same fluorescent excited state by either one- or two-photon excitations. Thus, for compounds **2a**−**d**, it seems to be impartial to the influence of the TPEF and OPEF properties except for a slight red-shift (no more than 5 nm). On the other hand, the different spectral selection rules for TPA and one-photon absorption (OPA) processes can lead to different excited states in these two cases.[23] For compound **2e**, a large red-shift (49 nm) was observed, and we assume that the distinction results from the reabsorption effect.[24] The effect occurs at high concentration; ($10^{-5}$ mol/L for the measurement of TPEF, and $10^{-7}$ mol/L for the measurement of OPEF). Furthermore, such red-shifted emission spectra can be ascribed to the different emitting states accessed by one- or two-photon excitation.[25]

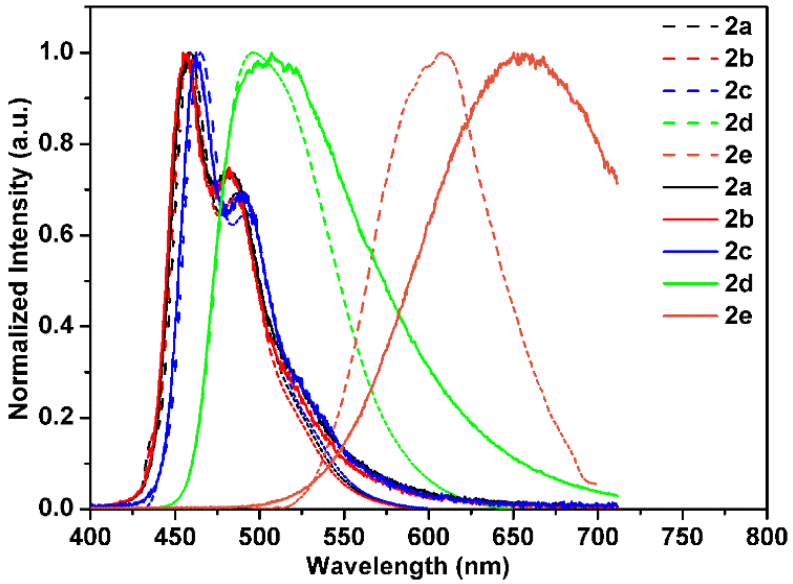


**Figure 8.** Normalized two-photon excited fluorescence spectra (solid line, $\lambda_{ex}$ = 800 nm) of compounds **2** in DMSO solution. One-photon excited fluorescence spectra are shown for comparison (dashed line).

Presented here, the OPEF and TPEF properties combined with theoretical calculations indicate that D–$\pi$–A pyrene systems exhibit excellent tunability for the design of large TPA cross sections and two-photon action cross sections. This type of molecule is not only a promising OPEF activator, but also an efficient TPEF fluorophor.

## 5.3 Conclusions

In conclusion, we have demonstrated an efficient and facile strategy for the design and synthesis of D–$\pi$–A pyrene-based fluorophors with large TPA cross section, which benefit from theoretical guidance. A microscopic rule was employed to prepare a series of dipolar molecules with graded energy gaps. Aided by this method, the first example of small pyrene-based dipolar molecules with $\delta$ above 2200 GM is reported, which can be attributed to the strong electron-donating nature of the $-N(CH_3)_2$ groups present. The electron-withdrawing nature of the –CHO groups results in a dipolar molecule with high quantum yield (93%) and large TP action cross section (1348 GM). Such OPEF and TPEF properties indicate a promising application in two-photon imaging materials. More studies are necessary to understand the underlying mechanisms of this type of molecule, and further detailed investigations are aimed at developing such TPA fluorophors in our laboratory.

## 5.4 Experimental Section

### 5.4.1 General

Synthetic routes for five compounds **2** are shown in Scheme 2. All reactions were carried out in a dry $N_2$ atmosphere. Solvents were Guaranteed reagent (GR) for cyclohexane, 1,4-dioxane, tetrahydrofuran (THF), dichloromethane ($CH_2Cl_2$), dimethylformamide (DMF), and dimethyl sulfoxide(DMSO), and stored over molecular sieves. Other reagents were obtained commercially and used without further purification. Reactions were monitored using thin layer chromatography (TLC). Commercial TLC plates (Merck Co.) were developed and the spots were identified under UV light at 254 and 365 nm. Column chromatography was performed on silica gel 60 (0.063-0.200 mm). All melting points (Yanagimoto MP-S1) are uncorrected. $^1H/^{13}C$ NMR spectra were recorded on a Varian-400MR-vnmrs 400 with $SiMe_4$ as an internal reference. Mass spectra were obtained with a Nippon Denshi JMS-HX110A Ultrahigh Performance mass spectrometer at 75 eV using a direct-inlet system. UV/ Vis spectra were obtained with a Perkin–Elmer Lambda 19 UV/Vis/NIR spectrometer in various organic solvents. Fluorescence spectroscopic studies were performed in various organic solvents in a semimicro fluorescence cell (Hellma®, 104F-QS, 10 × 4 mm, 1400 μL) with a Varian Cary Eclipse spectrophotometer. Fluorescence quantum yields were measured using absolute methods.

### 5.4.2 Synthetic Procedures

**Synthesis of 1,3-diphenyl-6,8-diarylethynylpyrenes (2a–e)**

A series of compounds **2a**–**e** were synthesized from 1,3-diphenyl-6,8-dibromopyrene **1**[14a] with the corresponding aryl alkyne by a Sonogashira coupling reaction.

**1,3-Diphenyl-6,8-bis-(4'-*N, N*-dimethylphenylethynyl)pyrene (2e)**

A mixture of 7-*tert*-butyl-1,3-diphenyl-6,8-dibromopyrene **1** (153 mg, 0.3 mmol), 4-ethynyl-*N, N*-dimethylaniline (174 mg, 1.2 mmol), $PdCl_2(PPh_3)_3$ (21 mg, 0.03 mmol), CuI (11.4 mg, 0.06 mmol), $PPh_3$ (8 mg, 0.03 mmol) were added to a degassed solution of $Et_3N$ (5

mL) and DMF (5 mL). The resulting mixture was stirred at 100 °C for 24 h. After it was cooled to room temperature, the reaction was quenched with water. The mixture was extracted with $CH_2Cl_2$ (2 × 500 mL), the organic layer was washed with water (2 × 30 mL) and brine (30 mL), and then the solution was dried ($MgSO_4$), and evaporated. The residue was purified by column chromatography eluting with a 2:1 of $CH_2Cl_2$/hexane mixture to give **2e** as a red granular solid (159 mg, 81.5%); Mp 297–298°C; $^1$H NMR (400 MHz, $CDCl_3$): $\delta_H$ = 3.03 (s, 12H, *Me*), 6.73 (d, *J* = 8.0 Hz, 4H, Ar-*H*), 7.46–7.51 (m, 2H, Ar-*H*), 7.53–7.59 (m, 8H, Ar-*H*), 7.68 (d, *J* = 6.9 Hz, 4H, Ar-*H*), 8.00 (s, 1H, pyrene-*H* ), 8.28 (d, *J* = 9.4 Hz, 2H, pyrene-*H*), 8.38 (s, 1H, pyrene-*H*), 8.64 (d, *J* = 9.4 Hz, 2H, pyrene-*H*) ppm; $^{13}$C NMR (100 MHz, $CDCl_3$): $\delta_C$ = 40.23, 86.34, 96.86, 110.30, 111.97, 118.83, 125.15, 125.20, 125.81, 126.13, 127.39, 128.34, 128.40, 129.77, 130.72, 131.06, 132.69, 132.86, 137.96, 140.97, 150.30 ppm; FAB-MS: m/z calcd for $C_{48}H_{36}N_2$ 640.2878 [$M^+$]; found 640.2878 [$M^+$].

A similar procedure using phenylacetylene, 4-fluorophenyl acetylene, 4-methoxyphenyl acetylene, 4-formylphenyl acetylene, was followed for the synthesis of **2a**–**d**.

**1,3-Diphenyl-6,8-bis-(phenylethynyl)pyrene 2a** was obtained as an orange solid (recrystallized from hexane:$CHCl_3$=4:1, 95 mg, 81.2%); Mp 195–196°C; $^1$H NMR (400 MHz, $CDCl_3$): $\delta_H$ = 7.41 (d, *J* = 7.3 Hz, 6H, Ar-*H*), 7.47–7.52 (m, 2H, Ar-*H*), 7.57 (t, *J* = 7.3 Hz, 4H, Ar-*H*), 7.68 (d, *J* = 6.3 Hz, 8H, Ar-*H*), 8.04 (s, 1H, pyrene-*H*), 8.35 (d, *J* = 9.4 Hz, 2H, pyrene-*H*), 8.45 (s, 1H, pyrene-*H*), 8.64 (d, *J* = 9.4 Hz, 2H, pyrene-*H*) ppm; $^{13}$C NMR (100 MHz, $CDCl_3$): $\delta_C$ = 88.02, 95.44, 117.65, 123.39, 124.93, 125.08, 125.45, 127.04, 127.54, 128.15, 128.45, 128.50, 130.00, 130.57, 130.71, 131.70, 132.03, 133.35, 138.60, 140.69 ppm; FAB-MS: *m/z* calcd for $C_{44}H_{26}$ 554.2035 [$M^+$]; found 554.2035 [$M^+$].

**1,3-Diphenyl-6,8-bis-(4'-fluorophenylethynyl)pyrene 2b** was obtained as a yellow solid (recrystallized from hexane:$CHCl_3$=3:1, 115 mg, 63.6%); Mp 263–264°C; $^1$H NMR (400 MHz, $CDCl_3$): $\delta_H$ = 7.12 (t, *J* = 8.1 Hz, 4H, Ar-*H*), 7.47–7.52 (m, 2H, Ar-*H*), 7.57 (t, *J* = 7.0 Hz, 4H, Ar-*H*), 7.67 (t, *J* = 7.1 Hz, 8H, Ar-*H*), 8.05 (s, 1H, pyrene-*H*), 8.35 (d, *J* = 9.4 Hz, 2H, pyrene-*H*), 8.41 (s, 1H, pyrene-*H*), 8.60 (d, *J* = 9.4 Hz, 2H, pyrene-*H*) ppm; $^{13}$C NMR (100 MHz, $CDCl_3$): $\delta_C$ = 87.70, 94.36, 110.08, 115.76, 115.98, 117.47, 119.49, 125.06, 125.36,

127.17, 127.61, 128.15, 128.49, 130.06, 130.73, 132.06, 133.26, 133.55, 133.64, 138.73, 140.67, 161.50 ppm; FAB-MS: *m/z* calcd for $C_{44}H_{24}F_2$ 590.1846 [$M^+$]; found 590.1846 [$M^+$].

**1,3-Diphenyl-6,8-bis-(4'-methoxyphenylethynyl)pyrene 2c** was obtained as a pale-yellow solid (recrystallized from hexane:$CH_2Cl_2$=2:1, 107 mg, 58.2%); Mp 169–170°C; $^1$H NMR (400 MHz, $CDCl_3$): $\delta_H$ = 3.87 (s, 6H, *Me*), 6.95 (d, *J* = 7.0 Hz, 4H, Ar-*H*), 7.47–7.52 (m, 2H, Ar-*H*), 7.57 (t, *J* = 7.3 Hz, 4H, Ar-*H*), 7.63 (d, *J* = 6.9 Hz, 4H, Ar-*H*), 7.68 (d, *J* = 7.8 Hz, 4H, Ar-*H*), 8.03 (s, 1H, pyrene-*H*), 8.33 (d, *J* = 9.4 Hz, 2H, pyrene-*H*), 8.41 (s, 1H, pyrene-*H*), 8.63 (d, *J* = 9.4 Hz, 2H, pyrene-*H*) ppm; $^{13}$C NMR (100 MHz, $CDCl_3$): $\delta_C$ = 54.45, 85.94, 94.57, 113.25, 114.60, 117.13, 124.06, 124.17, 124.63, 125.75, 126.57, 127.25, 127.52, 129.00, 129.80, 130.66, 132.07, 132.25, 137.40, 139.84, 158.92 ppm; FAB-MS: *m/z* calcd for $C_{46}H_{30}O_2$ 614.2246 [$M^+$]; found 614.2246 [$M^+$].

**1,3-Diphenyl-6,8-bis-(4'-formylphenylethynyl)pyrene 2d** was obtained as an orange solid (recrystallized from hexane:$CHCl_3$=1:1, 107 mg, 65.5%); Mp 177–178°C; $^1$H NMR (400 MHz, $CDCl_3$): $\delta_H$ = 7.49–7.54 (m, 2H, Ar-*H*), 7.58 (t, *J* = 7.6 Hz, 4H, Ar-*H*), 7.68 (d, *J* = 8.0 Hz, 4H, Ar-*H*), 7.81 (d, *J* = 7.9 Hz, 4H, Ar-*H*), 7.92 (d, *J* = 7.6 Hz, 4H, Ar-*H*), 8.08 (s, 1H, pyrene-*H*), 8.39 (d, *J* = 9.4 Hz, 2H, pyrene-*H*), 8.46 (s, 1H, pyrene-*H*), 8.60 (d, *J* = 9.4 Hz, 2H, pyrene-*H*) ppm; $^{13}$C NMR (100 MHz, $CDCl_3$): $\delta_C$ = 91.94, 94.60, 110.04, 116.70, 125.10, 127.71, 127.86, 128.01, 128.51, 129.50, 129.71, 130.23, 130.53, 130.70, 132.12, 132.68, 133.71, 135.61, 139.22, 140.43, 191.30 ppm; FAB-MS: *m/z* calcd for $C_{46}H_{26}O_2$ 610.1933 [$M^+$]; found 610.1933 [$M^+$].

## 5.4.3 X-ray Crystallography

Suitable single crystals of **2b**, **2c** and **2e** were obtained from chloroform/hexane mixtures, respectively. Diffraction data was collected at the ALS, beam line 11.3.1, using silicon 111-monochromated synchrotron radiation (λ = 0.7749 Å). Data were corrected for Lorentz and polarisation effects and for absorption from multiple and symmetry equivalent measurements.[26] The structures were solved by a charge flipping algorithm and refined by full-matrix least-squares methods on $F^2$.[27] For **2c** the absolute structure could not be reliably determined due to the lack of a heavy atom. In **2c** the chloroform molecule was positionally

disordered over two sets of positions with major component occupancy of 62.5(5)%. There was some evidence of low occupancy second component disorder in several of the Ph and $C_6H_4$ rings and the OMe groups, but this was not modelled. CCDC-1812898-1812900 contain the supplementary crystallographic data for this paper. Copies of the data can be obtained, free of charge, on application to CCDC, 12 Union Road, Cambridge CB2 1EZ, UK [fax: 144-1223-336033 or e-mail: deposit@ccdc.cam.ac.uk].

## 5.5 References


1. (a) Griesbeck, S.; Zhang, Z.; Gutmann, M.; Léhmann, T.; Edkins, R. M.; Clermont, G.; Lazar, A. N.; Haehnel, M.; Edkins, K.; Eichhorn, A.; Blanchard-Desce, M.; Meinel, L.; Marder, T. B., *Chem. - Eur. J.* **2016**, *22*, 14701−14706. (b) Yang, Z.; Zhao, N.; Sun, Y.; Miao, F.; Liu, Y.; Liu, X.; Zhang, Y.; Ai, W.; Song, G.; Shen, X.; Yu, X.; Sun, J.; Wong, W. *Chem. Commun.* **2012**, *48*, 3442−3444. (c) Jiang, M. J.; Gu, X. G.; Lam, J. W. Y.; Zhang, Y. L.; Kwok, R. T. K.; Wong, K. S.; Tang, B. Z. *Chem. Sci.* **2017**, *8*, 5440−5446.
2. (a) Fisher, W. G.; Jr, W. P.; Partridge, C.; Dees, E. A. Wachter, *Photochem. Photobiol.* **1997**, *66*, 141−155. (b) Shen, Y.; Shuhendler, A. J.; Ye, D.; Xu, J.-J.; Chen, H.-Y. *Chem. Soc. Rev.* **2016**, *45*, 6725−6741.
3. (a) Kawata, S.; Kawata, Y. *Chem. Rev.* **2000**, *100*, 1777−1788. (b) Fischer, J.; von Freymann, G.; Wegener, M. *Adv. Mater.* **2010**, *22*, 3578−3582. (c) Z. Gan, Y. Cao, R. A. Evans, M. Gu, *Nat. Commun.* **2013**, *4*, 2061.
4. (a) Albota, M.; Beljonne, D.; Brédas, J.-L.; Ehrlich, J. E.; Fu, J.-Y.; Heikal, A. A.; Hess, S. E.; Kogej, T.; Levin, M. D.; Marder, S. R.; McCord-Maughon, D.; Perry, J. W.; Röckel, H.; Rumi, M.; Subramaniam, G.; Webb, W. W.; Wu, X.-L.; Xu, C. *Science* **1998**, *128*, 1653−1656. (b) Zipfel, W. R.; Williams, R. M.; Webb, W. W.; *Nat. Biotechnol.* **2003**, *21*, 1369–1377. (c) Collins, H. A.; Khurana, M.; Moriyama, E. H.; Mariampillai, A.; Dahlstedt, E.; Balaz, M.; Kuimova, M. K.; Drobizhev, M.; Yang, V. X. D.; Phillips, D.; Rebane, A.; Wilson, B. C.; Anderson, H. L. *Nat. Photonics* **2008**, *2*, 420−424.
5. (a) Lin,G. T. C.; He, S.; Prasad, P. N.; Tan, L. S. *J. Mater. Chem.* **2004**, *14*, 982−991. (b) Beverina, L.; Fu, J.; Leclercq, A.; Zojer, E.; Pacher, P.; Barlow, S.; Van Stryland, E. W.; Hagan, D. J.; Bredas, J. L.; Marder, S. R. *J. Am. Chem. Soc.* **2005**, *127*, 7282−7283. (c) Sun, C. L.; Liao, Q.; Li, T.; Li, J.; Jiang, J. Q.; Xu, Z. Z.; Wang, X. D.; Shen, R.; Bai, D. C.; Wang, Q.; Zhang, S. X.; Fu, H. B.; Zhang, H. L. *Chem. Sci.* **2015**, *6*, 761−769.
6. (a) Rumi, M.; Ehrlich, J. E.; Heikal, A. A.; Perry, J. W.; Barlow, S.; Hu, Z. Y.; McCord-Maughon, D.; Parker, T. C.; Rockel, H.; Thayumanavan, S.; Marder, S. R.; Beljonne, D.; Bredas, J. L. *J. Am. Chem. Soc.* **2000**, *122*, 9500−9510. (b) Mongin, O.; Porrès, L.; Charlot, M.; Katan, C.; Blanchard-Desce, M. *Chem. - Eur. J.* **2007**, *13*, 1481−1498.

7. (a) Jiang, Y. H.; Wang, Y. C.; Hua, J. L.; Tang, J.; Li, B.; Qian, S. X.; Tian, H. *Chem. Commun.* **2010**, *46*, 4689−4691. (b) Shao, J.; Guan, Z.; Yan, Y.; Jiao, C.; Xu, Q.-X.; Chi, C. *J. Org. Chem.* **2011**, *76*, 780−790. (c) Poronik, Y. M.; Hugues, V.; Blanchard-Desce, M.; Gryko, D. T. *Chem. - Eur. J.*, **2012**, *18*, 9258−9266.
8. (a) He, G. S.; Swiatkiewicz, J.; Jiang, Y.; Prasad, P. N.; Reinhardt, B. A.; Tan, L. S.; Kannan, R. *J. Phys. Chem. A* **2000**, *104*, 4805–4810. (b) Alam, M. M.; Chattopadhyaya, M.; Chakrabarti, S.; Ruud, K. *Acc. Chem. Res.* **2014**, *47*, 1604−1612. (c) Dereka, B.; Koch, M.; Vauthey, E. *Acc. Chem. Res.* **2017**, *50*, 426−434.
9. Jérome, D.; Schulz, H. J. *Advances in Physics* **2002**, *51*, 293−479.
10. (a) Figueira-Duarte, T. M.; Müllen, K. *Chem. Rev.* **2011**, *111*, 7260–7314. (b) Feng, X.; Hu, J. Y.; Redshaw, C.; Yamato, T. *Chem. - Eur. J.* **2016**, *22*, 11898–11916.
11. (a) Kim, H. M.; Lee, Y. O.; Lim, C. S.; Kim, J. S.; Cho, B. R. *J. Org. Chem.* **2008**, *73*, 5127–5130. (b) Niko, Y.; Moritomo, H.; Sugihara, H.; Suzuki, Y.; Kawamata, J.; Konishi, G. *J. Mater. Chem. B* **2015**, *3*, 184–190. (c) Devi, C. L.; Yesudas, K.; Makarov, N. S.; Rao, V. J.; Bhanuprakash, K.; Perry, J. W. *J. Mater. Chem. C* **2015**, *3*, 3730—3744. (d) Gascón-Moya, M.; Pejoan, A.; Izquierdo-Serra, M.; Pittolo, S.; Cabré, G.; Hernando, J.; Alibés, R.; Gorostiza, P.; Busqué, F. *J. Org. Chem.* **2015**, *80*, 9915−9925.
12. Wan, Y.; Yan, L.; Zhao, Z.; Ma, X.; Guo, Q.; Jia, M.; Lu, P.; Ramos-Ortiz, G.; Maldonado, J. L.; Rodríguez, M.; Xia, A. *J. Phys. Chem. B* **2010**, *114*, 11737–11745.
13. Burn, P. L.; Lo, S. C.; Samuel, I. D. W. *AdV. Mater.* **2007**, *19*, 1675–1688.
14. (a) Feng, X.; Tomiyasu, H.; Hu, J. Y.; Wei, X. F.; Redshaw, C.; Elsegood, M. R. J.; Horsburgh, L.; Teat, S. J.; Yamato, T. *J. Org. Chem.* **2015**, *80*, 10973–10978. (b) Wang, C. Z.; Ichiyanagi, H.; Sakaguchi, K.; Feng, X.; Elsegood, M. R. J.; Redshaw, C.; Yamato, T. *J. Org. Chem.* **2017**, *82*, 7176−7182. (c) Wang, C. Z.; Do, J.-H.; Akther, T.; Feng, X.; Matsumoto, T.; Tanaka, J.; Redshaw, C.; Yamato, T. *J. Lumin.* **2017**, *188*, 388−393.
15. (a) Shizu, K.; Tanaka, H,; Uejima, M.; Sato, T.; Tanaka, K.; Kaji, H.; Adachi, C. *J. Phys. Chem. C* **2015**, *119*, 1291−1297. (b) Rajamalli, P.; Senthilkumar, N.; Gandeepan, P.; Huang, P. Y.; Huang, M. J.; RenWu, C. Z.; Yang, C. Y.; Chiu, M. J.; Chu, L. K.; Lin, H. W.; Cheng, C. H. *J. Am. Chem. Soc.* **2016**, *138*, 628−634.
16. (a) Lippert, V. E.; Z. *Naturforsch., A: Phys. Sci.* **1955**, *10*, 541−545. (b) Mataga, N,; Kaifu, Y.; Koizumi, M, *Bull. Chem. Soc. Jpn.*, **1956**, *29*, 465−470.

17. (a) Jadhav, T.; Dhokale, B.; Patil, Y.; Mobin, S. M.; Misra, R. *J. Phys. Chem. C* **2016**, *120*, 24030−24040. (b) Tayade, R. P.; Sekar, N. *J. Lumin.* **2016**, *176*, 298−308; (c) Lim, C.-H.; Ryan, M. D.; McCarthy, B. G.; Theriot, J. C.; Sartor, S. M.; Damrauer, N. H.; Musgrave, C. B.; Miyake, G. M. *J. Am. Chem. Soc.* **2017**, *139*, 348−355.
18. Zhu, H. N.; Wang, X.; Ma, R. J.; Kuang, Z. R.; Guo, Q. J.; Xia, A. D. *ChemPhysChem* **2016**, *17*, 3245–3251.
19. (a) Sheik-Bahae, M.; Said, A. A.; Wei, T.-H.; Hagan, D. G.; van Stryland, E. W. *IEEE J. Quantum Electron.* **1990**, *26*, 760−769. (b) Kamada, K.; Matsunaga, K.; Yoshino, A.; Ohta, K. *J. Opt. Soc. Am. B* **2003**, *20*, 529−537.
20. Xu, C.; Webb, W. W. *J. Opt. Soc. Am. B* **1996**, *13*, 481–491.
21. Demas, J. N.; Crosby, G. A. *J. Phys. Chem.* **1971**, *75*, 991–1024
22. (a) Chang, Z. F.; Jing, L. M.; Chen, B.; Zhang, M.; Cai, X.; Liu, J. J.; Ye, Y. C.; Lou, X.; Zhao, Z.; Liu, B.; Wang, J. L.; Tang, B. Z. *Chem. Sci.* **2016**, *7*, 4527–4536. (b) Tian, J.; Zhang, J.; Li, W.; Zhang, L. Q.; Yue, D. M. *J. Mater. Chem. C* **2016**, *4*, 10146–10153. (c) Ding, A. X.; Hao, H. J.; Gao, Y. G.; Shi, Y. D.; Tang, Q.; Lu, Z. L. *J. Mater. Chem. C* **2016**, *4*, 5379–5389.
23. (a) Xu, Y. Q.; Chen, Q.; Zhang, C. F.; Wang, R.; Wu, H.; Zhang, X. Y.; Xing, G. C.; Yu, W. W.; Wang, X. Y.; Zhang, Y.; et al. *J. Am. Chem. Soc.* **2016**, *138*, 3761−3768. (b) Han, Q. J.; Wu, W. Z.; Liu, W. L.; Yang, Y. Q. *RSC Adv.* **2017**, *7*, 35757−35764.
24. Wang, Y.; Li, X. M.; Zhao, X.; Xiao, L.; Zeng, H. B.; Sun, H. D. *Nano. Lett.* **2016**, *16*, 448–453.
25. (a) Liu, Z. Q.; Fang, Q.; Wang, D.; Cao, D. X.; Xue, G.; Yu, W. T.; Lei, H. *Chem. Eur. J.* **2003**, *9*, 5074–5084. (b) Chen, J.; Chábera, P.; Pascher, T.; Messing, M. E.; Schaller, R.; Canton, S.; Zheng, K.; Pullerits, T. *J. Phys. Chem. Lett.* **2017**, *8*, 5119–5124.
26. APEX 2 & SAINT (2012), software for CCD diffractometers. Bruker AXS Inc., Madison, USA.
27. (a) G. M. Sheldrick, *Acta Crystallogr.*, 2008, **A64**, 112–122; (b) G. M. Sheldrick, *Acta Cryst.*, 2015, **A71**, 3–8; (c) G. M. Sheldrick, *Acta Cryst.*, 2015, **C71**, 3–8.

# Summary

Almost 200 years have passed since its first description but still pyrene enjoys unbroken interest by chemists around the world. For 2017 alone more than 2000 publications are registered in the scientific search engine Thomson Reuters "Web of Science™". To a large extend this can be attributed to its interesting photophysical properties which can be exploited in biochemistry or material science.

Pyrene is a classical member of the family of PAHs, and possesses high thermal stability, photoluminescence efficiency, and enhanced hole-injection ability. Recently, many efforts have been devoted to the synthesis of pyrene-based materials for organic electronics. Generally, there are two strategies for effectively functionalizing pyrene core to control geometry. One way is to functionalize the K-region of the pyrene by bromination reaction. it involves expansion of the conjugation of the linear aromatic backbone using additional aromatic rings via sonogashira reactions. Another strategy is direct electrophilic substitution of the pyrene at the active sites, namely, 1-, 3-, 6-, and 8- positions, or directly to attack at the 1- and 3- positions by Suzuki, Sonogashira and Buchwald–Hartwig amination reaction.

In this thesis, we investigated the emission properties of pyrene-based fluorophores by constructing the different type molecules, such as D–$\pi$–D, D–$\pi$–A, and A–$\pi$–A pyrene-based derivatives.

In chapter 1, a brief introduction focus on the development of pyrene chemistry is presented at the beginning, including the application as organic materials, mechanism of luminescence, objects and motivation in our present work. Two main topics are summarized for pyrene-based materials science. Firstly, the synthesis of strong donor / acceptor based on the pyrene scaffold by functional group modification. Secondly, preparation of pyrene derivatives with tunable emission properties and large two proton absorption cross section.

In chapter 2, a series of *Y*-shaped arylethynyl-functionalized pyrenes derivatives were synthesized by a Pd-catalyzed Sonogashira coupling reaction in high yield. The Y-shaped, extended $\pi$-conjugated pyrene derivatives display strong face-to-face $\pi$-stacking with off-set head-to-tail stacking as compared with a *Y*-shaped carbon-carbon single bond arylsubstituted pyrene. Furthermore, the effects of the substituents and their position on the crystal packing structure and photophysical properties of the chromophores has been evaluated. Compounds

**2a**–**c** and **2e** in dichloromethane exhibited deep blue fluorescence with high quantum yield, while the chromophores **2d** and **2f** exhibit intermolecular charge-transfer (ICT) leading to intense optical absorbances over a wide spectral range. Strong fluorescence spectra of **2d** and **2f** show the maximum emission at 517 nm and 485 nm, respectively, with remarkable solvatochromic effects in polar solvents. Theoretical computation and experimental CV studies on their electrochemistry verify that Y-shaped extended π-conjugated pyrenes derivatives can be utilized in OLED devices as luminescent hole-transporting materials. In future, we will attempt to fabricate highly efficient OLED devices using these materials.

In chapter 3, a series of tuneable pyrene-based monomers 3a-e were designed and synthesized by a facile strategy, and their optical properties were investigated both experimentally and computationally. It was determined that these systems exhibited predictable photophysical properties by introducing different substituents at the para position of the phenyl moieties. Moreover, a positive correlation between the wavelength of the $\lambda_{em}$ max and the Hammett $\sigma_{para}$ constants for the functional groups provided evidence that these systems may be used to tune the emission color from blue to yellow or orange, which could be predicted and tuned by substitutions in the para position. And further investigations aimed at developing these optoelectronic materials for practical applications are ongoing in our group.

In chapter 4, we present an innovative, facile, and promising, controllable regioselective strategy for the functionalization at the active sites (1,3-positions) and K-region (5,9-positions) of pyrene. The resulting dipolar molecules, namely 1,3-diphenyl-5,9-diarylethynyl)pyrenes, exhibit thermal stability, and tuneable emission over the entire visible region. The chemistry (specifically the bromination and Suzuki reactions) now is in a supporting role in the study and the photo-physical properties is the main focus of the study. By drafting it this way, the authors have provided not only a good foundation for the further advancement of pyrene-based materials, but also a means to their synthesis. The combined experimental and computational results provide an increasing understanding of the emission mechanism for introducing substitution at the K-region of pyrene. This work opens up new avenues to explore strategy to functionalize pyrene and to greatly expand the scope for developing highly efficient pyrene-based photoelectric materials.

Finally, as we all know, rational design of pyrene-based dipolar molecules with two-photon absorption (TPA) properties is a challenge in practical photics and biological imaging

applications. Herein we developed a pyrene-based TPA fluorophores by constructing donor-π-acceptor (D-π-A) type structures by introducing the different electron-donating/withdrawing substituents, a series of dipolar pyrene-based molecules, with tunable LUMO and HOMO levels and large effective δ value are report. Specifically, a series of 1,3-diphenyl-6,8-diarylethynylpyrene compounds 2 with wide-range color tuning and large TPA cross-sections (up to 2.8 × 103 GM) are reported.

In summary, several kinds of pyrene-based fluorophores were investigated. Different strategies to design and synthesize pyrene-based organic materials with tunable emission properties were established. In this work, we have presented a novel and significative result, which can expand the new fundamental concepts, synthetic strategies, and application in organic electronics.

# Publications

1. Synthesis, structure and photophysical properties of pyrene–based [5]helicenes: an experimental and theoretical study

   **Chuan-Zeng Wang**, Rie Kihara, Xing Feng, Pierre Thuéry, Carl Redshaw, Takehiko Yamato, *ChemistrySelect*, **2017**, 2, 1436–1441.

2. Pyrene-Based Approach to Tune Emission Color from Blue to Yellow

   **Chuan-Zeng Wang**, Hisashi Ichiyanagi, Koya Sakaguchi, Xing Feng, Mark R.J. Elsegood, Carl Redshaw, Takehiko Yamato, *The Journal of Organic Chemistry*, **2017**, 82, 7176–7182.

3. D-π-D chromophores based on dithieno[3,2-b:2',3'-d]thiophene (DTT): Potential application in the fabrication of solar cell

   **Chuan-Zeng Wang**, Jung-Hee Do, Tahmina Akther, Xing Feng, Lynne Horsburgh, Mark R.J. Elsegood, Carl Redshaw, Takehiko Yamato, *Tetrahedron*, **2017**, 73, 307–312.

4. Synthesis and fluorescence emission properties of D-π-D monomers based on dithieno[3,2-b:2′,3′-d]thiophene

   **Chuan-Zeng Wang**, Jung-Hee Do, Tahmina Akther, Xing Feng, Taisuke Matsumoto, Junji Tanaka, Carl Redshaw, Takehiko Yamato, *Journal of Luminescence*, **2017**, 188, 388−393.

5. Regioselective substituted at 1,3- and 5,9-positions to achieve pyrene-based dipolar molecules and their optical properties

   **Chuan-Zeng Wang**, Xing Feng, Zannatul Kowser, Chong Wu, Thamina Akther, Mark R.J. Elsegood, Carl Redshaw, Takehiko Yamato, *Dyes and Pigments*. **2018**, In press.

6. Multiple Photoluminescence from Pyrene-Fused Hexaarylbenzenes with Aggregation Enhanced Emission Features

   **Chuan-Zeng Wang**, Yuki Noda, Chong Wu, Xing Feng, Perumal Venkatesan, Hang Cong, Mark R.J. Elsegood, Thomas G. Warwick, Simon J. Teat, Carl Redshaw, Takehiko Yamato, *Asian Journal of Organic Chemistry*. **2018**, In press.

7. Two-Photon Absorption Properties of Pyrene-based Bipolar D–π–A Fluorophores

   **Chuan-Zeng Wang**, Ruoyao Zhang, Koya Sakaguchi, Xing Feng, Xiaoqiang Yu, Mark R.J. Elsegood, Simon J. Teat, Carl Redshaw, Takehiko Yamato, *Chem. Eur. J.* Submitted.